Establishing a liquid chromatography-mass spectrometry method for the quantification of colistin A, a last line of defense against antibiotic resistance

Harald Røsand Moe

60 credits

Bioanalytical Chemistry

Department of Chemistry

Faculty of Mathematics and Natural Sciences

UNIVERSITY OF OSLO

7/2021

Preface

The work presented in this master's thesis was conducted at the Department of Chemistry at the University of Oslo, at the group for Bioanalytical Chemistry, from August 2019 to June 2021. The project was supervised by Professor Steven Ray Wilson (primary supervisor), Professor Elsa Lundanes, Associate Professor Hanne Røberg-Larsen, and Associate Professor Reidar Lund. Additionally, Cheng Cao, Marlene Andersen Nahm, and Lelaw Jalal Ali greatly aided me by supplying samples and solutions that proved imperative to this work.

I want to thank all my supervisors for their assistance, support, and guidance throughout this project and express my utmost sincere appreciation for how I was allowed to pursue my interests within a scientific field I found fascinating and exciting. This work could not have been performed without the technical, educational, and motivational support you provided throughout this work, and for this, I thank you.

Additionally, I would like to thank the people at VITAS AS at Forskningsparken, Oslo, for the competence and self-efficacy they helped me acquire during a kindly offered summer internship. The technical know-how and introduction to practical analytical chemistry helped accelerate this work tremendously.

Furthermore, I would like to express my tremendous gratitude towards my fellow students and friends at the group for Bioanalytical Chemistry, whose social, technical, and motivational support helped me tremendously through times of progress and significant setbacks. We shared some of the most nonsensical yet endlessly engaging, fun debates together.

Finally, I would like to send lots of love and appreciation to my parents and off-campus friends, who have cheered me on from day one and onwards, and have supported and encouraged me to persevere and continue with my work, half of which was conducted during the global COVID-19 pandemic. I couldn't have done this without you.

Thank you.

Harald Røsand Moe.

Oslo, 08 Jun 2021

1 ABBREVIATIONS

6-MHA	6-Methylheptanoic Acid
6-MOA	6-Methyloctanoic Acid
ACN	Acetonitrile
AMP	Antimicrobial Peptide
CE	Collision Energy
cLOD	Concentration Limit of Detection
Dab	2,4-Diaminobutyric acid
DAD	Diode Array Detector
DCM	Dichloromethane
DMPC	1,2-Dimyristoyl-sn-Glycero-3-Phosphocholine
DSPE-PEG	1,2-Distearoyl-sn-Glycero-3-Phosphoethanolamine-Polyethylene Glycol
EMA	European Medicines Agency
ER	Endoplasmic Reticulum
ESI	Electrospray Ionization
FMOC-Cl	Fluorenylmethyloxycarbonyl chloride
FT-ICR	Fourier Transform Inductively Coupled Resonance
HAI	Hospital-Acquired Infection
HAVcr-1	Hepatitis A virus Cellular Receptor 1
HESI	Heated Electrospray Ionization
HILIC	Hydrophilic Interaction Liquid Chromatography
HPLC	High Performance / Pressure Liquid Chromatography
HPSEC	High Performance / Pressure Size Exclusion Chromatography
HRPTEpC	Human Renal Proximal Tubule Epithelial Cells
ICU	Intensive Care Unit
ID	Inner Diameter
IU	International Unit(s)
KIM-1	Kidney Injure Molecule 1
LC	Liquid Chromatography
Leu	Leucine
LLOQ	Lower Limit of Quantification
LOD	Limit of Detection
LOQ	Limit of Quantification

LPS	Lipopolysaccharide
m/z	Mass-to-charge Ratio
MALDI	Matrix-Assisted Laser Desorption Ionization
MCR	Mobilized Colistin Resistance
MDR	Multi-Drug-Resistant
MeOH	Methanol
MIC	Minimum Inhibitory Concentration
mLOQ	Mass Limit Of Quantification
MRM	Multiple Reaction Monitoring
MS	Mass Spectrometry
MS/MS	Tandem Mass Spectrometry
NPC	Normal Phase Chromatography
PEG	Polyethylene Glycol
Phe	Phenylalanine
PTM	Post Translational Modification(s)
RF	Radio Frequency
RI	Refractive Index
RPLC	Reversed Phase Liquid Chromatography
RSD	Relative Standard Deviation
SEC	Size Exclusion Chromatography
Ser	Serine
SIM	Selected Ion Monitoring
SPE	Solid Phase Extraction
SRM	Selected Reaction Monitoring
ST.DEV.	Standard Deviation
Thr	Threonine
TIM-1	T-cell immunoglobulin 1
TOF	Time of Flight
UHPLC	Ultra-High Performance / Pressure Liquid Chromatography
ULOQ	Upper Limit of Quantification

Table of contents

Abstract

Antibiotic resistance has become an increasingly pressing issue in recent times. With a dwindling discovery rate of new antibacterials, gram-negative bacteria threaten to return humanity to the pre-antibiotic era where mere paper cuts could result in fatal outcomes. The antimicrobial peptide colistin is our present-day last line of defense against gram-negative infections. Nevertheless, despite the recent surge in use and research on colistin, research on its biological effects and chemical behavior remains somewhat scarce. Colistin was initially abandoned due to numerous reports of neuro- and nephrotoxicity. Slow leakage from colistin-loaded liposomes may reduce this toxicity significantly. In this work, an LC-MS method for separating and quantifying colistin and polymyxin B1 was developed to measure colistin leakage from loaded liposomes over time. Isocratic elution provided adequate separation of polymyxin E1 and the internal standard, polymyxin B1, and measurements were done using a triple-quadrupole MS. Widely unreported and uninvestigated adsorption and degradation mechanisms of colistin were observed and addressed by adding a 100 mM ammonium formate buffer at pH 3 to solutions of colistin. The LC-MS method provides a reliable and accurate approach for measuring colistin at lower concentrations (< 10 µg/mL) in ammonium formate buffered solutions, and the future challenges and potential approaches for further research upon colistin are discussed. The LC-MS method described serves as a solid platform for further research on colistin, colistin toxicity negation, and more may be built upon.

2 BACKGROUND

It is generally accepted that antibiotic resistance in bacteria has become a rising issue over the past decades. Following the discovery of penicillin by Alexander Fleming, antibiotics have been used for various applications, ranging from life-saving treatments to preventative additives in livestock feed [1]. As a result of this widespread use, multidrug-resistant (MDR) bacteria have become a significant and still growing public health issue. Gram-negative bacteria, bacteria with not one but two bacterial membranes, are of particular concern as they are naturally more resistant to most antibiotics [2]

Thus far, two main approaches have been used to mitigate the threat posed by antibiotic resistance: discovering brand-new antibiotics or through chemical modifications of preexisting antibiotics already in use. The former proved highly efficient until the 1970s where the discovery of new antibiotics came to a crawl. Lately, the latter method has been the significant source of new antibiotics; however, bacteria rapidly continue to develop resistance with the copious overconsumption of antibiotics. For this reason, many new antibiotics are currently administered alongside inhibitors designed to bypass or neutralize antibiotic resistance mechanisms already evolved by many bacteria. With the current rate of development of new antibiotics, these inhibitors may prove essential in the immediate future to manage the pressing issue that is antibiotic resistance [3].

For example, *Staphylococcus aureus*, a common hospital-acquired infection (HAI), was typically highly susceptible to penicillin G. Nowadays, virtually all samples of this strain of bacteria readily present resistance to standard antibiotics such as aminopenicillins and ureido-penicillins [4].

2.1 NATURALLY ANTIBIOTIC-RESISTANT GRAM-NEGATIVE BACTERIA

Compared to their gram-positive counterparts, gram-negative bacteria are naturally more resistant to antibiotics and antibacterials. This resistance arises from an additional membrane around their cellular membrane and peptidoglycan coating. Gram-positive bacteria possess only a thicker layer of peptidoglycan around their cellular membrane [5, 6]. Furthermore, gram-negative bacteria have a coating of lipopolysaccharides (LPS), which play an essential role in maintaining the stability of the bacterial cell membrane. In many cases, LPS also function as a potent endotoxin, capable of inducing strong reactions from the immune system of a given organism, sometimes with acute and potentially fatal consequences [7, 8]. These also serve a

protective function: embedded into the outer membrane, any alteration in the LPS will inherently affect the membrane's hydrophobic permeability and stability. This outer membrane is responsible for the increased antibiotic resistance in gram-negative bacteria. While hydrophobic compounds can readily diffuse through the membrane, hydrophilic compounds must pass through narrow porins embedded in the outer layer before approaching the inner membrane. For many antibiotics, such as vancomycin, the structure is incompatible with these passages, preventing them from doing so. As such, only minor alterations in the outer membrane, be it of the hydrophobic properties, embedded porins, and even an increased expression of efflux pumps, are required for resistance to emerge. In summary, not only are gram-negative bacteria generally more resistant by their structure alone, but they can readily develop or improve this resistance by relatively minor changes [9]. For an illustration of gram-negative membranes versus the gram-positive counterparts (see **Figure 1**).

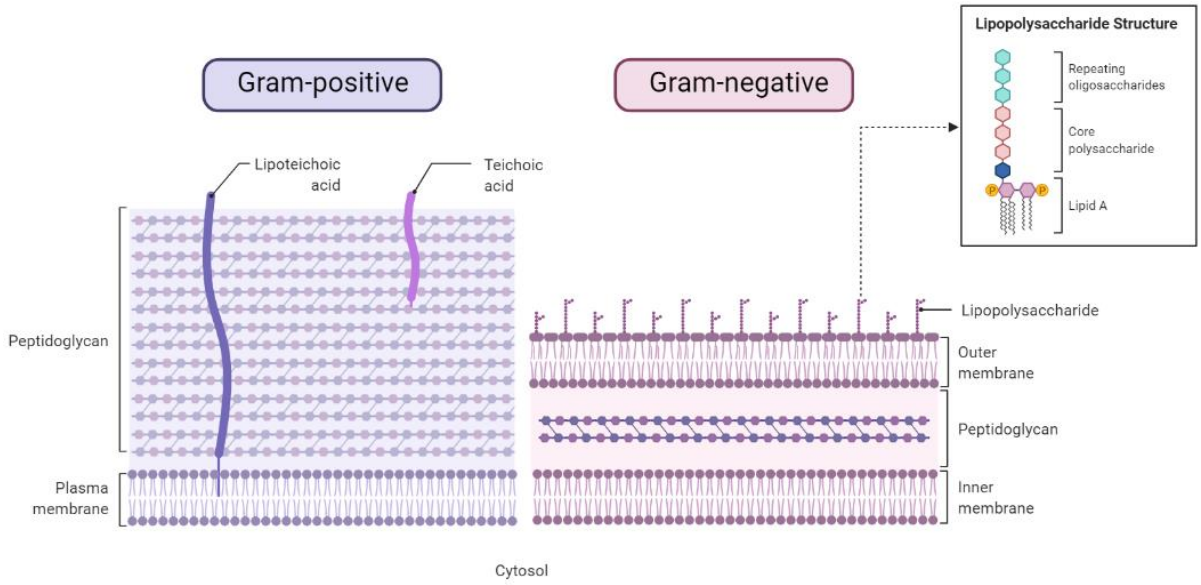

Figure 1 Illustration of the differences and similarities between gram-negative and gram-positive bacterial membranes. Gram-negative bacteria have an additional cellular membrane, with the intermembrane space containing a layer of peptidoglycan. Gram-positive bacteria have a single cellular membrane and a more prominent layer of peptidoglycan [5, 6]. Lipoteichoic and teichoic acid are also significant constituents of the gram-positive bacterial membrane. Illustration created using BioRender [10].

HAI generally have a significantly higher incidence of antibiotic resistance than other infections, as found by a study performed by Zhang et al. [11]. Furthermore, a statistical approach conducted in a study by Falagas and Rafaildis in 2007 concluded that the probability that a given bacteria in the intensive care unit (ICU) of a hospital would be susceptible only to polymyxins, an antibacterial class used in last resort efforts, was as high as approximately 50% [12].

2.2 POLYMYXINS AS ANTIMICROBIAL PEPTIDES

As a result of the rapidly emerging antibiotic resistance observed nowadays, there has been a widespread investigation into alternatives to antibiotics. Exotic treatments such as viral treatments using bacteriophages [13] and formerly near-abandoned drugs (such as polymyxins) are rapidly becoming promising candidates for the antibacterial therapies of tomorrow. Antimicrobial peptides (AMPs) such as the polymyxins are also frequently referred to as host defense peptides [14] and represent a part of the innate immune system employed by many organisms in nature, representing the first line of defense against bacteria, viruses, and even cancerous cells [15, 16]. AMPs prevent infections in the cornea of the eye, enable germination of a seed amidst a blanket of soil microbes, and even allow insects to thrive without antibodies [17] (see **Figure 2**).

Figure 2 The cornea of the eye (left), many insects (middle), and germinating seeds (right) are examples of how crucial AMPs are throughout nature, allowing these to thrive without a complete immune system, thanks to their employment of AMPs [17]. Illustration created using BioRender [10].

While AMPs represent the first line of defense for many organisms, many of these antibacterial compounds have become our very last line of defense. Polymyxins are a prime example of this. They have become the present-day last class of drug we have to treat MDR gram-negative bacterial infections (frequently referred to as 'superbugs' in popular media) [18, 19].

Initially discovered in 1947, the polymyxins constitute a class of AMPs produced by the gram-positive bacteria *Bacillus polymyxa* [20]. They are similar to one another in structure and contain a mixture of L- and D-amino acids. Structurally, they all contain a heptapeptide ring, an exocyclic tripeptide, and a fatty acid bound to this tripeptide (see **Figure 3**) [21]. Furthermore, they all contain a relatively high percentage of a somewhat uncommon amino acid, 2,4-diaminobutyric acid (Dab), making up six out of ten amino acids. The polymyxins are cationic decapeptides and only available as salts. At physiological pH, the terminal γ-amine groups present on Dab are positively charged. In total, six primary polymyxins exist, ranging from polymyxin A, B, C, D, E, and polymyxin M, albeit subvariants within these structures do

exist [21, 22]. The four primary points of difference; the fatty acid, and the three amino acids, are identified in **Table 1** and **Figure 3** below.

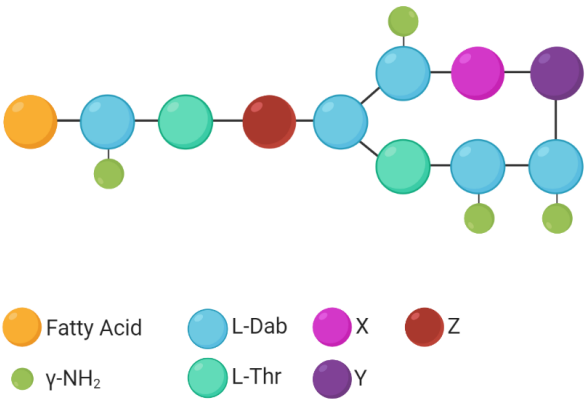

*Figure 3 General structure of a polymyxin. The only variable parts are the fatty acid (orange), X (pink), Y (dark purple), and Z (dark red), identified in **Table 1** for the various polymyxins. L-Dab: 2,4-diaminobutyric acid. L-Thr: Threonine. Created using BioRender [10].*

Table 1 Structural differences between some polymyxins, as reported in the literature. Data on the structure of polymyxin C proved challenging to locate. 6-MOA: 6-Methyloctanoic acid. 6-MHA: 6-Methylheptanoic acid[1]. L-Dab: 2,4-Diaminobutyric acid. D-Phe: Phenylalanine. L-Thr: Threonine. D-Ser: Serine.

Polymyxin	Fatty acid	X	Y	Z	Reference(s)
A1	6-MOA	D-Leu	L-Thr	D-Dab	[23]
A2	6-MHA	D-Leu	L-Thr	D-Dab	[23]
B1	6-MOA	D-Phe	L-Leu	L-Dab	[24-26]
B2	6-MHA	D-Phe	L-Leu	L-Dab	[24-26]
D1	6-MOA	D-Leu	L-Thr	D-Ser	[23, 26]
D2	6-MHA	D-Leu	L-Thr	D-Ser	[23, 26]
E1	6-MOA	D-Leu	L-Leu	L-Dab	[24-26]
E2	6-MHA	D-Leu	L-Leu	L-Dab	[24-26]
M1[2]	6-MOA	D-Leu	L-Thr	L-Dab	[23]
M2	6-MHA	D-Leu	L-Thr	L-Dab	[23]

2.3 POLYMYXIN E - COLISTIN

Produced by the subspecies of *Bacillus polymyxa*, *var. colistinus*, polymyxin E, also called colistin, is used in nature by gram-positive bacteria to kill off their gram-negative resource competitors. However, in a human setting, the compound is used as an antibacterial, and mildly antifungal [28] drug, specifically to combat gram-negative infections, increasingly more so in recent years [20, 29-31]. Initially discovered in 1949 and put into clinical use shortly after as an antibacterial agent, it showed high promise as an alternative to antibiotics to treat gram-negative bacterial infections [20, 32, 33]. However, following reports of an increased incidence

[1] Also referred to as isooctanoic acid (typically abbreviated IOA) in some literature.
[2] Polymyxin M is also commonly referred to as mattacin [27].

of neuro- and nephrotoxic side effects, clinical usage of colistin was widely discontinued in favor of other, safer drugs shortly after [31, 33, 34].

Colistin has become increasingly relevant (see **Figure 4**) in recent years, as it is among the still-viable candidates of drugs capable of combating the increasingly pressing issue that is antibiotic resistance (see **Figure 4**). Highlighting this, colistin was classified by the WHO as critically important for human medicine in 2012 [35].

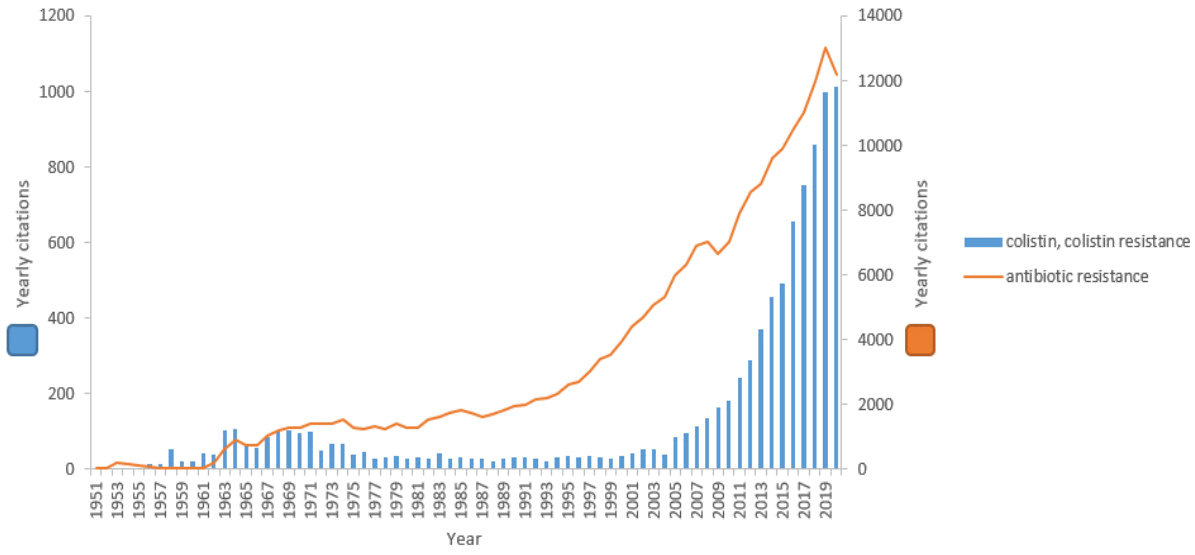

Figure 4 Number of citations found using the phrases 'colistin' and 'colistin resistance' (blue) and 'antibiotic resistance' (orange) in the PubMed database, ranging from 1.1.1951 to 31.12.2020. Data downloaded 6th of June 2021, from PubMed.

Presently, colistin is used mainly as a so-called 'salvage therapy' drug, in which the potential positive results are thought to outweigh the known adverse side effects. Salvage therapy is frequently referred to as 'rescue therapy,' to be applied after all other therapeutic options have failed [36]. Such treatments are typically only used in extreme therapeutic situations or, today, MDR gram-negative bacterial infections such as those of *Pseudomonas aeruginosa* [29, 37-39].

Structurally, colistin shares the same central structure as the other polymyxins (see **Figure 3**). However, it is essential to note that colistin refers not to one singular structure but rather a set of structures. For instance, polymyxin E1 and E2 (often referred to as colistin A & B, respectively) make up the vast majority of a solution of colistin. However, the specific ratios of these molecules vary depending on the supplier [40]. In total, colistin is recognized as a mixture of 12 highly similar compounds, varying only slightly between one another [41]. At physiological pH, colistin has a net charge of +5 due to the presence of five Dab units with

primary amine groups [29]. Colistin is highly soluble in water and near-insoluble in organic solvents [21]. The structure of colistin is shown in **Figure 5**.

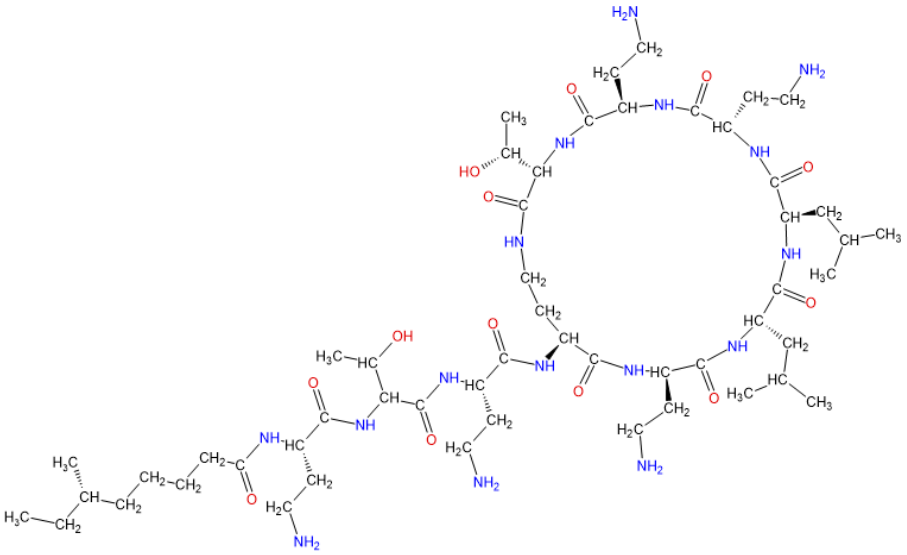

*Figure 5 Structure of colistin A (polymyxin E1), consisting of six Dab residues, a fatty acid (6-methyloctanoic acid, 6-MOA), two leucine residues, and two threonine residues. For CMS, a colistin prodrug, see **Figure 6**.*

As a drug, colistin is available in two forms: colistin sulfate and colistin methanesulfonate sodium (CMS). The latter is a derivatized inactive prodrug of colistin. CMS differs from colistin by possessing methyl sodium sulfate groups attached to the γ-amines by covalent bonds (see **Figure 6**). Recent studies suggest that not all five Dab units repeatably include these groups, however. As such, further research is required to evaluate whatever effects this may have on any therapeutic or chemical properties [42]. CMS is slowly hydrolyzed back into colistin in an aqueous solution by reacting with surrounding water molecules [21, 40, 43-45].

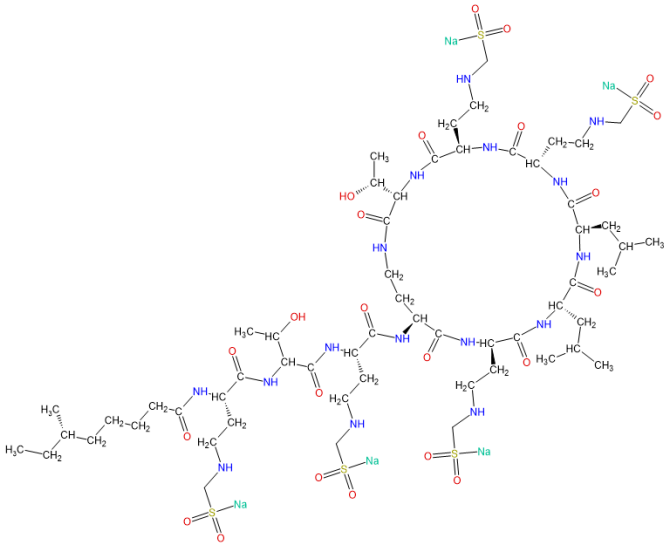

*Figure 6 Illustration of colistin methanesulfonate, which bears five sodium methanesulfonate groups on the γ amine side chains. Structurally, colistin A (polymyxin E1) is identical, except for these methanesulfonate groups. For colistin, see **Figure 5**.*

2.3.1 Present-day lack of international dosing standards

Despite the current therapeutic use of colistin and CMS, proper dose regulations vary from region to region. Lack of international dose regulations and brand specifications in studies examining dose-effect relationships make it difficult to establish collaboratively established ideal dosages, and presently, none exist [46-48]. For instance, in a review by Li et al. from 2006 [49], two CMS formulations; Colomycin (DumexAlpharma A/S) and Colo-Mycin (Parkedale Pharmaceuticals), offered two widely different dosages due to different labels, with the former using international units (IU) and the latter using 'colistin base activity' equivalents, resulting in the latter suggesting almost double the amount of the former [49].

The lack of proper standards is a recurring pattern regarding colistin due to the lack of a single dosage unit. With milligrams, IU, and 'colistin base equivalents,' study findings and their dosage recommendations vary widely. This becomes especially harmful when prescribed dosages only provide insufficient colistin concentrations, encouraging resistance to the last line of defense against gram-negative infections [44]. While the incidence of colistin-resistant bacteria remains relatively low on average, it is a significant and growing concern. Some studies report an incidence of up to 58.2% of clinically isolated bacterial strains proving resistant [50]. Perhaps even more alarmingly are the recent reports of outbreaks of colistin-resistant bacteria, such as *Klebsiella pneumoniae*, with inter-institutional spread [51]. As a result of this development, exotic alternatives to colistin, such as bacteriophages, are already being investigated as possible therapies to be co-administered alongside colistin [52].

Misuse of colistin, especially as an animal feed additive, is a known issue [53]. This was especially observable in China, which drastically contributed to the rise of colistin resistance in more recent years [54]. A study conducted by Liu et al. published in 2015, and picked up by The Lancet in 2016, reported the first instance of horizontal (plasmid-mediated) gene transfer of the first colistin resistance gene, mobilized colistin resistance 1 (MCR-1) during routine surveillance of antimicrobial resistance present in livestock in China [55]. Thankfully, the government was quick to respond in 2016, mandating that the approximate 8000 tons of colistin they used for livestock feed annually must be replaced by other non-human antibacterials [56]. Other countries, such as Thailand, India, Brazil, Malaysia, and Argentina, followed suit shortly after, prohibiting the use of colistin in animal feed [53, 57, 58].

Since 2016, the MCR-1 gene has spread to over thirty countries across five continents (see **Figure 7**) [59, 60], and most likely continued to spread since, with known vectors such as the common housefly and wild gulls enabling spread within and between ecosystems in addition to

livestock and travel based transmission [61, 62]. Other variations of the MCR gene have been discovered [63], and more research is required to assess the status quo regarding the spread and variations of the MCR genes. [16, 40].

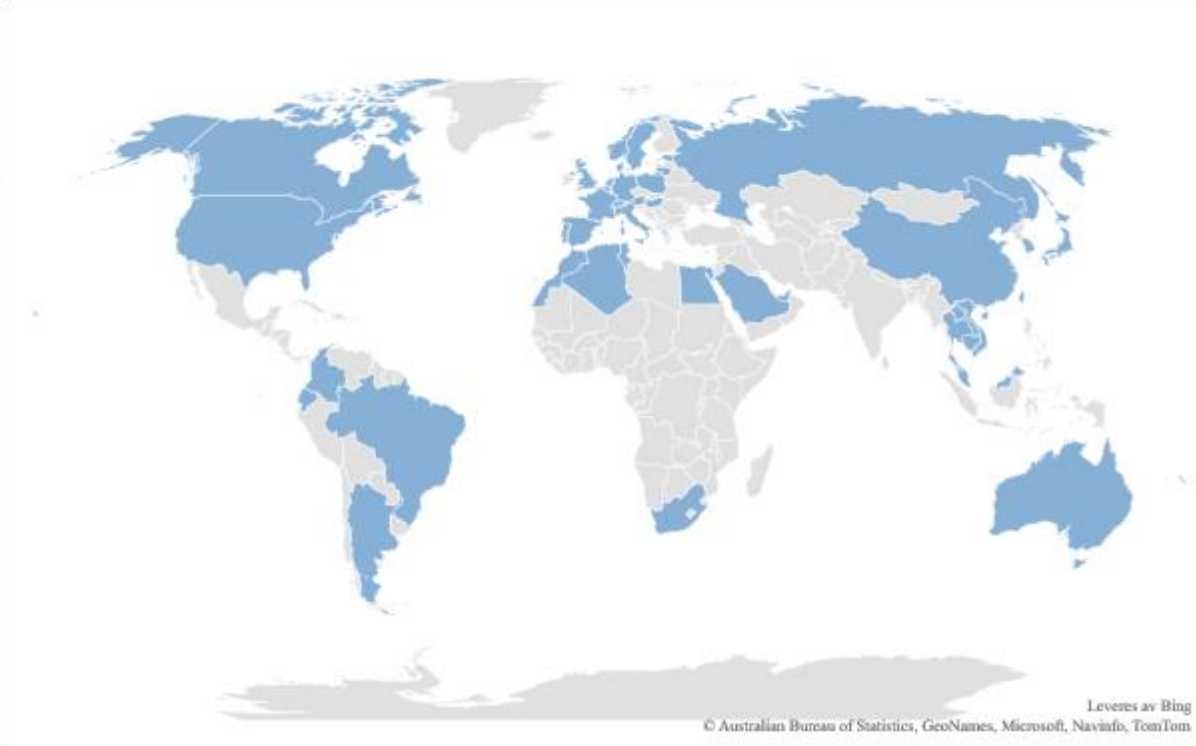

*Figure 7. Global map highlighting countries that have reported instances of the MCR-1 gene. For a complete list of the countries and references used, see **Table 19** in **Appendix F** – Countries that have reported instances of the mobilized colistin resistance 1 gene.*

2.3.2 **Mode of action**

While data on the mode of action of colistin (polymyxin E) remains sparse, the mode of action is thought to be somewhat similar to polymyxin B due to the high degree of structural similarity between the two compounds. As such, there is a consensus that the antibacterial properties displayed by colistin originate from its ability to destabilize the outer membrane of the gram-negative bacteria it preferentially targets, increasing the membrane permeability and eventually causing cell death [17, 32, 50]. Moreover, there is strong evidence that colistin and other AMPs can engage in anti-endotoxin activity through interactions with the LPS of the gram-negative bacteria, significantly reducing the inflammatory immune response [64-67]. However, the clinical significance is yet to be fully understood due to the rapid binding of endotoxin-like LPS to LPS-binding proteins *in vivo* [68, 69].

While still not entirely understood, the mode of action of colistin is thought to follow the so-called *Shai-Matsuzaki-Huang* model (see **Figure 8**) as former theories, such as those suggesting

the mode of actions follows detergent-like activity, have failed to reconcile with experimental data [17, 33]. The *Shai-Matsuzaki-Huang* model currently remains the leading theory as to how colistin acts upon cellular membranes. The model gives a sufficiently believable explanation of why the observed toxic side-effects center only around the nervous and renal system, both being systems fitted with numerous protein pumps specifically designed to draw in organic ionic compounds [70, 71]. Furthermore, this model is compatible with the preferential antibacterial activity colistin exhibits against gram-negative bacterial membranes versus the gram-positive counterparts.

The model itself states that the process in which colistin affects the membrane goes as follows: The polycationic peptide ring of colistin is attracted by the negatively charged headgroups and the LPS on the outer membrane surface. The negatively charged LPS are typically stabilized by calcium and magnesium ions, however, as the polycationic ring has proven to have an affinity for the LPS (at least 10^3 times stronger than Ca^{2+} and Mg^{2+}) they effectively displace these ions, destabilizing the LPS, disrupting and destabilizing the outer membrane [21, 50, 63, 72, 73]. The theory of calcium and magnesium displacement is supported by how the antibacterial activity of colistin readily diminishes with increasing concentrations of these ions [29]. The model is illustrated in **Figure 8**.

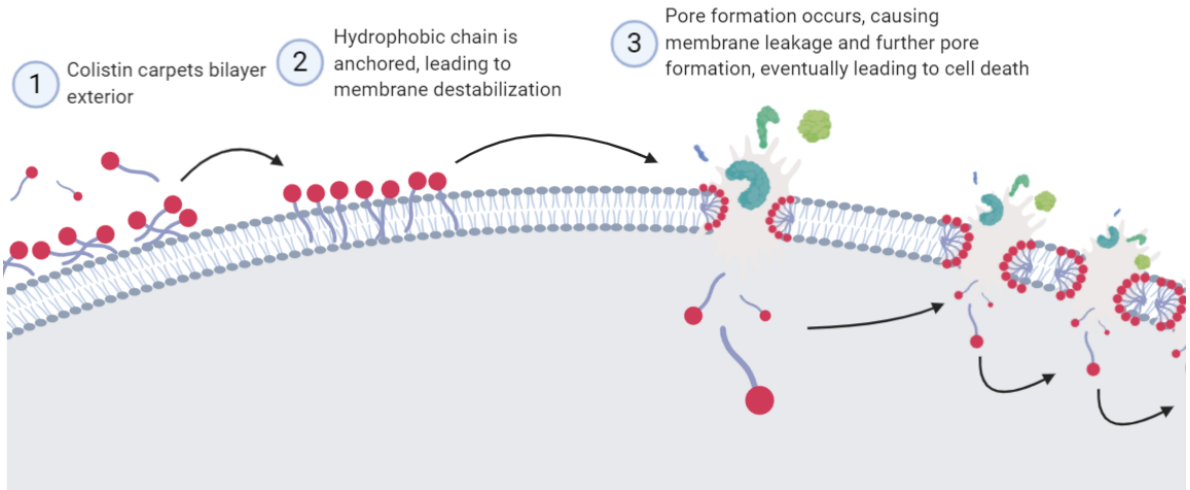

Figure 8 The Shai-Matsuzaki-Huang model of antimicrobial peptide activity against cellular bacterial membranes. (1) Colistin (red head, blue tail) carpets the bilayer exterior. (2) Hydrophobic tail is anchored, leading to membrane destabilization. (3) Transient pore formation occurs, causing leakage and further pore formation by a self-promoted uptake pathway, eventually leading to cell death. Sizes are not correct relative to one another. Adopted from [17], made using Biorender [10].

The *Shai-Matsuzaki-Huang* model is highly compatible with the innate differences between eukaryotic and prokaryotic cell membranes and explains why the compound exhibits minimal effect towards most eukaryotic cells (with the notable exception of those located within the

renal or nervous system). Gram-negative prokaryotic cells generally possess a net negative charge on the exterior of their outer membrane due to the distribution of headgroups within the bilayer (see **Figure 9**). These headgroups can be either cationic, anionic, or zwitterionic [74, 75]. LPS present on the gram-negative prokaryotes are typically also negatively charged, with the opposite being the case for their gram-positive counterparts [76]. The negative charges strongly favor interactions between the highly positively charged colistin, as opposed to positive-positive interactions with the eukaryotic membranes.

Once the electrostatic attraction has brought colistin close to the membrane, the fatty acid chain readily inserts itself into the membrane, anchoring the peptide in place [32]. From here, once a sufficient concentration of colistin is reached and enough peptides become anchored to the membrane, transient pores or even tears are thought to form in the outer membrane. Transient pore formation drastically increases the membrane permeability, enabling the leakage of cell contents, exposes the inner membrane, and allows for the penetration of more colistin peptides, ultimately leading to cell death [17, 33, 72, 77-80]. By definition, colistin is among the class of drugs that follow a self-promoted uptake pathway, in which uptake of the drug encourages further uptake of itself [33, 81, 82]. For this reason, the observed rise in colistin resistance described in section 2.3.1 appears to predominantly originate from modifications made to the outer membrane of these gram-negative bacteria [21, 63, 80, 83].

As previously described, another significant difference between prokaryotic and eukaryotic membranes is the presence of cholesterol (see **Figure 9**). While serving as both lubricant and softener in the eukaryotic membrane, cholesterol remains absent in prokaryotic membranes (with the notable exception of those able to obtain it from their environment [84]). Due to the stabilizing effects of colistin, a partial negation of the effects colistin exerts on cellular membranes is exerted, further reducing its ability to affect eukaryotic cells [33].

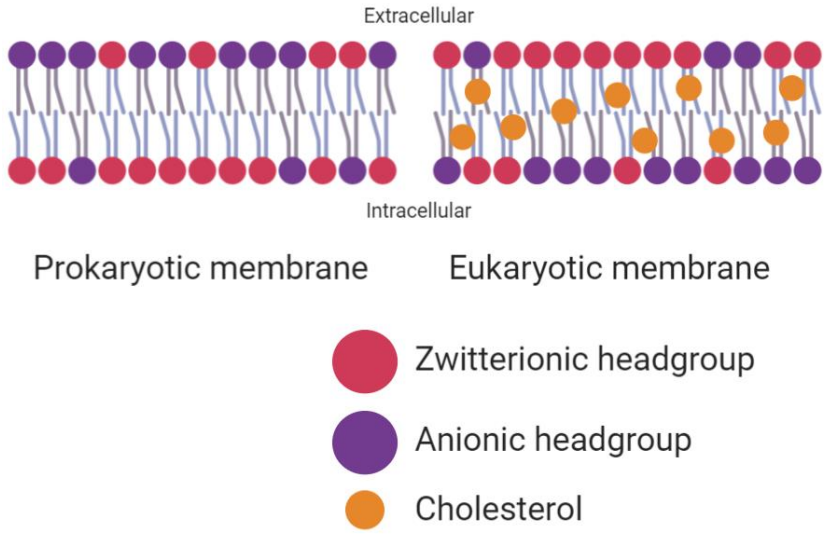

Figure 9 Differences in the distribution of anionic and zwitterionic headgroups present in the outermost membrane in prokaryotes and eukaryotes. Prokaryotes have a net negative charge on the exterior of the lipid bilayer, whereas eukaryotes have a net negative. Furthermore, cholesterol is absent in the vast majority of bacteria [33]. Made using BioRender [10].

2.3.3 Intracellular effect of colistin in eukaryotic cells

Despite the strong preference colistin exhibits for prokaryotic membranes, interactions between eukaryotic cells and colistin still occur. However, movement across the cellular membrane does not occur through diffusion, readily prevented by the polycationic nature colistin possesses at physiological pH. Because of this, membrane-bound transport proteins remain the strongest suspect to explain the intracellular effects induced by colistin [33]. The mode of action colistin enacts in the intracellular milieu on both neural and renal cells, those observed to be vulnerable to colistin, appears to center around interactions with other organelles containing bilayers. In particular, the mitochondria and endoplasmic reticulum (ER) [33, 85, 86]. Further reading on the toxic side-effects of colistin can be found in **Appendix B** – Colistin toxicity.

2.4 LIPOSOMAL NANOCARRIERS TO REDUCE TOXICITY

Today, most drugs are either delivered in the form of liquid solutions or ingestible tablets and capsules. An increasingly popular option is the formulation of nanoparticles to be used as drug delivery systems. Per definition, a nanoparticle is a particle not exceeding 1 and 100 nm in any dimension. The term is broad and includes everything from colloidal solid gold particles to PEGylated liposomes [87]. These particles have a wide range of applications and numerous advantages. For one, they remain a highly viable option to fight intracellular bacterial infections [88]. Liposomes, spherical liposomes with a lipid bilayer, are of particular interest, as the bilayer membrane allows for a slow leakage of the encapsulated compounds, in stark contrast

to most other methods of drug administration, which frequently produce a so-called ‘burst release.’ A ‘burst release’ occurs when an administered drug obtains a high concentration around the immediate tissue it is administered to, while a significantly lower concentration is present elsewhere in the body, diminishing the therapeutic effect of the drug in question [88] (see **Figure 10**).

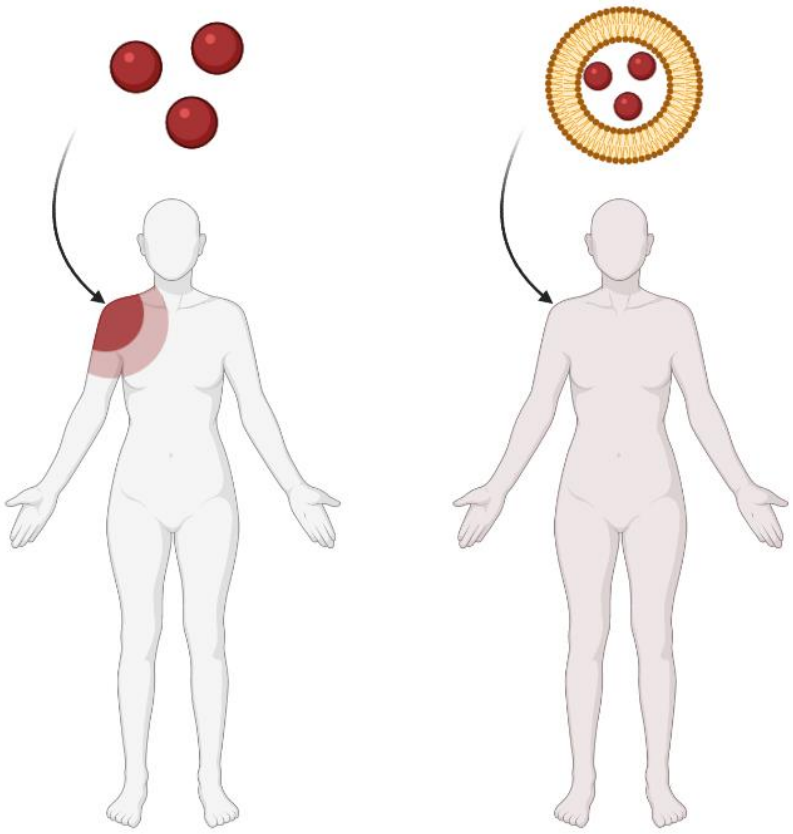

Figure 10 Difference between localized administration (via. injection, in this case, in the upper shoulder) with free and liposomal encased drugs. Note: The figure illustrates only the concept and has been exaggerated for clarity. Once administrated, free drugs (left) rapidly reach a high concentration in a small area before slowly spreading throughout the body, with local tissue near the administration site initially taking a high dose. In contrast, liposomal encased drugs that slowly leak through the membrane (right) release their contents slowly as they circulate the body, avoiding burst release as described in section 2.4. Illustration created using BioRender [10].

These liposomes can also readily be PEGylated, a process in which polyethylene glycol (PEG) is applied to the exterior of the liposome bilayer. PEGylation increases the blood circulation time of the liposome, as the liposome is made more resistant to degradation by the immune system and other forms of biological activity, which may degrade the liposome [87]. For this reason, PEGylated liposomes are also frequently referred to as ‘stealth liposomes’ [89, 90].

2.4.1 Preparation of liposomes

Liposomes in an aquatic solution, loaded with one or more drugs or not, can be prepared by numerous methods. Reversed phase evaporation, the freeze-thaw method, sonication, and the so-called ‘injection technique’ are just a few of these. By subjecting a dispersion of aqueous

phospholipids to sonication, unilamellar (single layer) liposomes of varying sizes form spontaneously in solution. Multilamellar (multi-layered) liposomes form without the sonication merely by adding an aqueous buffer to the dry solution. The creation of large (> 100 nm diameter) liposomes requires the use of the reversed phase evaporation technique (see **Figure 11**), in which an emulsion of aqueous buffer, suspended in a solution of phospholipids, has the organic phase slowly removed by pressure-driven evaporation, creating a suspension of large, unilamellar liposomes [91-94].

However, to obtain liposomes with a relatively narrow size range, extrusion, a form of filtration, is required. In this method, the solution of particles is driven through filters with fixed pore sizes, which filter out and retain particles with a diameter too large to move through the pores. This results in a filtrate containing liposomes with a size distribution below or equal to the diameter of the pores and is necessary to obtain sufficient control over the size distribution of the liposomes created by one of the above methods [95-98] The thin film hydration method is shown in **Figure 11**.

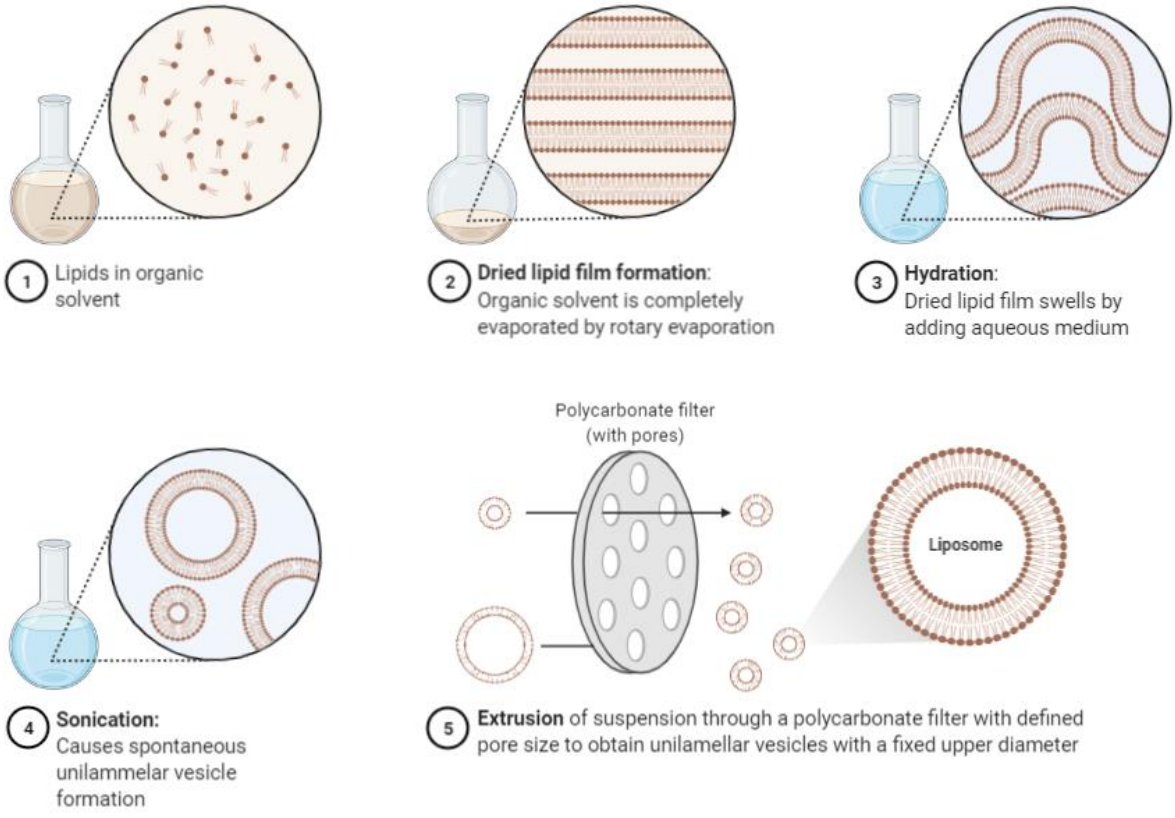

Figure 11 Illustration of the thin film hydration method used to create unilamellar liposomes with a fixed upper diameter. (1) Initially, lipids are weighed out and added to an organic solvent, left to dry. (2) The dried lipid film is left behind, and upon the addition of an aqueous medium (3), the film swells. Upon sonication (4), unilamellar liposomes of varying sizes form spontaneously in solution. These are then extruded (5) to obtain liposomes with an upper size limit. Illustration obtained and modified from BioRender [10]

2.4.2 Trends in the analysis of liposomes

There are numerous ways liposomes, loaded or otherwise, may be analyzed to evaluate their size distribution, content, and kinetics. Often used methods are static and dynamic light scattering [91, 99, 100], atomic force- and cryoelectron microscopy [100-102], as well as other forms of electron microscopy also prove viable to measure liposome sizes. However, these require more elaborate sample preparation, induce distortions in size and shape, are unfit for routine measurements, and are not described further in this thesis [103]. Another method used, called field-flow-fractionation [104-106], separates nano- and microparticles depending on their size and liquid mobility in a column-like environment [107]. This method is somewhat similar to size exclusion chromatography (SEC), another viable method used to assess liposome size distributions [108-110], in which tiny species such as proteins and liposomes are separated based on their size on a temporal level. This method is described in detail in section 2.5.2.2.

2.5 LIQUID CHROMATOGRAPHY

Liquid chromatography, or high-performance liquid chromatography (HPLC), is a method employed for the high-resolution separation of compounds present in a solution. It is common to utilize before detection, as separation before detection typically yields much higher selectivity. The general setup of an HPLC system is shown in **Figure 12**.

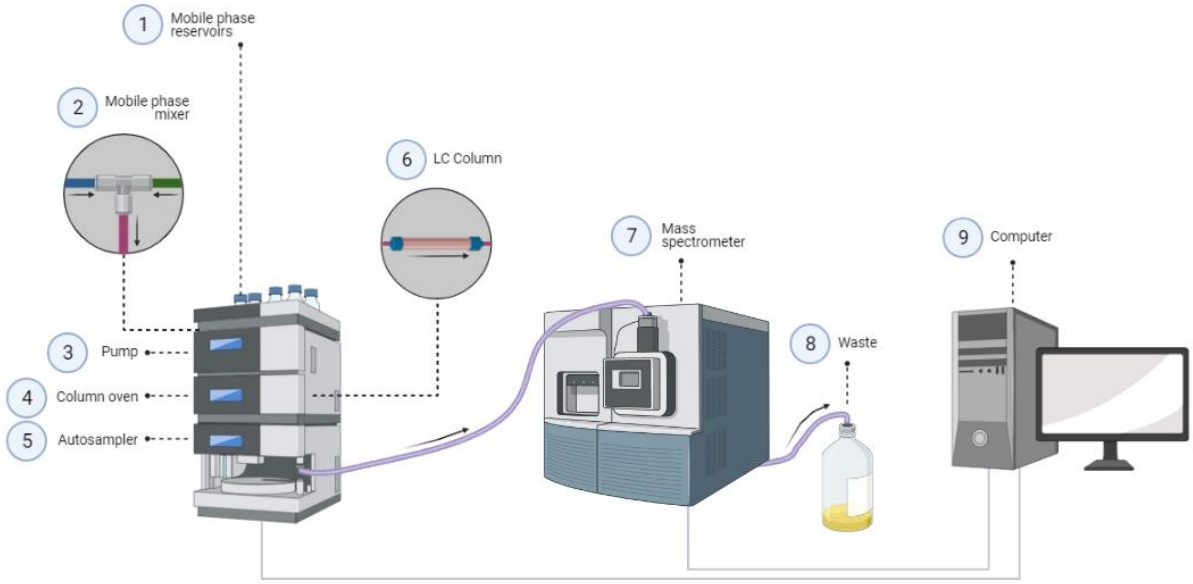

*Figure 12 Typical setup for an HPLC-MS system. Mobile phases (**1**) are kept in separate reservoirs. While the mobile phase may consist only of one solution, gradient elution (programs where the ratios of two solutions change during the separation procedure) is quite common. If more than one mobile phase is used, these must be mixed (**2**) in either a T-port or a mixing unit. A pump (**3**) drives this liquid flow. The moving mobile phase passes through an injection system (**5**) or a six-port valve (not shown), where a sample is injected. It is common to have a pre-column or a filter (not shown) in front of the LC column, often to remove larger particles that are undesired in the column. Once these particles are largely removed, the injected sample and mobile phase pass through the column (**6**), where separation occurs. Typically, this column is kept in a column oven (**4**), where the temperature may be controlled and adjusted as needed. Finally, the ideally separated compounds pass through a detector (7), either a non-destructive type (like the UV detector) or a destructive type (like a mass spectrometer, as shown). Waste is collected in a separate reservoir (8). The entire system is controlled by a computer or other control unit (**9**), where data is typically also stored and processed. Illustration made using BioRender [10].*

2.5.1 Columns

Analytical liquid chromatography (LC) columns chiefly come in three forms. Packed, monolithic, and open tubular, which vary in structure and stationary phase binding/distribution (see **Figure 13**). Packed columns are by far the most common in LC, in which the stationary phase is bonded to solid particles, most often wholly porous silica. These particles are held in place by filters at either end. The particles vary in size, nowadays typically from 3.5 µm to 1.7 µm [111]. Smaller particles yield better efficiency than larger particles; however, this comes with the cost of additional backpressure, which can be a limiting factor in a given analysis.

Smaller particles around 1-2.5 µm can be used in a high-pressure subcategory of HPLC, known as ultra-high performance/pressure liquid chromatography (UHPLC). The pressure may reach

several thousand bars depending on the conditions, but a pressure above approximately 600 bar is expected [112] (see section 9.3.1.2).

In a monolithic column, the inner volume is filled with a single structure, filling up the entirety of the column. This structure has a sponge-like structure, with numerous pores of varying sizes provide a large surface [111, 113, 114]. Finally, open tubular (OT) columns have their stationary phase bonded to the inner column wall. OT columns provide very low backpressure at the cost of surface area. For these columns to be comparably efficient, an inner diameter (ID) of approximately 5-20 µm is required [115].

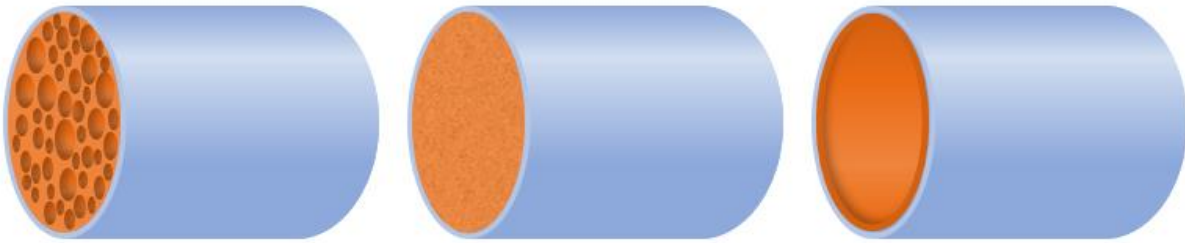

Figure 13. Concept difference between monolithic columns (left), packed columns (center), and open tubular columns (right).

2.5.2 Stationary phases & chromatographic principles of separation

There are several principles utilized for the separation of analyte molecules in LC. These all utilize different aspects, but they all take advantage of the different physicochemical properties of the analyte molecules. In the following subchapters, a short description of the most used ones is described.

Normal phase chromatography (NPC) and hydrophilic interaction liquid chromatography (HILIC) are two examples of less common chromatographic principles. In NPC, a polar stationary phase is used with a mostly nonpolar mobile phase, and compounds are separated based on their hydrophilicity [116-118]. HILIC is often referred to as a subcategory of NPC. In HILIC, the stationary phase is a thin film of water covering the particles held by weak intermolecular bonds. Separation is driven by differences in polarity, with retardation increasing with polarity [117-120].

2.5.2.1 Reversed phase

In reversed phase liquid chromatography (RPLC), the stationary phase is hydrophobic, while the mobile phase hydrophilic, and the analyte molecules at least partially hydrophobic. These columns separate compounds based on their interactions with the hydrophobic stationary phase,

often an alkyl chain. These chains can range from C2 (ethyl) upwards to C32 and above. The length used depends on the degree of retention desired; a longer (more hydrophobic) chain will have increased retention for hydrophobic analytes and vice versa. Typically, fused, porous silica particles are used, where the stationary phase is chemically bonded to the surface of these. [117-119].

2.5.2.2 Size exclusion

Size exclusion chromatography (SEC) is a principle primarily used to determine the molecular size of larger polymers. In SEC, the column is filled with porous particles. The pores have a fixed size, and since larger particles and molecules will not enter these, they are separated from their smaller molecules, which have a chance of moving into the pores and the small cavities within. A stationary phase is not defined for SEC, as the primary principle of separation is by size.

Because of the nature of SEC, it is particularly good at separating free and liposomally encapsulated compounds.[108, 116-118, 121], as described in section 2.4.2. However, a problem with using a SEC column for the separation of liposomes from free particles is the loss of nanoparticles that readily adhere to the column surface [92, 108, 109]. To prevent nanoparticle loss, pre-saturation of sonicated (perturbed) liposomes is required to allow non-liposomal lipids to enter the narrow pores (if their size allows) and saturate the polymeric coating inside the particulate pores [92, 108, 109].

Furthermore, the mobile phase needs to be relatively isosmotic to prevent osmotic shock of the liposomes. For this reason, the mobile phase should be as identical to the buffer solution within the liposomes as possible. When using organic polymer-based SEC particles, the pressure should be minimized to avoid compression or deformation of the beads in the column, as polymer-based particles do poorly under high pressure. However, high-performance SEC (HPSEC) may prove more suitable for studies concerning the release kinetics of liposomes. HPSEC typically offers faster run times, better reproducibility, and a higher peak resolution than traditional SEC, at the potential expense of column lifetime [108].

2.5.3 Trends in the analysis of colistin

Studies on developing LC-based methods for measuring colistin in aqueous media remain numerous. This is best highlighted in a recent review article by Zabidi et al. [122], which looked at 26 articles describing LC-based analytical methods for the measurement of colistin (from biological samples). For most of these, as they were designed for biological samples, sample-cleanup was performed using protein precipitation or solid phase extraction (SPE). Generally, polymyxin B1 was used as an internal standard, although others have also been used[3]. The detection methods used in these articles were either fluorescence- (9/21) and mass-spectrometry (MS) (12/21) based. For fluorescence-based detection, derivation was required and performed using fluorenylmethyloxycarbonyl chloride (FMOC-Cl) or dansyl chloride. For mass spectrometry-based detection (the basis of which is explained further in the next section), positive-mode electrospray ionization (ESI) was favored. [122]. Some published methods for measuring colistin can be seen in **Table 2**.

[3] Other internal standards used include netilmicin sulfate, reserpine, fibrinopeptide B and amphetamine [122]

Table 2 Some reported methods from literature, on the measurement of colistin or a colistin subvariant (such as polymyxin E1, E2, etc.). Column dimensions, means of detection, and the standard solution matrix are included. For studies using MS-based detection, polarity is written in parentheses. Means of elution, run time, and the method limit of quantification (LOQ) are listed for studies where this is specified. Methods using fluorescence-based methods were omitted from this table, as this required chemical modification of the analyte (colistin). ACN: Acetonitrile. MeOH: Methanol. FA: Formic acid.

Column (ID x length, particle size)	Standard solution matrix	Detection	Elution	Total run time (minutes)	LOQ (µg/mL)	Ref.
Poroshell 120 SB-C18 (4.6 x 150 mm, 2.7 µm)	0.1 % FA 20% MeOH (v/v %)	ESI-MS (+)	Gradient	20	-	[123]
Synergi Fusion-RP (200 x 2 mM, 2 µm)	Plasma/urine	ESI-MS (+)	Isocratic	-	0.028	[124]
Phenomenex Luna C18 (2.1 x 150 mm, 5 µm)	-	ESI-MS (+)	Gradient	15	-	[125]
Ultrasphere C18 (250 x 4.6 mm, 5 µm)	Plasma	ESI-MS (+)	Isocratic	10	0.194	[126]
Acquity BEH C18 (2.1 x 50 mm, 1.7 µm)	-	ESI-MS (+)	Gradient	5.5	-	[127]
MC C8 (50 x 4.0 mm, 3 µm)	20% MeOH	ESI-MS (+)	Isocratic	2	0.027	[128]
MassTox[4]	Plasma	ESI-MS (+)	Gradient	3.5	0.1	[129]
C18 Xbridge (150 x 2.1 mm, 5 µm)	-	ESI-MS (+)	Isocratic	3.8	0.024	[130]
Symmetry C18 (150 x 4.6 mm, 5 µm)	-	ESI-MS (+)	Gradient	15	0.014	[131]
Acquity BEH C18 (100 x 2.1 mm, 1.7 µm)	0.2 % FA 10% ACN	ESI-MS (+)	Gradient	5	-	[132]
Kinetex C18 (50 x 2.1 mm, 2.6 µm)	-	ESI-MS (+)	Isocratic	10	0.13	[133]
C8 BEH (100 x 2.1 mm, 1.7 µm)	Plasma	ESI-MS (-)	Gradient	4.5	0.05	[134]

2.6 MASS SPECTROMETRY

Mass spectrometry is an analytical technique that functions by measuring the mass-to-charge (*m/z*) ratio of the different molecules in a sample. It is generally used for highly accurate measurements, usually providing a low limit of detection (LOD) and high selectivity, both quantitative and qualitative.

The general setup of a mass spectrometer remains relatively simple (see **Figure 14**). Highly simplified, a mass spectrometer (MS) consists of four main parts. The ion source at the front is responsible for converting the neutral analyte molecules into a stream of either positive or

[4] Further information could not be located in the article referenced.

negatively charged ions. These ions may be polycationic/polyanionic or possess a single charge, positive or negative [135, 136].

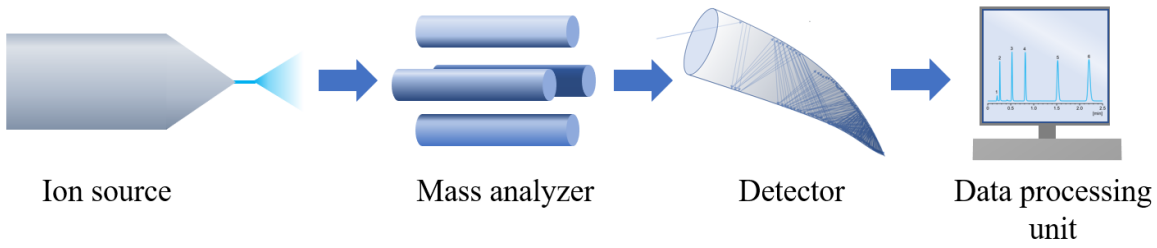

Figure 14. Principle sketch of a typical mass spectrometer. The ion source converts the compounds in a sample (either from an inlet or a plate introduced before analysis). The mass analyzer separates, stabilizes, and destabilizes ions of various m/z values, enabling the filtering of selected m/z-ranges or values, leading to an ion guide/collision cell, possibly another mass analyzer. Both the detector and the mass analyzer are maintained in a high vacuum. The detector measures the unfiltered (remaining) ions from the mass analyzer, and through the use of a dynode, produces an electric signal corresponding to the ion stream. Finally, the data processing unit interprets and illustrates the incoming data from the detector. Chromatogram presented in the 'Data processing unit' has creative commons license but was not modified.

Pre-separation of the sample on a gas chromatography (GC) or an LC-system is common for analyzing samples by mass spectrometry because separating the compounds present allows for a much higher selectivity and sensitivity. Furthermore, this typically vastly reduces ion suppression/enhancement instead of injecting the whole sample at once into an MS instrument. Pre-separation of sample constituents significantly reduces interferences of non-analyte-compounds with an identical *m/z*-value. Furthermore, pre-separation of analytes allows for a much more accurate determination of multiple analytes (with different retention times) since the dwell time of the mass analyzer (the amount of time the MS measures a certain *m/z*-value) can be increased, raising the measurable signal response from the detector.

2.6.1 Electrospray ionization

Electrospray ionization is one of many ionization methods used in mass spectrometry when a liquid sample is introduced (see **Figure 15**). The interface providing ionization consists of a nebulizer and an initial skimmer. In positive (ionization) mode, the capillary nebulizer voltage is typically maintained at 3.5 kV, while the skimmer plate voltage is typically maintained at 0 V (this varies from instrument to instrument, however). An aqueous solution is ejected from the nebulizer to create a localized aerosol, typically already containing (aqueous) ions. The electric field produced by the voltage difference pulls the ion-containing liquid as a stream towards the skimmer. After a certain distance, however, this stream becomes unstable and forms a stable plume (see (2) in **Figure 15**). Droplets containing more than one ion are exposed to a drying gas (typically N_2 or Ar) and shrink as the solvent evaporates. At a certain threshold, the charged ions get too close to one another, favoring separation of the droplet, typically through

a Coulomb explosion, in which droplets of around 1 µm explode due to internal repulsion into numerous smaller droplets. This process is repeated multiple times before the droplets are too tiny, and the solvent readily evaporates, leaving free ions ready to enter the mass analyzer [117, 137-140].

ESI is commonly referred to as a ‘soft’ ionization technique. It ionizes molecules largely without affecting covalent bonds, effectively leading to little fragmentation, mainly retaining the non-fragmented molecular ions [137, 141]. In ESI, ions are typically pre-formed in the solution, but some can be formed by redox reactions in the capillary nebulizer [142-144] or proton transfer reactions in the gaseous phase [145]. Increasing the number of analytes by these redox reactions increases the overall number of ions, encouraging coulomb explosions and free ion generation. However, pre-formed ions are mainly formed by the regulation of pH of the mobile phase solution. For basic compounds, a low pH is preferable to encourage protonation and ionization of the target compounds. The opposite remains true for acidic compounds [117].

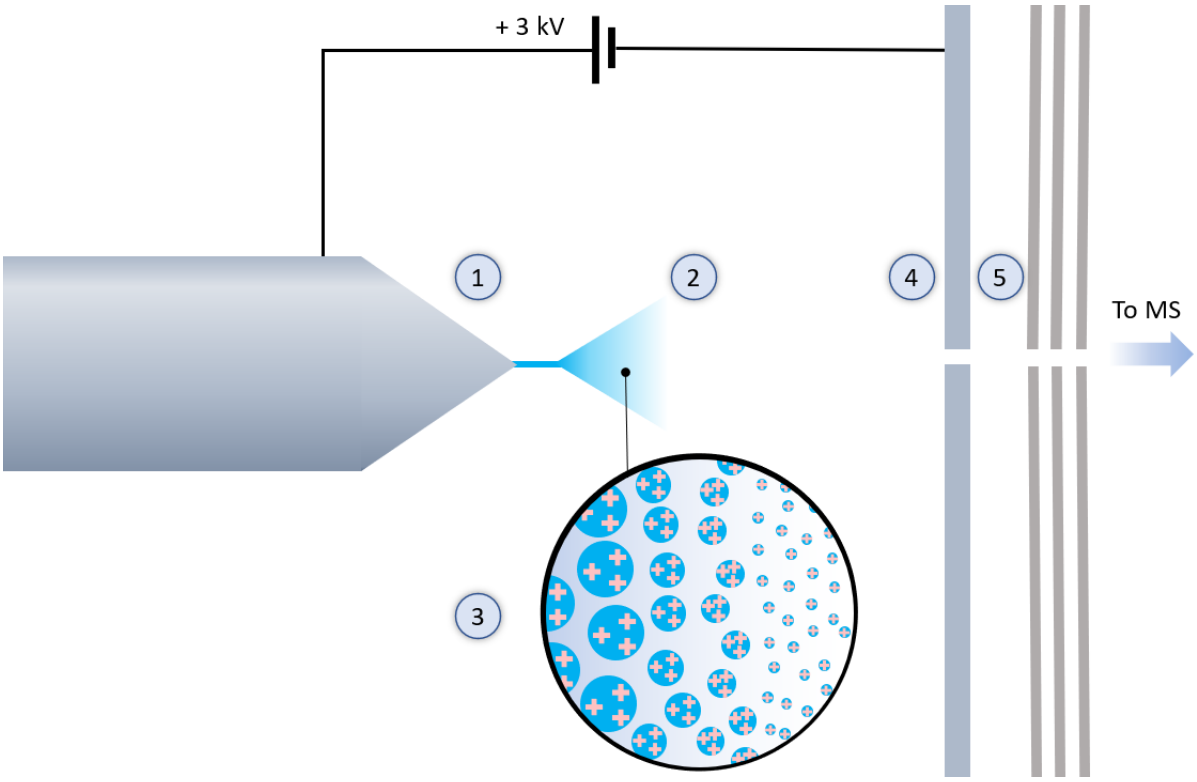

Figure 15 Principle illustration of electrospray ionization (ESI). (1) Liquid sample is ejected through a thin needle that is approximately 1-10µm wide, depending on instrument specifics [146]. A voltage is applied on the needle, opposite to that of the electrode plates on the other side (see (4)). (2) After a specific range, however, the liquid stream becomes unstable, and it becomes a stable plume (aerosol spray) of charged droplets. (3) Suspended in a heated gas, these droplets promptly shrink as their material begins to evaporate. However, the ions remain, and the charge-to-volume ratio reaches a threshold where the droplets undergo a Coulomb explosion [147], in which the droplets collapse, and free ions are formed. (4) The electrostatic attraction pulls the ions towards a narrow entrance hole to the MS, leading to subsequent skimmers (5) preceding the mass analyzer (to remove neutral molecules) and finally leading to the mass analyzer (MS) itself. Illustration made in PowerPoint.

2.6.2 Quadrupole mass analyzers

The (transmission) quadrupole mass analyzer is a highly common mass analyzer used in mass spectrometry. Low cost, easy maintenance, and a lower lab space requirement than that of time of flight (TOF) or orbitrap mass spectrometers make quadrupole mass analyzers an attractive choice [117]. Quadrupole mass analyzers consist of four opposing metal rods, with each pair having a voltage opposite of the other (see **Figure 16**). A constant voltage and a radio frequency (RF)-oscillating voltage is applied to each. By rapidly alternating the positive and negative voltages, complex ion trajectories are stabilized in a cylindrical spiral orbit. By varying the voltages applied, ions of different *m/z* values have their orbits stabilized or destabilized, enabling the filtering and selection of *m/z*-ranges or values. Generally, a higher voltage will cause ions of a low mass to deflect strongly by the electric field, throwing them out of the quadrupole or making them hit one of the rods. When a low voltage is applied, heavier ions are not sufficiently deflected and are either ejected out between the quadrupole rods or collide with

them. In this way, by varying the constant and RF voltage applied, ions of different *m/z*-values can be selectively allowed to pass through the quadrupole [137].

These quadrupoles may also be attached in a series, typically three, referred to as a 'triple quadrupole,' which allows for MS/MS analysis of ions. In this setting, the first and the final quadrupole function as mass analyzers, whereas the centermost quadrupole functions as a collision cell. Unlike in the other quadrupoles, there is no high vacuum in the collision cell. Instead, a collision gas is introduced, which encourages fragmentation of the ions allowed to pass through the first quadrupole. The energy applied to the transitions molecules undergo here is called the collision energy (CE). By identifying product fragment ions specific to the analyte in question, the final quadrupole may then be adjusted to only permit transferal of these very ions, enabling a very high selectivity [117, 137].

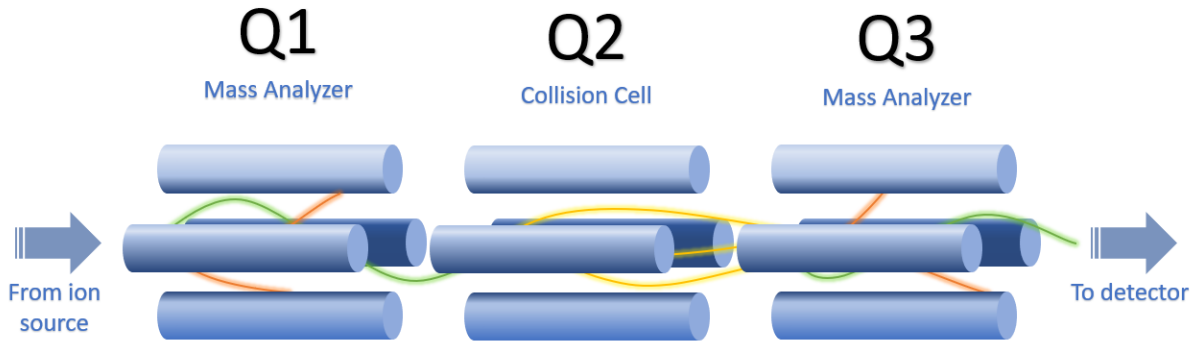

Figure 16. ***Sketch of a triple quadrupole mass analyzer****. A single quadrupole (shown: three) consists of four rods connected in opposing pairs so that two opposing rods produce an identical electrical field. The polarity of these fields is rapidly swapped back and forth at adjustable frequencies. By alternating the field strength and frequencies, only the orbits of ions with specific m/z values are given stable trajectories. The first and third quadrupoles are used as mass analyzers, allowing only selected m/z values to pass through (green). Orbits of ions with different m/z values are unstable, and these ions promptly collide with one of the four quadrupole rods (orange). The second quadrupole functions as an ion guide and collision cell, allowing all m/z values to pass through. However, in doing so, they collide with a collision gas and subsequently shatter into fragments to be analyzed (yellow). The final mass filtering is performed in the third quadrupole, where only fragments of a selected m/z value are allowed to continue to the detector.*

Quadrupole mass spectrometers typically operate in selected- or multiple reaction monitoring (SRM / MRM) mode. In these modes, one (SRM) or more (MRM) transitions from parent molecule to fragment ion are exclusively permitted and measured [148-150]. This allows for multiple transitions to be observed for each molecule. Typically, two transitions are used for each compound, a quantifier transition, whose signal is used to quantify detected amounts, and qualifier transitions. Qualifier transitions are used to verify that the quantifier signal is from the analyte in question and not from another, co-eluting compound that shares the quantifier transition, vastly improving selectivity. New method development typically starts with a full scan mode. All *m/z* values are permitted through a full scan, providing highly qualitative data

and poor sensitivity for quantitative work [149, 150]. Following the full scan mode, one or more parent ions are selected, and a product ion scan is conducted, where all fragments from the parent ion(s) are recorded [148]. One or more of these are selected, producing an SRM/MRM method. Finally, selected ion monitoring (SIM) involves no fragmentation. However, it provides high sensitivity as one or more unfragmented molecules are measured by themselves, drastically increasing sensitivity at the expense of qualitative data [151]. Using SIM also comes at the cost of data reliability, as other compounds may share a near-identical *m/z* value. For a visual illustration of these modes, see **Figure 17**.

2.6.3 Resolution in mass spectroscopy

In mass spectrometry, the mass resolution is defined as the minimum mass difference between two mass spectral peaks, m_1 and m_2 so that the valley between their sum is equal to a specific ratio of the smaller peak, typically 50% [152]. However, in mass spectrometry, mass resolving power is more frequently used to describe the resolution, which is determined by Formula 1:

$$Mass\ resolving\ power = \frac{m_2}{m_2 - m_1}$$

Formula 1 Mass resolving power in mass spectrometry, where m_2 is the higher mass between m_1 and m_2.

This approach is more intuitive and shows more readily why a higher mass resolving power is required to resolve ions with a higher mass. If the difference between m_1 and m_2 are kept constant, but the masses of both ions increase, so must the mass resolving power increase for the equation to hold [152].

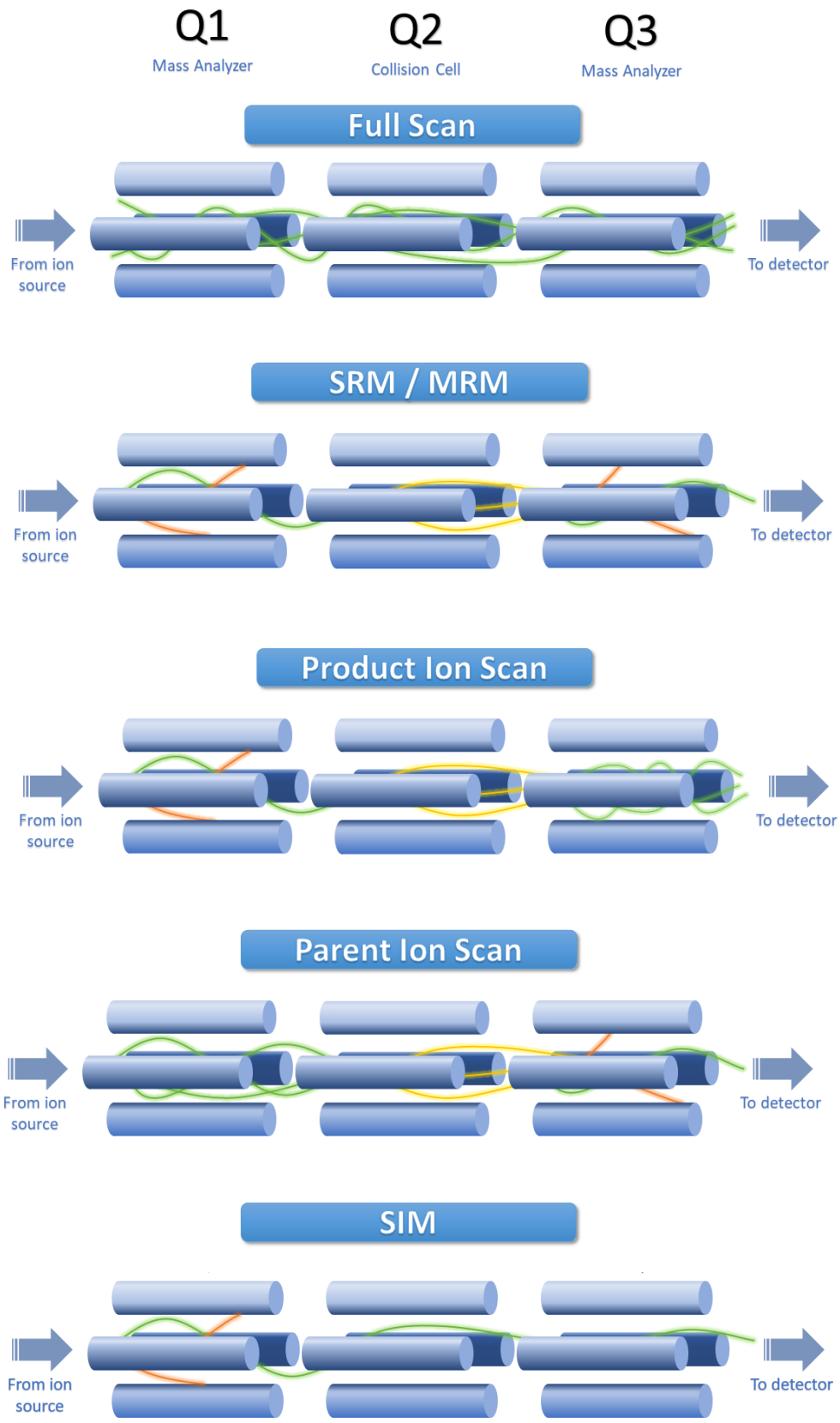

Figure 17. Illustration of four common modes used with quadrupoles. Q1-Q3 represent the three quadrupoles, in order. In a Full scan, all masses are allowed through Q1 and Q2, and a scan is conducted in Q3 so each can be quantified. In SRM, A single reaction is monitored, using a selected parent molecule, and measuring a selected fragment ion filtered in Q3. In MRM, multiple SRM reactions are monitored in tandem. A product ion scan scans all fragments in Q3 generated from a specific m/z value. In parent ion scan, a selected m/z value is permitted through Q3, and parent ions that produce this product ion are scanned. In SIM, a single m/z value is observed, and no fragmentation is performed in Q2.

3 AIM OF STUDY

This work aimed to develop an analytical LC method suitable for measuring aqueous colistin in solution, both free and liposomally encapsulated, with an end goal of assessing how viable liposomes are as colistin drug carriers. Furthermore, the suitability of various detectors for measuring colistin, and an internal standard, polymyxin B1, is to be evaluated. Colistin-liposome mechanics (adsorption and leakage) were to be examined through liposome release studies over time, with the ultimate goal of reducing the toxic side-effects colistin exerts upon human bodies, to brace and postpone the upcoming era of broad antibiotic resistance in gram-negative bacteria.

4 EXPERIMENTAL

4.1 CONSUMABLES

Nonbleeding Fisherband pH indicator strips were purchased from Thermo Fisher Scientific (Oslo, Norway). F1 Finnpipettes with delivery volume ranges of 100-100 µL, 20-200 µL, and 5-40 µL from Thermo Scientific were used. 1000 µL and 200 µL pipette tips were purchased from Sarstedt (Oslo, Norway).

4.2 CHEMICALS

4.2.1 For the analytical work

Polymyxin B1 sulfate (10 mg, 95.2% purity) and polymyxin E1 sulfate (10 mg, 96.1% purity) were purchased from TOKU-E (Gent, Belgium). LC-MS grade water, LC grade ACN, and formic acid (99%, LC-MS grade) were purchased from VWR (Oslo, Norway). Type 1 water was obtained from a Milli-Q® integral water purification system from Merck Millipore (Billerica, MA, USA). Ammonium formate (99.995% purity, Sigma-Aldrich) was purchased from Merck Life Science AS (Oslo, Norway).

4.2.2 For the creation of the liposomes

1,2-Dimyristoyl-sn-glycero-3-phosphocoline (DMPC) (Avanti Polar Lipids Inc. Alabaster, AL, USA), and 1,2-dimyristoyl-sn-glycero-3-phosphoethanolamine-N-[methoxy(polyethylene glycol)-2000] (DMPC-PEG) were purchased from Avanti Polar Lipids Inc. (Alabaster, AL, USA).

4.3 SAMPLES

Solutions of liposomes consisting of 97.5% 1,2-dimyristoyl-sn-glycero-3-phosphocholine (DMPC) and 2.5% 1,2-distearoyl-sn-Glycero-3-Phosphoethanolamine-PEG (DSPE-PEG) (n/n %) were premade in aqueous solutions containing a phosphate-buffered saline (PBS) buffer at pH 7.4 (50mM) or a tris buffer (tris(hydroxymethyl)aminomethane) at pH 7.2 (50mM), prepared and supplied by master student Marlene Andersen Nahm (Bio3 – Chemical life sciences, Department of Chemistry, University of Oslo, Norway). These were prepared by sonicating a Tris-buffered, aqueous solution (pH 7.2) extruded an odd number of times

(minimum of 21). Liposomes were prepared using the thin-film hydration method, described in section 2.4.1. Details can be found in **Appendix G** – Liposome preparation method.

In the first liposome release study, liposomes were loaded with a solution of polymyxin E1 at a concentration of approximately 1.8 mg/mL, and samples were obtained (via. dialysis) 1.5, 4, 24, and 96-hours post-liposome preparation, in which the liposomes had been removed from the solution to be analyzed. The delivered sample volume was low (apx. 200µL for each sample). These were prepared by Marlene Andersen Nahm (from the group for Bio-inspired materials at the University of Oslo) and delivered ready for analysis.

In the second liposome release study, liposomes loaded with polymyxin E1 were left idle for varying amounts of time (from 0 to 72 hours), and the liposomes were removed through dialysis. The remaining solution was then used to determine the amount of polymyxin E1 that had leaked from these liposomes. These were pre-prepared by Cheng Cao (Bio3 – Chemical life sciences, Department of Chemistry, University of Oslo, Norway) and delivered ready for analysis.

4.4 SOLUTIONS – METHOD A

4.4.1 Stock solutions

Stock solutions of polymyxin B1 sulfate and polymyxin E1 sulfate were prepared in the same manner, using the following procedure for both substances: The compound was dissolved in a total of 10 mL of LC-MS-grade water to produce a 1 mg/mL solution. Following thorough homogenization for 1 minute, by 3000 rpm on an IKA Topolino Minishaker (Fischer Scientific (Leicestershire, England)), aliquots of 1 mL were transferred to Low-bind PCR Eppendorf tubes, purchased from SARSTEDT (Nümbrecht, Germany). Aliquots not expected to be used within a month were stored at -80 ºC (MyBio, DAIREI (Kuala Lumpur, Malaysia)). Aliquots were only thawed once. Aliquots for daily usage were stored at 4 ºC (for up to 1 month), see **Figure 18**.

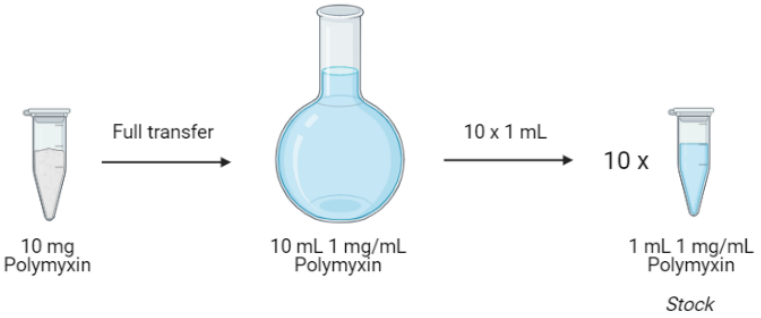

Figure 18 Illustration of how the stock solutions of both polymyxins were prepared.

4.4.2 Working solutions

Working solutions of 10 µg/mL were made by transferring 100 µL of the above stock solutions of polymyxin E1 and B1 (1 mg/mL) into separate 10 mL volumetric flasks. LC-MS-grade water was added to the 10 mL mark, followed by homogenization. Working solutions were homogenized on the IKA Topolino Minishaker for 1 minute before being transferred into amber vials. From these working solutions, standard solutions were prepared (see **Figure 19**). Solutions for quantitative use (i.e., standard solutions) were used within 24h of preparation, whereas for qualitative use, these were stored for up to three days.

4.4.3 Standard solutions

Standard solutions were prepared in 5 mL flasks. These were prepared from the working solution described in section 4.4.2. Standard solutions were prepared and used the same day (see **Figure 19**).

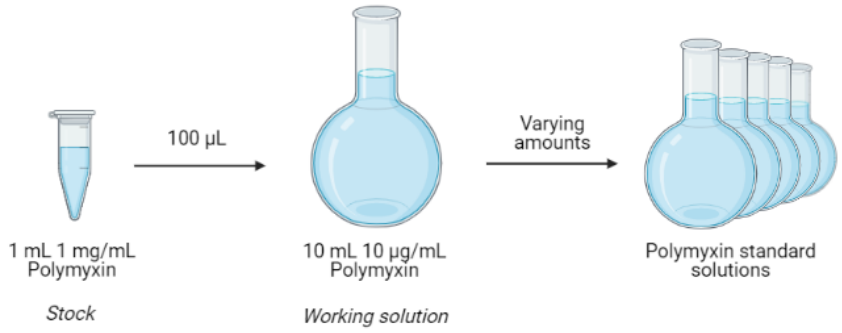

Figure 19 Illustration of how the working solutions and standard solutions of polymyxins were prepared.

4.4.4 Mass spectrometry method optimization solutions

The method was optimized manually by continuous, direct injection of a 10 µg/mL solution of either polymyxin (one at a time), dissolved in 50/50 water/methanol (v/v %) to ensure a stable spray. These solutions consisted of either polymyxin dissolved in LC-MS grade water.

4.5 SOLUTIONS – METHOD B

4.5.1 Buffer solutions

100 mM ammonium formate buffer was produced by dissolving 0.631 g ammonium formate salt in 100 mL type 1 water. The pH was then adjusted to approximately 3-4 using formic acid. The approximate pH was determined using the pH strips described in section 4.1.

Other buffered solutions used (Tris (50mM, pH 7.2), citric acid/phosphate (50mM, pH 5.5) and PBS (50mM, pH 7.4)) were delivered pre-prepared by master student Lelaw Jalal Ali (Bio3 – Chemical life sciences, Department of Chemistry, University of Oslo, Norway).

4.5.2 Working solutions

Working solutions produced using method B were produced identically to those in method A (described

in section 4.4.2), with the exception of the diluent; in method B, the diluent used was a 100 mM ammonium formate buffer (described in section 4.5.1). From these working solutions, standard solutions were prepared. Solutions for quantitative use (i.e., calibration solutions) were used within 24h of preparation, whereas for qualitative use, these were stored for up to three days (see **Figure 19**).

4.5.3 Standard solutions

Standard solutions produced using method B were produced identically to those in method A (described in section 4.4.3), with the exception of the diluent, being a 100 mM ammonium formate buffer solution (described in section 4.5.1). Standard solutions were prepared and used on the same day.

4.5.4 The first adsorption/degradation study

In the first adsorption/degradation study, three modifications were performed. Ammonium formate (10 mM) was added to all solutions. The pH was adjusted using formic acid until the pH was approximately 3-4. Polymyxin B1 concentrations were kept approximately five times as high as the highest concentration in the standards. 50µL 1 mg/mL polymyxin B1 was added before the addition of the buffer described above. 20 mM ascorbic acid was also used and was prepared by weighing out 0.141 g ascorbic acid and transferring it into 40 mL of the 10 mM buffer solution described above. Control solutions were prepared similarly, with pure type 1 water as the diluent. The final volume for all solutions was 1 mL. These four sets of standard solutions were then repeatedly measured while stored in an autosampler holding 4 ºC and

analyzed at 4h intervals, for a total of eight times (28 h). A summary of the four sample sets prepared can be seen in **Table 3**.

Table 3 Contents of the four sets compared in the first adsorption/degradation study.

Set	10 mM ammonium formate buffer (pH 3-4)?	Ascorbic acid?	Polymyxin B1?
Control	-	-	-
Buffer only	Yes	-	-
Buffer + Ascorbic acid	Yes	Yes	-
Buffer + Polymyxin B1	Yes	-	Yes

4.5.5 The second adsorption/degradation study

In the second adsorption/degradation study, a 100 mM ammonium formate buffer (pH 4) solution was used in one set, the preparation of which is described in section 4.5.1. A second set containing 10% ACN had polymyxin E1 added first, followed by water and ACN at the end. Finally, the control set consisted of polymyxin E1 dissolved in pure type 1 water. A summary of the three sets prepared can be seen in **Table 4**.

Table 4 Contents of the four sets compared in the second adsorption/degradation study.

Set	100 mM ammonium formate buffer (pH 3-4)?	10% ACN
Control	-	-
Buffer only	Yes	-
Buffer + ACN	Yes	Yes

4.5.6 Validation solutions

For the method validation described in section 5.3, four concentration levels were used to assess the precision, retention times, and carry-over. The lower limit of quantification (LLOQ) was determined by injecting solutions containing increasingly higher concentrations (see **Table 5)**.

Table 5 Concentrations of solutions used to determine the method LLOQ, injected in increasingly higher concentrations.

Injection #	Polymyxin E1 concentration (µg/mL)
1	0
2	0.0001
3	0.00025
4	0.0005
5	0.001
6	0.0025
7	0.005
8	0.01
9	0.025
10	0.05
11	0.1
12	0.25
13	0.5
14	1
15	5
16	10

In addition to the LLOQ and the upper limit of quantification (ULOQ, 10 µg/mL), two other concentrations were used; one 20% higher than the LLOQ (1.2LLOQ) and one at 50% of the ULOQ (0.5ULOQ) (see **Table 6)**. All of these solutions were prepared each day anew.

Table 6 Concentrations of the standard solutions used for the method validation.

Name	Polymyxin E1 concentration (µg/mL)
LLOQ	0.025
1.2LLOQ	0.030
0.5ULOQ	5.00
ULOQ	10.00

Matrix effects were assessed with the signal-to-concentration linearity, ranging from the LLOQ to the ULOQ. The concentrations used can be seen in **Table 7**. Diluents used were the various buffers described in section 4.5.1.

Table 7 Concentrations used in solutions used to assess matrix effects.

Polymyxin E1 concentration (µg/mL)
0
0.025
0.05
0.1
0.25
0.5
1
5
10

4.6 COLUMNS

Several analytical columns were tested and used for various purposes; see **Table 8** below.

Table 8. Analytical LC columns used in this thesis

Column	Produced by	Used for	See section
ACE C18 (2.1 mm ID x 100 mm, 3 µm particle size)	ACE (Aberdeen, Scotland)	Separation of polymyxin E1 and B1 in an LC-MS system	4.7
xBridge C18 (4.6 mm ID x 50mm, 3.5 µm particle size)	Waters (Milford, MA, USA)	Attempted separation of polymyxin E1 and B1 in an LC-UV-RI system	**Appendix** J – Attempted liquid chromatography with ultraviolet and refractive index detection
BIOBASIC SEC 300 (2.1 mm ID x 150 mm, 5µm particle size, 300 Å pore size)	ThermoFisher (Waltham, MA, USA)	Separation of liposomes from free polymyxin E1 in the LC-MS system	

4.7 INSTRUMENTATION

The components in the LC-MS system were all purchased from ThermoFisher (Waltham, MA, USA). It consisted of a Dionex ultimate 3000 pump, a Dionex 3000 column oven, and a Dionex 3000 autoinjector (holding 4 ºC, unless otherwise stated). The mass spectrometer used was a Thermo TSQ Vantage equipped with a heated electrospray ion source (HESI).

The oven temperature used was 40ºC, and the flow rate was set to 0.3 mL/min for all methods used on this instrument. Chromeleon Xpress was used to control the LC instrumentation, including autosampler, oven, and pumps. Thermo TSQ Tune Master was used for the direct control of the MS. Thermo Xcalibur Roadmap assumed control for both during runs using the established methods. An ACE C18 (2.1 mm x 100 mm) column was used for the LC-MS system. The system parameters are described in detail in section 4.7.1.

A binary mobile phase system was used for the LC-MS work, with isocratic elution of 83 % mobile phase A (Type 1 water + 0.1 % formic acid) and 17 % mobile phase B (HPLC grade ACN + 0.1 % formic acid). The elution program included a washing step to ensure no remaining compounds were present when the following sample was injected (see **Table 9**).

Mobile phases were degassed for a minimum of 10 minutes before use using a BRANSON 5510 ultrasound bath. The system was then auto purged for five minutes before flow

initialization. The injection volume for all experiments conducted was 20 µL. Overlap injection was not used.

Table 9 Flow program for the LC-MS method used for the separation and quantification of polymyxin E1 and B1.

Time (minutes)	% A	% B
0	83	17
3	83	17
3.5	10	90
4	83	17
7.5	83	17

4.7.1 Mass spectrometry method optimization

Direct injection was conducted using a Harvard Apparatus Syringe Pump 11 Elite with a 100 µL SGE syringe. Method optimization was conducted manually with a 10 µg/mL solution of either analyte (solved in 50/50 (v/v %) water/methanol to ensure a stable spray) at a rate of 5 µL/min. Full scan mode was used, and full ion scans were conducted to observe the most prevalent ions in these solutions, with an *m/z* range from 180 to 1300 for both polymyxins.

Parameters were adjusted, and the signal intensity for the transitions was used to indicate whether the adjustment had a positive/negative/neutral effect. Parameters were adjusted with increasingly smaller increments until no observable change in signal strength was found. This approach was used for both polymyxins. Half a year later, the method was optimized automatically, and the parameters had no significant difference from those achieved with manual optimization. The optimized parameters for the LC method for the analysis of free polymyxin E1 and polymyxin B1 can be seen in **Table 10**.

Table 10 MS parameters used during method development for the analysis of free polymyxin E1

Property	Value
Nozzle voltage	3000 V
Vaporizer temperature	70 C
Sheath gas pressure	15 psi
Capillary temperature	380 C

5 RESULTS AND DISCUSSION

A part of the aim of this thesis was to establish a suitable method for the determination of polymyxin E1, both free and liposomal encapsulated. For this, both UV, MS, and RI-based detection were evaluated. Preliminary attempts with an LC-UV-RI system were made with little success due to insufficient absorbance of both polymyxin E1 and B1. Experimental data and preliminary results from the LC-UV-RI system can be found in **Appendix J** – Attempted liquid chromatography with ultraviolet and refractive index detection. As such, MS-based detection proved most viable. Hence, an LC-MS method was developed and applied to analyze samples (method A). However, following practical applications of method A, extensive analyte adsorption proved to be a significant challenge. Method A was promptly modified into method B, identical except for the sample preparation approach. An illustrative timeline of this development can be seen in **Figure 20**.

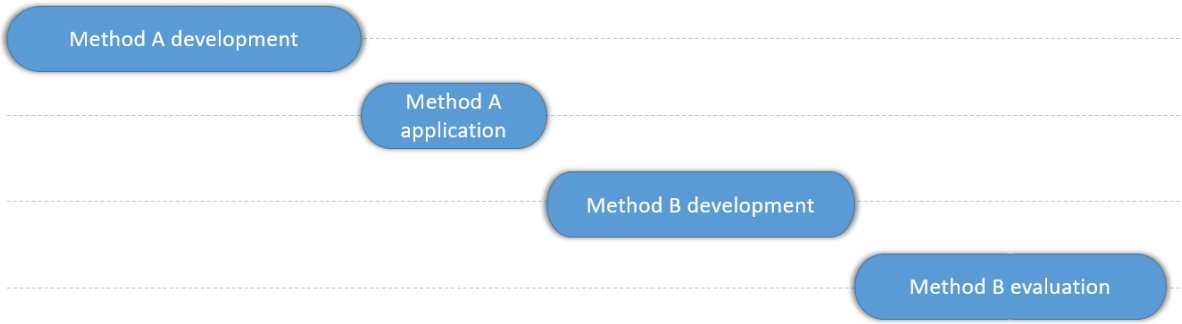

Figure 20 Flowchart for the work presented, showing an illustrative timeline of the work presented. Method A, a method for the measurement of colistin, was initially developed and applied to provided samples. Following observations of analyte adsorption, method A was modified into method B, which was later evaluated and compared to method A. Temporal constraints prevented practical applications of method B.

5.1 METHOD A DEVELOPMENT

5.1.1 Choice of internal standard

Polymyxin B1 was chosen as the internal standard (IS) in this study due to the structural similarity to colistin A (polymyxin E1). The two AMPs differ exclusively in one of their amino acids; where polymyxin E1 possesses a D-leucine, polymyxin B1 has a D-phenylalanine. The rest of the structure in these molecules is identical (see **Figure 21**).

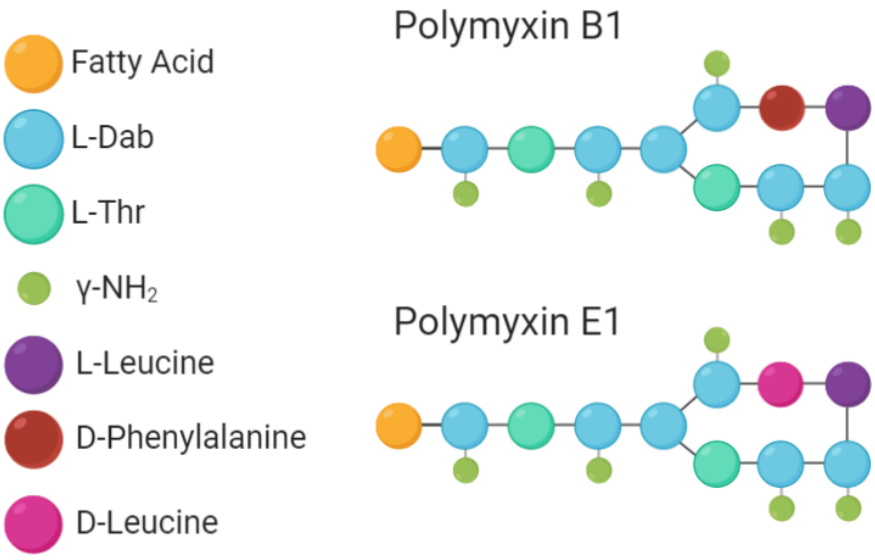

Figure 21. Simplified illustration of polymyxin B1 (Above) and polymyxin E1 (Below). The fatty acid for both is 6-methyloctanoic acid (6-MOA). The only difference between the two polymyxins is the structures, with polymyxin B1 having a D-phenylalanine (Red), as opposed to D-Leucine (Dark pink) in polymyxin E1 [29, 38, 153, 154]. Made using BioRender [10].

Furthermore, of the 5 polymyxins (A to E), mostly polymyxin E and polymyxin B have been used in a clinical setting [42], rendering it far easier to obtain these standards. The choice of polymyxin B1 as an internal standard is also supported by numerous other studies arriving at the same conclusion [129-131, 155-157]. It is worth noting that despite intending to use polymyxin B1 as an internal standard throughout this work, revelations of degradation/adsorption effects of polymyxin E1 raised suspicions regarding the suitability of polymyxin B1 as an IS due to the high structural similarity. As such, polymyxin B1 was not used as an internal standard in this work. However, the method was developed so that it has the capacity to determine polymyxin E1 quantitatively and separate and qualitatively determine polymyxin B1.

5.1.2 Optimization of mass spectrometry parameters

While ultraviolet (UV) and refractive index (RI) detection was initially attempted, this proved a fruitless effort and was therefore abandoned. It was concluded that these detectors had insufficient sensitivity for measuring colistin. Further reading can be found in **Appendix J** – Attempted liquid chromatography with ultraviolet and refractive index detection. Compared to UV, mass spectrometry remains a considerably more sensitive analytical method [158] and provides a higher specificity (as described in section 2.6). Transitions to be used for quantification and qualification were optimized manually for both compounds through direct

infusion. The expected ions produced by ESI-MS, reported through literature, are listed in **Table 11**.

Table 11 Expected ions produced by ESI-MS for polymyxin B1 and polymyxin E1, respectively. The transition used is highlighted in blue.

Ion	Polymyxin B1 (m/z)	Polymyxin E1 (m/z)
$[\boldsymbol{M+H}]^{+}$	1203.1[h]	1169.8 [a]
$[\boldsymbol{M+2H}]^{2+}$	602.4 [c, d, g]	585.4 [b, c, g]
$[\boldsymbol{M+3H}]^{3+}$	401.2[f, g]	390.6 [d, e, f, g]
$[\boldsymbol{M+4H}]^{4+}$	301.2[h]	293.2[h]
$[\boldsymbol{M+5H}]^{5+}$	241.6[h]	234.8[h]

a: [126, 134], b:[124, 131], c: [129, 130, 159, 160] ,d: [156], e: [125, 132, 161], f: [128, 133, 157], g: [162], h: determined by calculation.

5.1.2.1 Polymyxin E1

Ions at *m/z* 390 and *m/z* 585 were found to have the highest intensity in the full scan spectrum, and these *m/z* values were selected as the parent ions to observe. Auto-SIM was then used to detect the most prevalent product ions with *m/z* 390 as the parent ion, with a CE of 10 V. The same was done for *m/z* 585. Following auto-optimization of the collision energies, the resulting transitions were compared simultaneously. The transitions, collision energies, and approximate relative intensity are listed in **Table 12**.

Table 12 Transitions, collision energies, and relative intensities observed for polymyxin E1. Relative intensity shows intensity relative to the first transition (390.3 → 101.3). The transition used is highlighted in blue.

Transition	CE	Relative intensity
$\boldsymbol{390.3 \rightarrow 101.3}$	19 V	100%
$\boldsymbol{390.3 \rightarrow 241.3}$	13 V	40%
$\boldsymbol{585.7 \rightarrow 101.3}$	33 V	15%
$\boldsymbol{585.7 \rightarrow 241.3}$	21 V	10%

The transition giving the strongest signal, $390.3 \rightarrow 101.3$, was selected as the quantifier, while $390.3 \rightarrow 241.3$ was selected as the qualifier. These transitions are described in further detail in section 5.1.3.

5.1.2.2 Polymyxin B1

The same procedure as the one described in section 5.1.2.1 was repeated for polymyxin B1. The selected transitions for qualification and quantification of polymyxin B1 are summarized in **Table 14** in section 5.1.5.

5.1.3 Liquid chromatography optimization

Various flow programs were attempted for the elution of polymyxin E1 and B1. While gradient elution was attempted for polymyxin E1 (not shown), this option was discarded rapidly once the internal standard had been selected. The internal standard (polymyxin B1) should be treated as similar to the analyte in question as possible, and for this reason, identical elution conditions remained preferable. The benefit of isocratic elution is the similar elution and henceforth ionization conditions of analytes and internal standards, especially when using an internal standard. Isocratic elution was therefore chosen, but with a washing step (90% B) to flush out impurities and contaminants that might otherwise have become fixated or strongly retarded on the column.

Isocratic elution was attempted with various amounts of mobile phase B, and the separation and peak shapes were used as qualitative measurements of the mobile phase ratio fitness. Separation was prioritized over peak shape (tailing is a known issue for colistin, described in section 5.1.5). Separation was found to be significantly sensitive to the percentage of the organic modifier, but not to the extent where above-average care had to be taken during the creation of either mobile phase.

Table 13 Isocratic elution programs attempted for the separation of polymyxin E1 and polymyxin B1. Comments included regarding the peak shapes and separation of the two polymyxins, with a final conclusion of the mobile phase B ratio. A mobile phase constitution of 17 % B was found to be the ideal ratio.

% mobile phase B	Peak shape	Separation	Conclusion
25	Unacceptable	None	Unacceptable
20	Acceptable	Poor	Suboptimal
18	Acceptable	Poor	Suboptimal
17	Acceptable	Acceptable	Acceptable
16	Poor	Acceptable	Suboptimal

The washing step was added after the selection of the mobile phase ratios. A brief 90 % organic phase step was thought sufficient to elute strongly retarded compounds.

5.1.4 Mass spectrometry fragmentation

By comparing the mass of the product ions (see **Table 14**, next section) to the masses of the amino acids making up polymyxin E1, likely candidates for the quantifier product ions have been deduced and are presented in **Figure 22**. As described in the previous section, these product ions are expected and reported elsewhere in the literature.

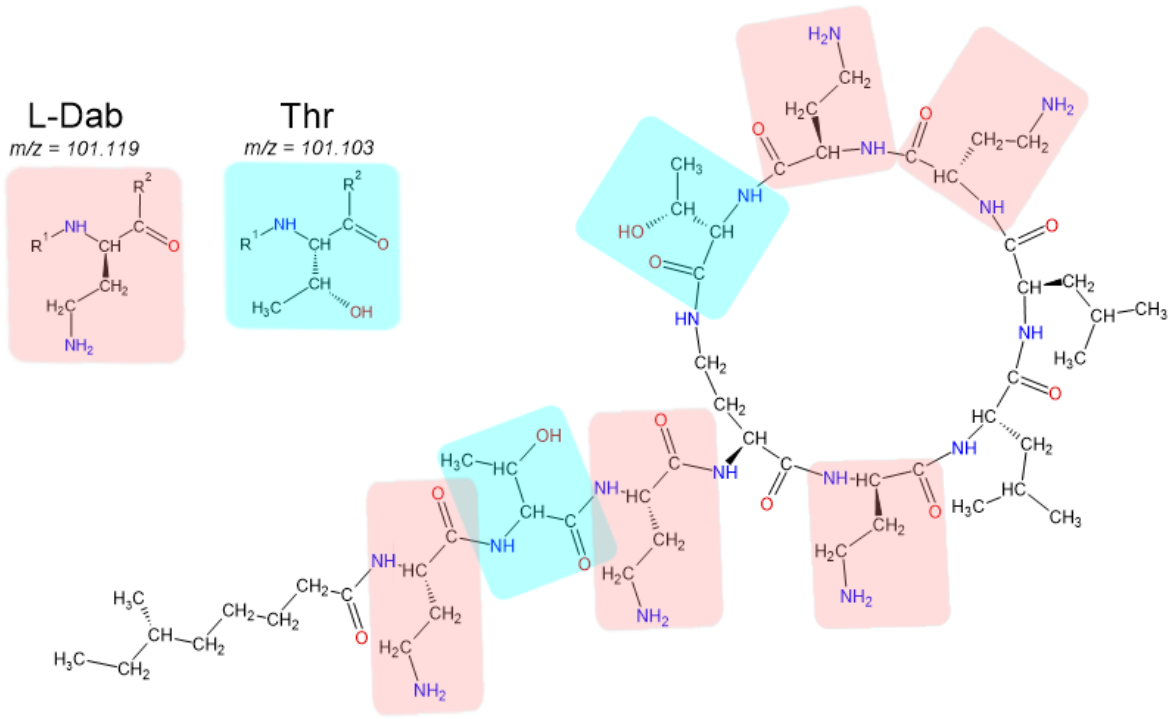

Figure 22 Amino acids thought responsible for the high signal of the quantifier product ion used in this work. Shown: Polymyxin E1 / Colistin A, with red and blue highlighting of the two amino acids L-Dab and Thr, have a mass to charge ratio of 101.1.

The quantifier ion signal can come from either L-dab or Thr or be a combination of these two. While the mass spectrometer used in this thesis lacked the resolution to differentiate between these, a mass spectrometer of a higher mass resolution should be able to separate this. For this, a resolution of roughly 6320 is required, as shown below, using Formula 1 and inserting $m_1 = 101.119$ and $m_2 = 101.103$.

$$\frac{101.119}{101.119 - 101.103} \approx 6320$$

For this, a triple-quadrupole time of flight (TOF) mass spectrometer should be sufficient, with typical resolutions of up to 10 000. Alternatively, an orbitrap mass spectrometer should be viable [163]. The qualifier product ion is thought to consist of the fatty acid (6-MOA) and one unit of the amino acid L-Dab, as shown in **Figure 23**. The polymyxin B1 quantitative transition

product ion could be a dimer of either L-Dab or Thr or a combination thereof. However, it remains more likely that this *m/z* value originates from a product ion consisting of a combination of L-dab and/or Thr with the peptide bond intact

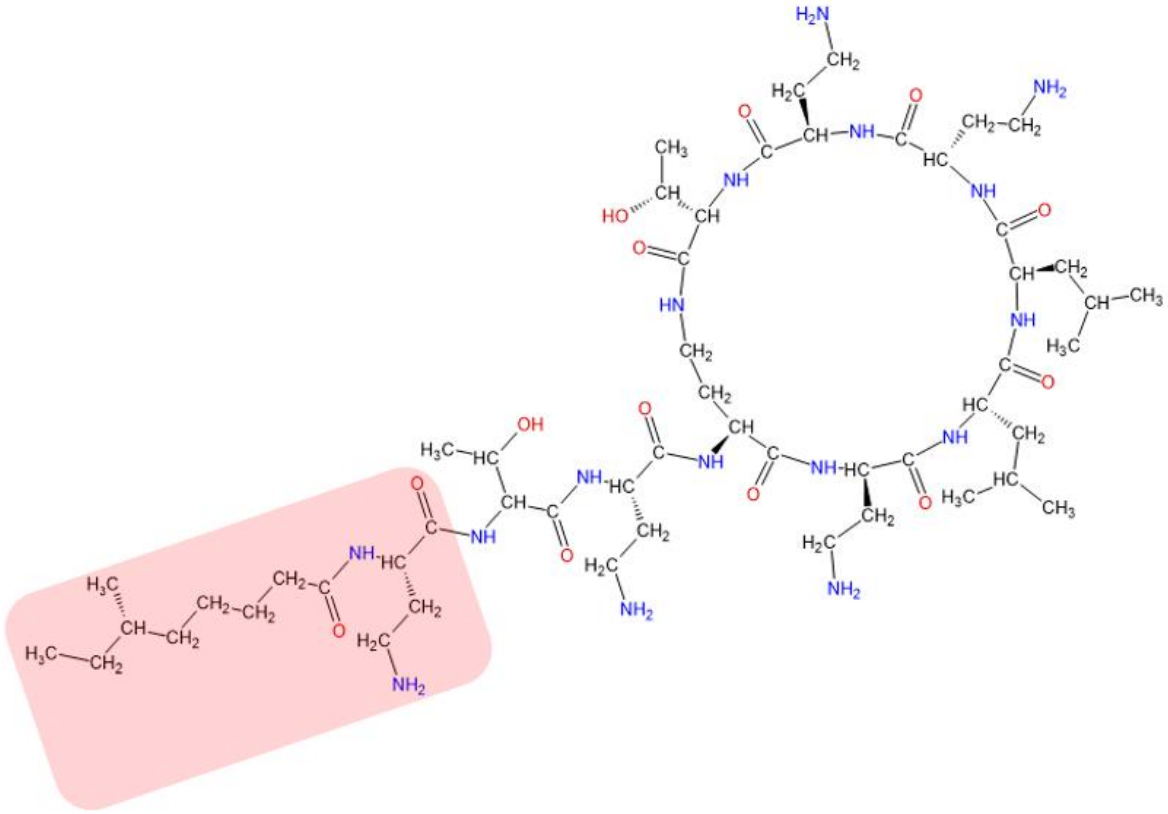

Figure 23 The 6-MOA fatty acid chain and L-dab amino acid are thought responsible for the qualifier product ion used in this work (highlighted in red). The average expected m/z value for this product ion is 241.35, with a monoisotopic mass of 241.19.

5.1.5 Method A summary

For a complete overview of the selected MRM transitions, alongside their respective collision energies, see **Table 14**. A representative multichannel chromatogram of the method can be seen in **Figure 24**.

Table 14 Complete overview of the selected MRM transitions for polymyxin E1 and B1, respectively.

Analyte	Transition	CE	Type
Polymyxin E1	390.3 → 101.3	19 V	Quantifier
	390.3 → 241.3	13 V	Qualifier
Polymyxin B1	401.937 → 202.3	16 V	Quantifier
	401.937 → 241.3	14 V	Qualifier

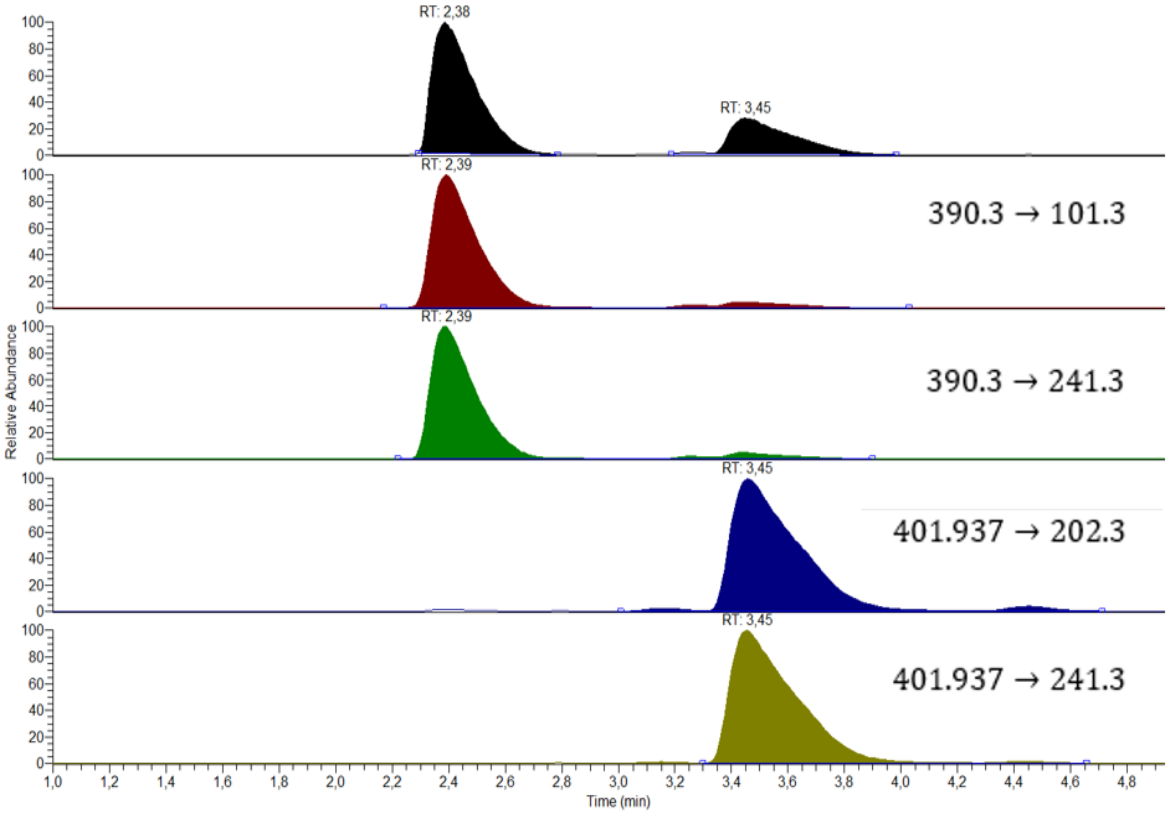

Figure 24 Representative multichannel chromatogram for a mixture of polymyxin E1 and polymyxin B1, showing the total ion current (TIC, black), quantifier (red), and qualifier (green) transitions for polymyxin E1, and the quantifier (blue) and qualifier (orange) transitions for polymyxin B1. The injection volume for all experiments was 20 µL.

As shown in the top two chromatograms in **Figure 24**, polymyxin B1 shares some of the transitions of polymyxin E1, making adequate separation vital to avoid errors. There was a significant asymmetry in the form of tailing for all peaks. However, tailing is expected due to the five amine groups present on both analytes, suspected to engage in extensive secondary interactions with silanol groups in the analytical columns [124, 125].

In summary, an LC-MS method for the separation and measurement of polymyxin E1 and polymyxin B1 was developed. Quantifier and qualifier transitions were used to add confidence of analyte presence if the method was to be used for complex samples. The transitions shared some overlap, although this was a non-issue due to sufficient retention.

5.2 METHOD A APPLICATION

The method developed and described in section 5.1.5 was applied to samples of liposomally encapsulated colistin. A preliminary study was first conducted to determine whether the method was viable or not (described in section 5.2.1). A second, more in-depth study was performed shortly after, with more samples and data points (described in section 5.2.2).

5.2.1 Preliminary pseudoquantitative time study on the liposomal release of polymyxin E1

A preliminary test analysis of polymyxin E1 obtained from dialyzed liposomes (see section 4.3) was conducted to evaluate the developed method without excessive resource consumption. The purpose of this analysis was to get a sense of how much polymyxin E1 could leak through the liposomal barrier on its own, given time.

A calibration curve covering the concentration range of the delivered samples was created by observing the area of a chromatographic peak in a sample, comparing it to the lowest calibration standard, diluting appropriately, and repeating this procedure as required until sufficiently low concentrations were achieved. No internal standard was used in this experiment. Quantification was not possible for the first sample of 1.5 h. It had a signal below the limit of detection (Here defined as a signal to noise ratio below 3), estimated to be around 0.02 ng/mL at the time of analysis.

Low sample volume required the use of cone-shaped vials. However, the position of the needle of the autoinjector proved to be slightly inaccurate, being unable to sample from the center of these vials. Therefore, while three injections from each sample were performed, only one analytical run proved viable for each, as the injector needle managed only to sample a sample volume accurately once.

Calibration solutions with concentrations of 0.008, 0.01, 0.05, 0.19, 0.5, and 1 µg/mL were created from the 100 µg/mL polymyxin E1 stock solution. A correlation coefficient of 0.9938 was found. Due to the unreliable nature of the sample measurement, however, the measured concentrations can be considered pseudo-quantitative at best.

The calibration curve can be seen in **Figure 25**. The data used to create the calibration curve and the calculated concentrations can be seen in **Appendix H1** – Raw data from the first liposome release study.

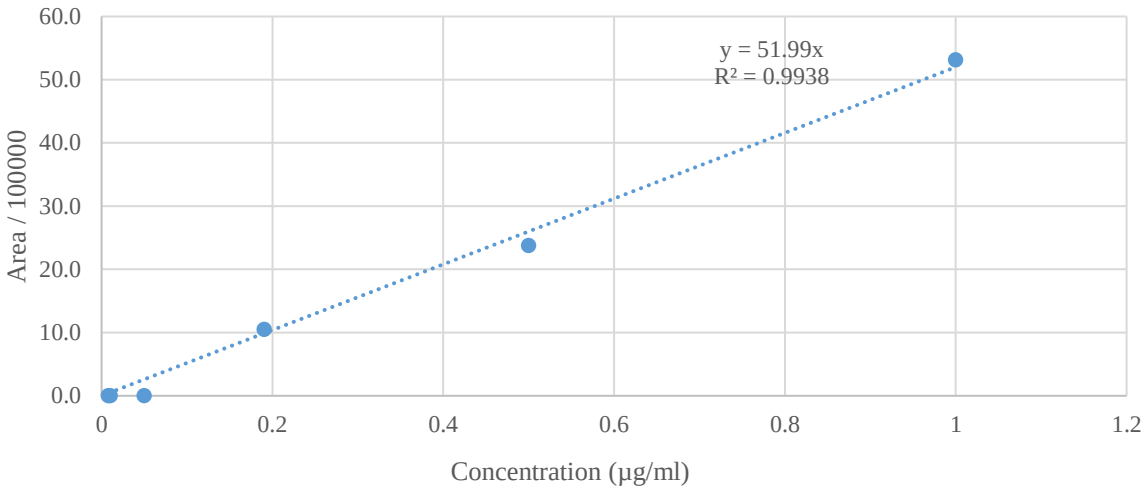

Figure 25. Calibration curve of quantifier transition signal versus concentration of polymyxin E1, measuring reduced area (area / 100000) against the concentration of polymyxin E1. The area was scaled down for all measurements by a factor of 100000 due to complications with the software used at the time (Excel 2016).

For this analysis, method A, as described in section 5.1.5, was used with a 20 µL injection volume. Transitions used are listed in **Table 14**. The calibration curve, albeit consisting of few data points, appeared relatively flat in the lower concentration range. This was found slightly suspicious and was examined further in a later experiment (see section 5.3).

The measurements followed the expected trend of a high initial release and a slow equilibration, suggesting polymyxin E1 heavily favors binding to the liposome wall or liposome interior instead of the free solution otherwise. However, this requires further investigation to evaluate as true or not. The measurements are displayed graphically in **Figure 26**, showing the concentration outside the liposomes as a function of the time the sample spent idle before analysis.

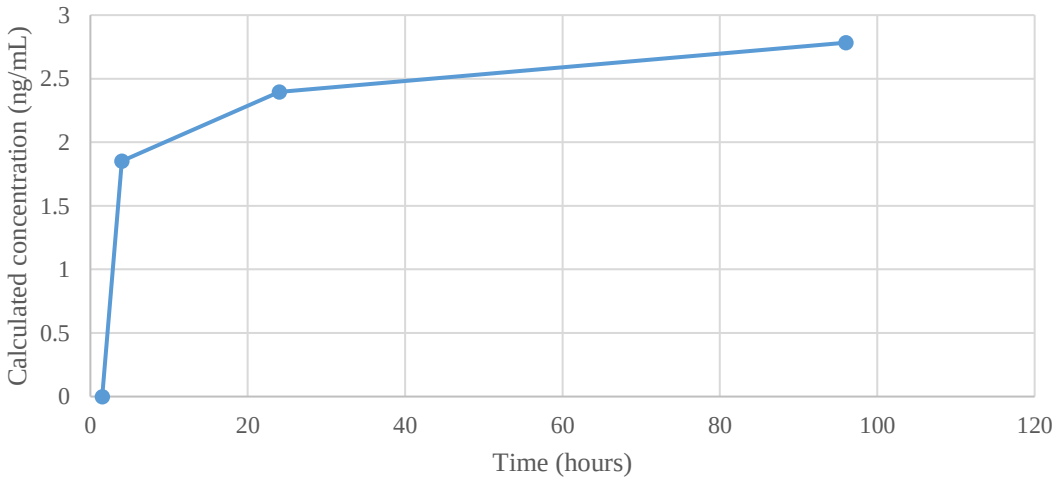

Figure 26. Polymyxin E1 concentration versus time, from the pseudoquantitative time study, as described in section 5.2.1. . Sample 1, whose concentration was below the concentration limit of detection (cLOD), had the measured concentration set to 0.

5.2.2 A more thorough pseudoquantitative study of polymyxin E1 release from liposomes

Since only polymyxin E1 was to be measured and not polymyxin B1, the percentage of mobile phase B was increased from 17 to 19 percent, giving an elution time of 1.1 minutes for polymyxin E1. This is the only deviation from method A, developed and described in section 5.1 and 5.1.5, respectively. The sample preparation is described in section 4.3. Due to the instrument encountering an error halfway through the sequence, the measurements were conducted for two days, and two calibration curves were used, one for each day. The calculated concentrations from day 1 and day 2 are shown in **Figure 27** and show a promising trend of increasing polymyxin E1 concentrations, though only after 36 hours. The first data point (0 hours) has been omitted from **Figure 27** due to an error in the sample preparation (see **Figure 45** in **Appendix H2** – Raw data from the second liposome release study).

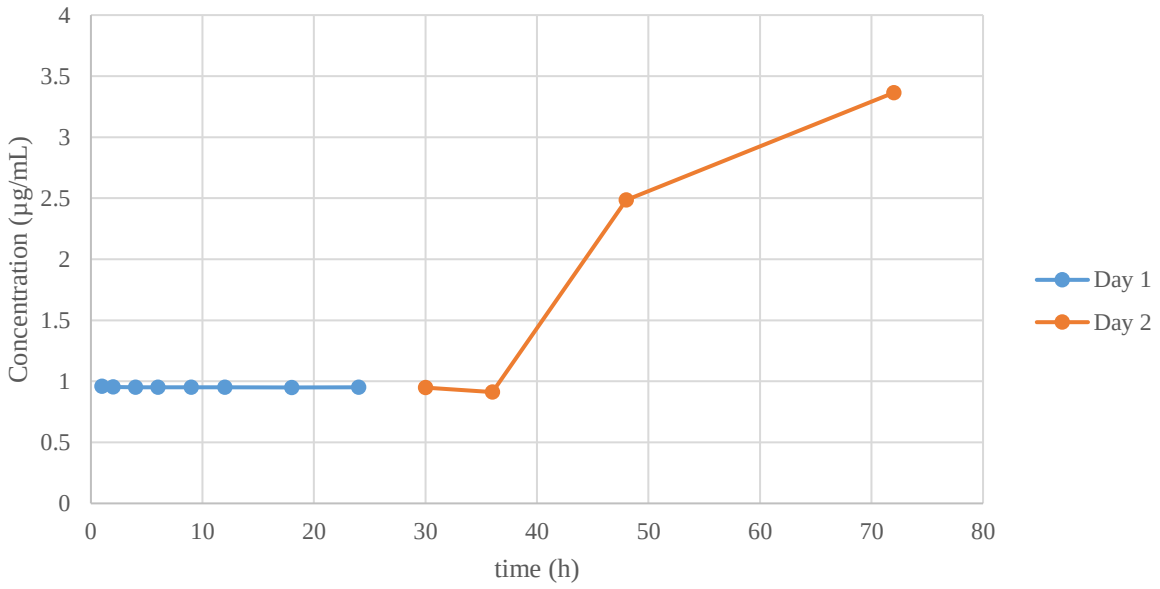

*Figure 27. Measured polymyxin E1 concentration in provided pre-prepared and aliquoted samples measured on day 1 (blue) and day 2 (orange) containing liposomes loaded with polymyxin E1, left to stand for varying amounts of time. The graph was constructed using data from **Table 22** in **Appendix H2** – Raw data from the second liposome release study.*

These samples were left to stand at the lab benchtop at room temperature during the polymyxin E1 release. As a later section (5.3) explains in further detail, polymyxin E1 concentrations proved to be unstable without careful control of both temperature and pH, in part explaining the flat curve from day 1 in **Figure 27**.

The concentration appeared constant in the beginning for all samples left up to 24 hours (blue dots in **Figure 27**) before it suddenly appeared to increase. The low peak area measured (see

Table 22 in **Appendix H2** – Raw data from the second liposome release study) relative to the intersect of the calibration curve (see **Figure 44** in **Appendix H2** – Raw data from the second liposome release study) implies that the pseudo-constant concentration of 1 µg/mL up until 36 h is due to poor curve fitting. The calculated concentrations are only rendered artificially high due to this and are most likely far lower in reality. Colistin adsorption and degradation effects, unknown at the time of measuring, were presumably responsible for a drastic loss of what the polymyxin E1 concentration would otherwise be. This, and low inter-day repeatability of tentative experiments (not shown) raised suspicions that non-instrumental factors were at play, prompting an investigation into the stability and behavior of colistin.

As later discovered, solutions with polymyxin E1 concentrations < 2 µg/mL rapidly lose polymyxin E1 to surfaces unless this effect is mitigated. Additionally, as investigated in a later experiment, polymyxin E1 was not stable when left at room temperature.

With the assumption that polymyxin E1 slowly leaked from the liposomes, samples in this second quantitative study with lower concentrations were subject to adsorption and degradation. As such, samples subject to the most polymyxin E1 release and the least amount of time spent at room temperature are expected to have higher concentrations (above the artificial 1 µg/mL). The suddenly skyrocketing trend on day 2 (orange in **Figure 27**) suggests that the adsorption effects were of more significance than those of degradation, as the polymyxin E1 leakage appears to have overcome room-temperature degradation.

In summary, liposome release studies were promising but ultimately inconclusive. Instead, they prompted an investigation into the chemical behavior of colistin, revealing that colistin concentrations were not stable in aqueous conditions and that colistin was readily adsorbed to various surfaces.

5.3 METHOD B DEVELOPMENT

Following the inconclusive data from the second colistin release study (see section 5.2.2) and other inconsistencies observed on a semi-regular basis (such as nonlinearity in the calibration curves, see section 5.5.2), it was suspected that polymyxin E1 might not be as stable as once thought, despite this not being reported in most published articles on colistin. This suspicion arose at the same time method validation had begun, based on the Guideline on Bioanalytical Method Validation proposed by the European Medicines Agency (EMA) in 2011 [164]. A deeper look yielded surprising results from a handful of studies, namely that colistin was neither stable nor inert against surfaces. As such, the method evaluation was halted until adequate control of polymyxin E1 concentration stability could be achieved.

A stability study conducted by Elimam et al. [165] concluded that sunlight did not affect the degradation rate of polymyxin E1 to a measurable extent when irradiated for six hours. The same study concluded that the colistin degradation reaction, thought to be a form of hydrolysis, is linearly dependent upon temperature (increasing degradation rate as temperature increases). Furthermore, it was concluded that the degradation reaction rate was linearly dependent upon the concentration of hydroxide ions, with the rate increasing with increasing pH. The rate appeared constant below pH 6, however. At room temperature, this study found colistin to have a half-life of roughly four hours at a pH < 6. Another study supported this evidence, noting a colistin loss of nearly 50% after 2 hours [166]. However, this study did not have any pH control, so the basic nature of colistin quite possibly helped accelerate the degradation. Another study, however, conducted by Nation et al. [167], concluded that colistin remained stable at pH 4 and stable at 37 degrees when stored in pure water without pH modifications but unstable when a phosphate buffer was used. Furthermore, they concluded that colistin was not stable when dissolved in plasma.

In its most basic state, colistin is predicted to have a pK_a of 10.2 [168]. Without using a buffer to control the pH, the pH of a solution of colistin at 10 µg/mL is therefore loosely estimated to be around 10, see **Appendix K** – Colistin pH estimation. Aqueous colistin will therefore encourage its own degradation unless the pH is carefully controlled. The instability of polymyxin E1 at room temperature in basic conditions was confirmed by repeated measurements of polymyxin E1 solutions at pH 3, 6, and 9 and are explained in further detail in **Appendix I8** – Effect of pH. The data obtained support the already presented evidence that polymyxin E1 concentrations remained unstable at non-acidic pH levels at room temperature.

Not only does it appear that colistin degrades at a significant rate without careful control of pH and temperature, but a few studies also suggest that colistin is significantly adsorbed to various surfaces when in a solution. Studies suggested colistin was adsorbed to even Low-bind polypropylene vials (vials with a less hydrophobic surface, as to reduce adsorption effects [169]) in solution, but more research should be conducted [170-173]. Surface adsorption appears to be more substantial the lower the colistin concentration was throughout the materials tested. The same study also found that serial dilution caused extensive loss of colistin; up to 80% of colistin appeared to be lost to surface adsorption after six serial dilutions. Both glass and plastic readily adsorbed colistin, with binding capacities of 1.3 µg/cm^2 and 0.5 µg/cm^2 for glass and polypropylene, respectively. Low-bind materials appeared to help significantly, but even then, a loss of up to 40% was observed [170]. Hence, further research was required on both the stability and adsorption of colistin.

In order to reduce polymyxin E1 adsorption and degradation, three modifications were applied to polymyxin E1 standards and compared against a control, supposing that the amine groups on polymyxin E1 were responsible for the adsorption to various surfaces. In that case, the addition of an ammonium-based buffer (in this case, ammonium formate) could reduce adsorption and degradation (adsorption through competitive inhibition, degradation through pH control). A 10 mM ammonium formate buffer was used and adjusted to approximately pH 4 using formic acid. Ascorbic acid was also attempted in case the degradation reaction could be partially mitigated by using an antioxidant. Thirdly, polymyxin B1 was applied to the surface of the third set of vials to be used. With the structure differing only slightly from polymyxin E1 (see section 5.1.1), it was thought polymyxin B1 could be used as a competitive inhibitor if applied before polymyxin E1 was added to the solution. Experimental details can be found in section 4.5.4. A summary of the modifiers can be seen in **Figure 28**. It is worth noting that all four sets (except the control) contained ammonium formate.

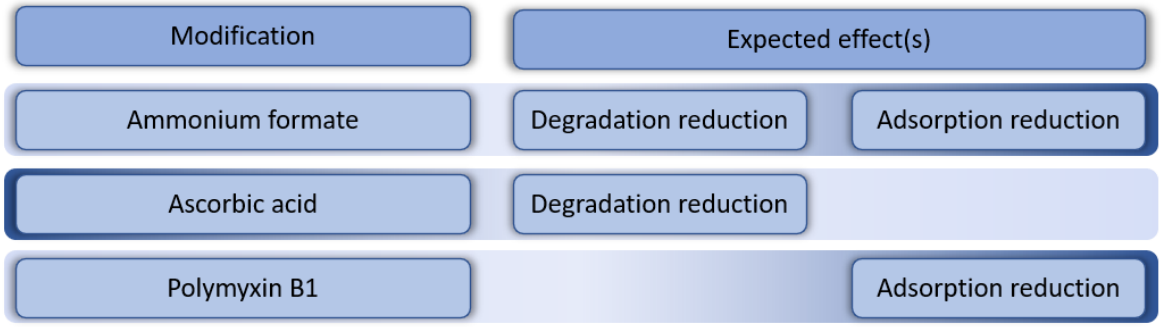

Figure 28 Summary of the three modifications examined in this preliminary adsorption/degradation study on polymyxin E1. Ammonium formate was expected to reduce both adsorption and degradation. Ascorbic acid potentially only degradation, and polymyxin B1 only adsorption.

If ascorbic acid or polymyxin B1 had a beneficial effect, this effect should be visible compared to the set containing only ammonium formate. A steady decline in signal over time was found, with ascorbic acid seemingly accelerating degradation rather than reducing it, see **Figure 29** for the peak area of the highest concentration investigated for each set.

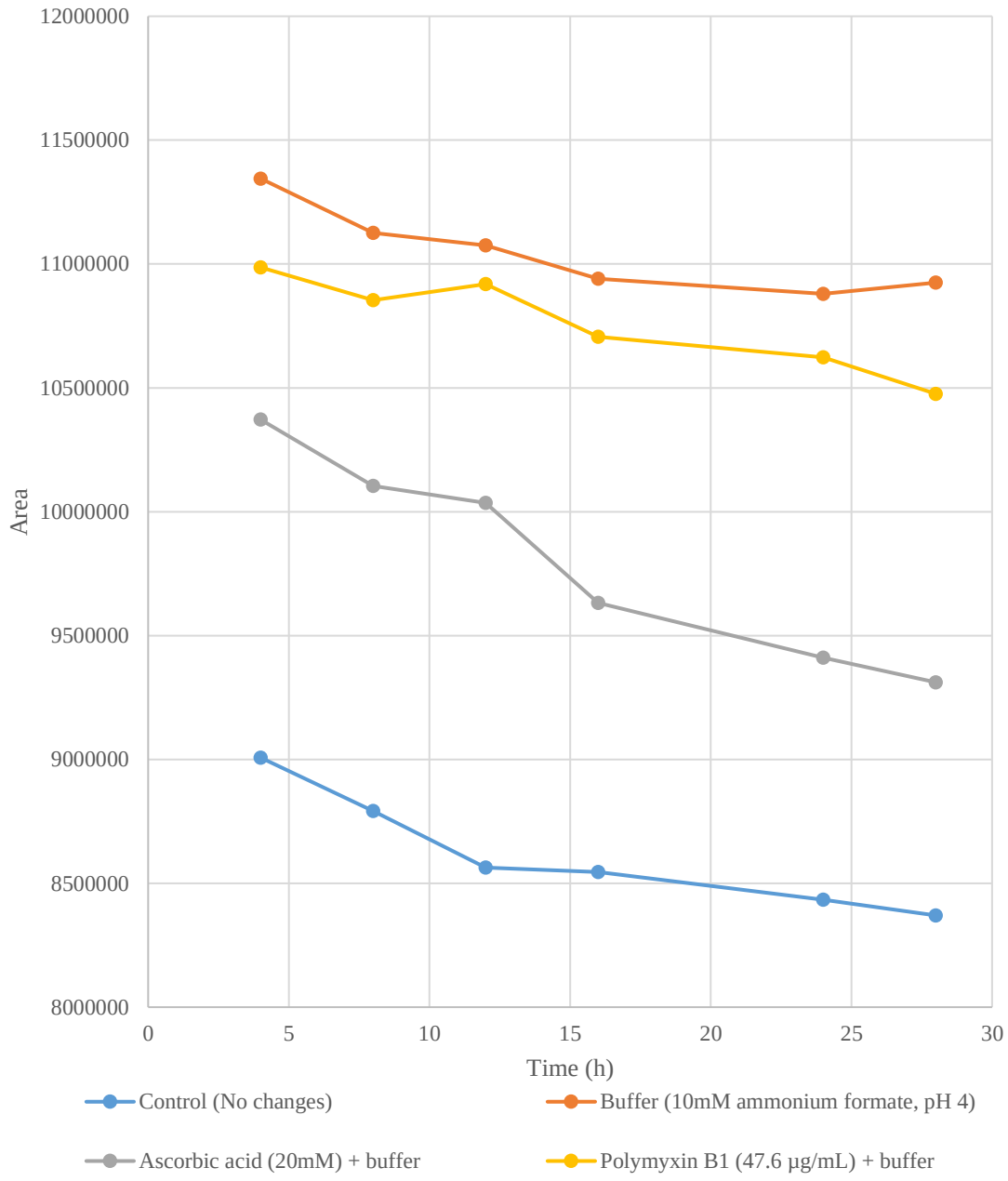

Figure 29 Plots of a 10 µg/mL solution, showing a slowly decreasing trend. Data points for 0h and 20h were omitted, as an instrumentational error caused all data points for this sequence to have a loss of signal of almost 50%. The graph was created using ***Appendix H3*** *– Raw data from the first stability/adsorption test.*

This experiment was performed by running a single, four-hour sequence a total of eight times. It was noted that in two of these sequences, the area measured seemed reduced by almost 50 percent relative to all other runs of the same samples. Interestingly enough, the use of ascorbic acid appeared to accelerate the degradation reaction. The use of a buffer seemed to help significantly with polymyxin E1 loss. As the solutions containing polymyxin B1 and ascorbic acid also contained the ammonium formate buffer, it would appear that for some reason, these enhance the degradation or reduce the effects of the buffer. Further investigation should be conducted on this topic before any conclusions are drawn, however. The calibration curves

remained linear, but no explanation was found for the 50% signal loss, and it was concluded to be due to a bug in the instrument software. As such, the experiment was repeated three days later with the same concentrations, but in a single, 28-hour sequence instead of eight four-hour sequences, the results of which can be seen in **Figure 30**.

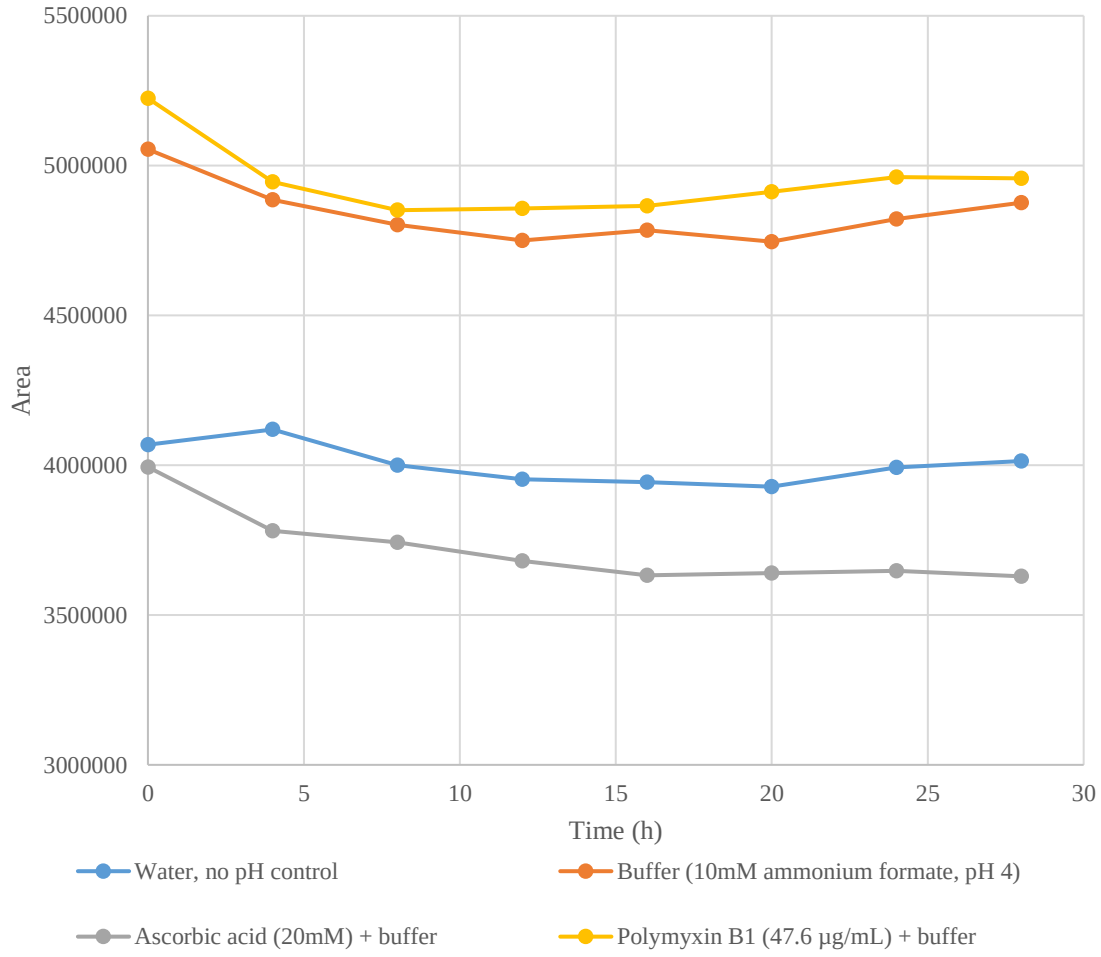

*Figure 30 Plots of the highest calibration point for each calibration curve (10 µg/mL) from the second stability test, produced using data from **Appendix H4** – Raw data from the second stability/adsorption test.*

This experiment yielded inconclusive data. These are the exact solutions as were measured three days prior, and so the lack of a clear trend may be a result of degradation that occurred the three days between the first and second time the solutions were measured. Overall, a signal (area) decrease can be seen for all solutions up until approximately 10 hours, after which the area appears to be somewhat stable. The cause for this is not fully understood, but adsorption and surface saturation were suspected, and the time passing between the sample preparation and measurement may be of significance. However, before the experiment was repeated, another search through literature revealed that colistin concentrations were not only unstable and 'sticky' towards various surfaces but also self-aggregates in aqueous solutions to form

fixed-size micelles [174, 175]. These micelles have a hydrophobic core consisting of the fatty acid attached to colistin.

Micelle formation is believed to reduce the degradation rate of colistin by reducing the amount of colistin surface area exposed to water molecules [174, 175]. As far as the practical implications of this go, while not examined in this work, two studies found that when a surfactant was added (polysorbate-80, also referred to as 'tween 80'), the minimum inhibitory concentration (MIC) drastically sunk. The MIC, the lowest concentration of an antimicrobial substance that inhibits bacterial growth, of colistin was reduced by factors of 4 to 8, suggesting that breaking up micellar colistin effectively increased the concentration of 'free' colistin able to engage in antimicrobial activity [172, 176]. Further research on this could yield vital insight into the self-assembly of colistin, ways to negate adsorption/instability, and potential alternative means of therapeutic administration.

The use of an ammonium formate buffer at pH 4 seemed to contribute to analyte stability mildly and significantly reduce the surface adsorption of polymyxin E1 (see **Figure 29** and **Figure 30**). For this reason, a third stability/adsorption study was conducted. This time, the ammonium formate concentration was increased to see if the effect could be more significant at higher buffer concentrations. A control set was compared against a set containing 100mM ammonium formate at pH 4 and a set containing the ammonium formate buffer in addition to 10% v/v ACN. For experimental details, see section 4.5.5.

It is worth noting that since a buffer was not used in the stock solutions described in section 4.4.1, the buffer concentration in the buffered working solutions was not precisely 100 mM as stated, as the 100 µL stock solution used did not contain this buffer. However, this difference was considered negligible and is not considered significant (as 100 µL makes up 1% of the 10 mL working solution, giving a negligible dilution factor). This final set was produced to see if breaking up micelles of polymyxin E1, as described in the previous paragraph (and [174, 175]), could reduce adsorption, potentially by freeing up micellar polymyxin E1 molecules that had gotten stuck on the surface of its container. The control set consisted of polymyxin E1 dissolved in type 1 water (no pH control).

In the third stability/adsorption study, lower polymyxin E1 concentrations were examined to see the effect of an ammonium formate buffer on the lower endpoint of the linear range. The signal trend was inconclusive; there was a clear decrease of signal over time for the first 14

hours, after which the signal began to increase, suggesting the presence of some unexplained mechanism (see **Figure 31**), potentially an unexplained inducement of desorption.

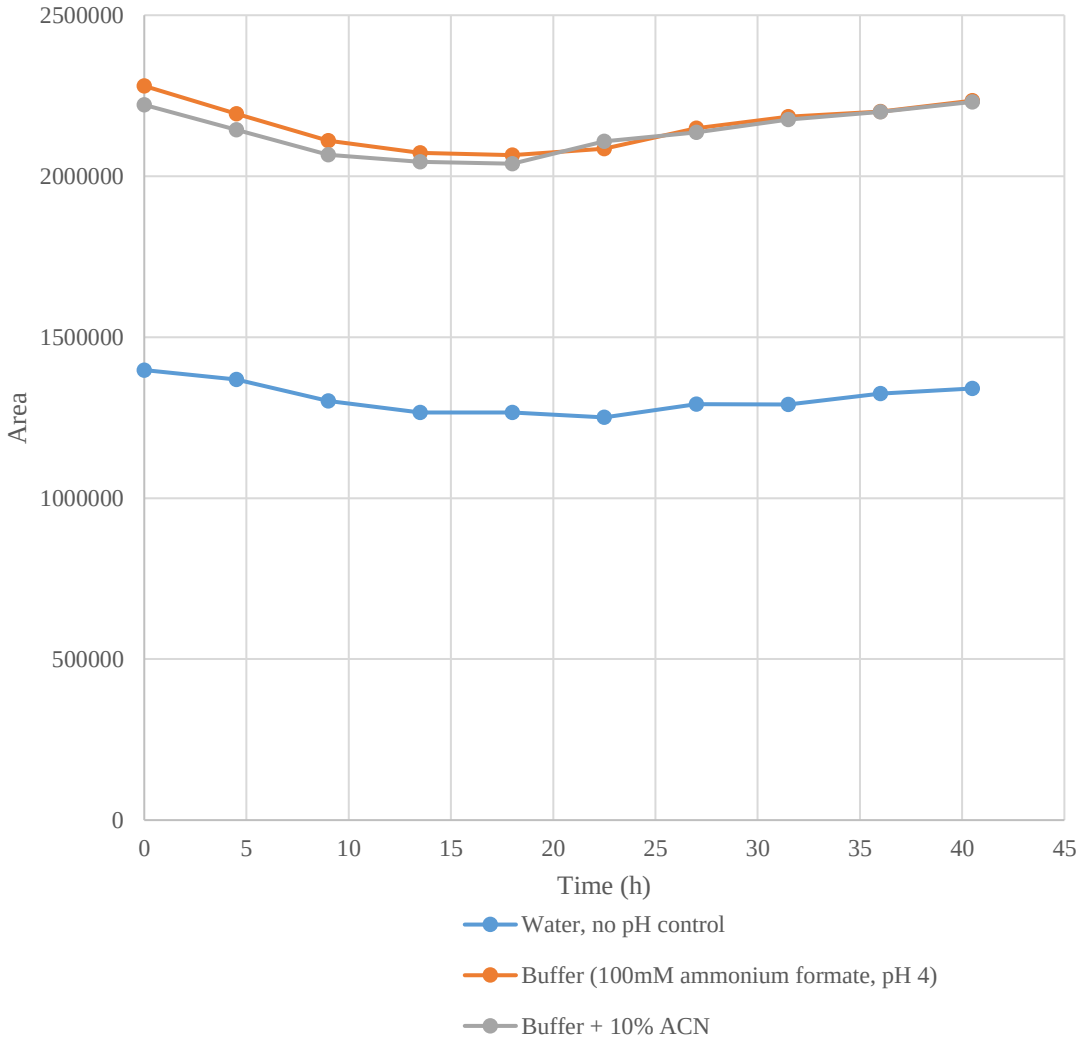

*Figure 31 Plots of the peak areas of 2 µg/mL polymyxin E1 solutions from the third stability test. This graph was produced using raw data from **Appendix H5** - Raw data from the third stability/adsorption test.*

The difference between the highest and lowest signal in one set was roughly 10 % and was therefore not believed to originate due to MS instability. This trend can be vaguely observed in **Figure 30** as well, adding confidence to this assumption. Whatever the mechanism, it appeared to increase the polymyxin E1 concentration back to roughly where it was initially after a certain amount of time (40.5 h). This decrease can therefore not be attributed to colistin instability.

The effects of using a buffered polymyxin E1 solution are stark, however, with a dramatically higher signal in solutions containing buffered polymyxin E1 in contrast to the control solutions (containing no buffer). It is worth noting that this third stability/adsorption test was conducted at a lower concentration (2 µg/mL) than the former two. Adsorption may be more pronounced, and therefore of higher significance at lower than higher concentrations, though further research should be conducted to verify or disprove this. Furthermore, the mechanism appears to be slightly more prominent in the buffered solutions, as seen in **Figure 31**. A longer time study on these solutions might yield exciting insight into the unknown mechanism(s) at play and the potential implications.

While **Figure 31** remains just an excerpt, the entire data set can be seen in **Figure 32** (control solutions) and **Figure 33** (buffered solutions). Buffered solutions containing ACN are not shown due to the strong similarity between these and those without ACN. The difference between peak area intensities on buffered versus non-buffered solutions was highly promising on the limit of quantification (LOQ), as a higher colistin signal would mean that lower concentrations may become detectable. This data also suggested that ammonium formate reduces colistin adsorption. However, whether this is due to the competitive binding of ammonium to surfaces or the formate counter ions preventing the ammonium groups on polymyxin E1 from binding remains unknown. As shown in **Figure 32**, not using ammonium formate (as per method A) produces a lower limit of quantification, as the lower point of the linear range begins around 0.75 µg/mL. In contrast, when using a buffer as per method B (see **Figure 33**), there was no precise breakpoint from the linear range that determined the LOD but rather the instrument itself. In the case of non-buffered solutions, the LOQ must be determined by the curvature of the calibration (as the lower limit of the linear range). In contrast, in buffered solutions, the linearity is sufficient to render the LOQ dependent only upon the signal-to-noise ratio. This highlights the superiority of method B over method A. As such, it is concluded that the use of ammonium formate is required to achieve reliable

quantification and measurements of lower concentrations near and below 1 µg/mL. Using 10%, v/v ACN in the solutions had no significant effect and was not investigated further. Polymyxin E1 micelle formation was therefore not thought to pose an issue.

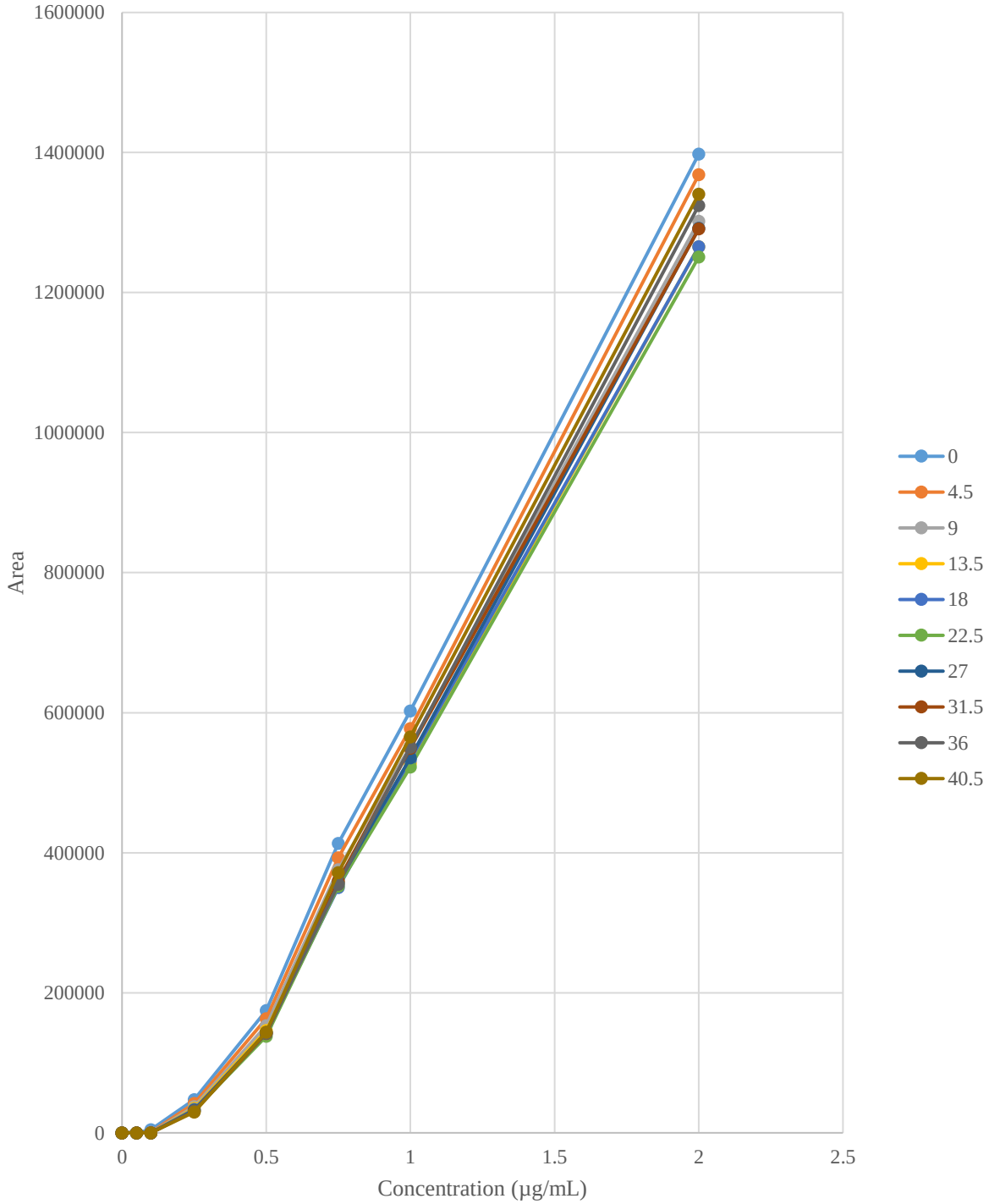

*Figure 32 Standard curves from the third stability/adsorption study from the control set. The legend shows the times (in h) the solutions were measured after the start of the measurements. An apparent lack of linearity can be seen below 1 µg/mL, unlike in **Figure 33**. This graph was produced using data from **Appendix H5** - Raw data from the third stability/adsorption test.*

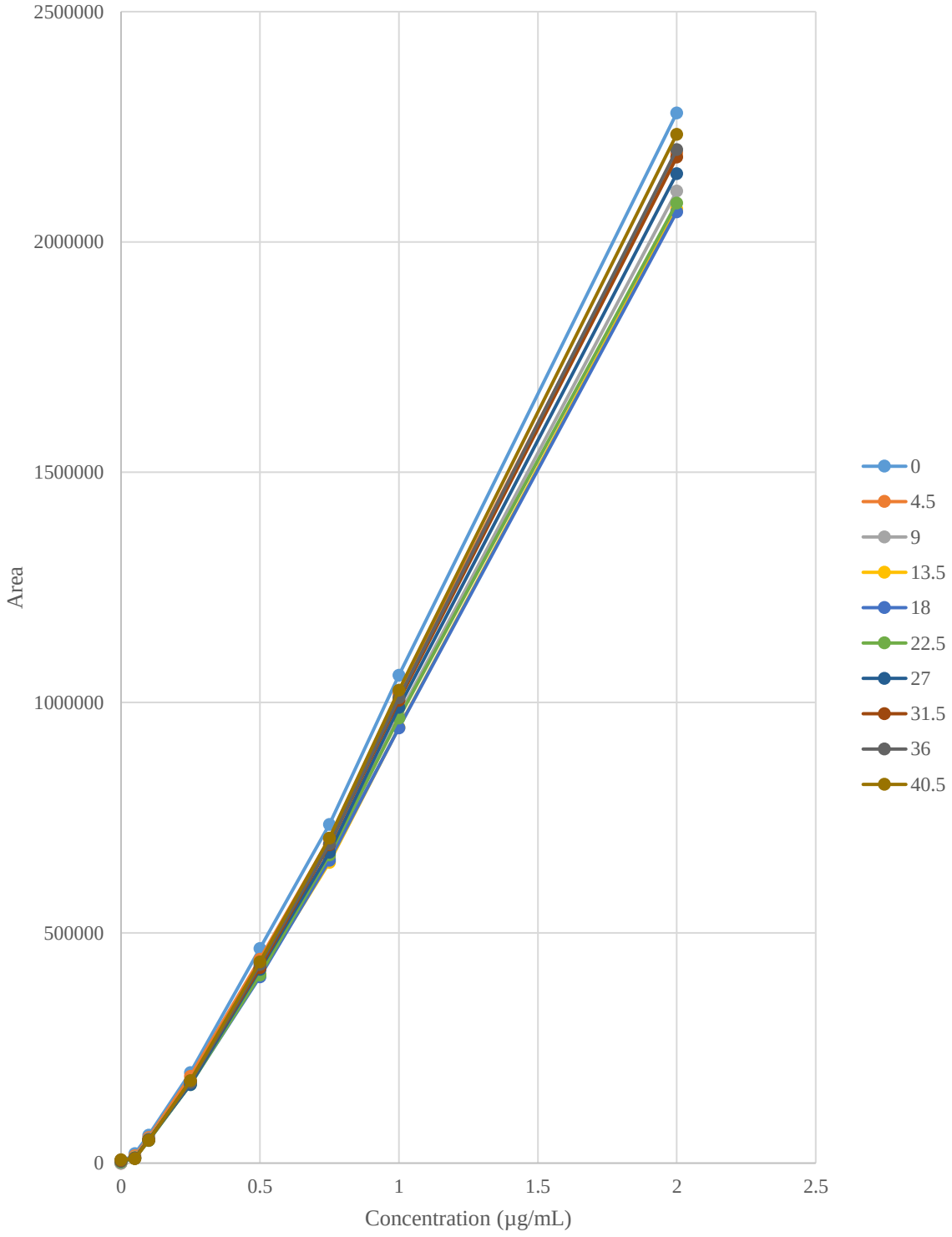

Figure 33 Standard curves from the third stability/adsorption study from the buffered set (100mM ammonium formate, pH 4). The legend shows the times the solutions were measured after the start of the measurements. Linearity can be seen down to the lowest calibration point at 0.1 µg/mL, in contrast to ***Figure 32.*** *This graph was produced using data from* ***Appendix H5*** *- Raw data from the third stability/adsorption test.*

Finally, to confirm the conclusion drawn from the third stability/adsorption study, a fourth stability study was used to confirm the effectiveness of buffer used in aqueous solutions of polymyxin E1 at room temperature, with concentrations of 1, 5, and 10 µg/mL. This study differed from the others as the autosampler held a constant 20ºC. The concentration instability should become more pronounced at a higher temperature, and kinetic effects should accelerate, making the polymyxin E1 adsorption effect reach equilibrium faster. In this study, buffered solutions with these concentrations (1, 5, and 10 µg/mL) were prepared using working solutions containing buffer, and non-buffered solutions were prepared using working solutions without buffer. The data obtained were used to interpret the short-term (15 h) benchtop stability of polymyxin E1 solutions of low concentrations (see **Figure 34**).

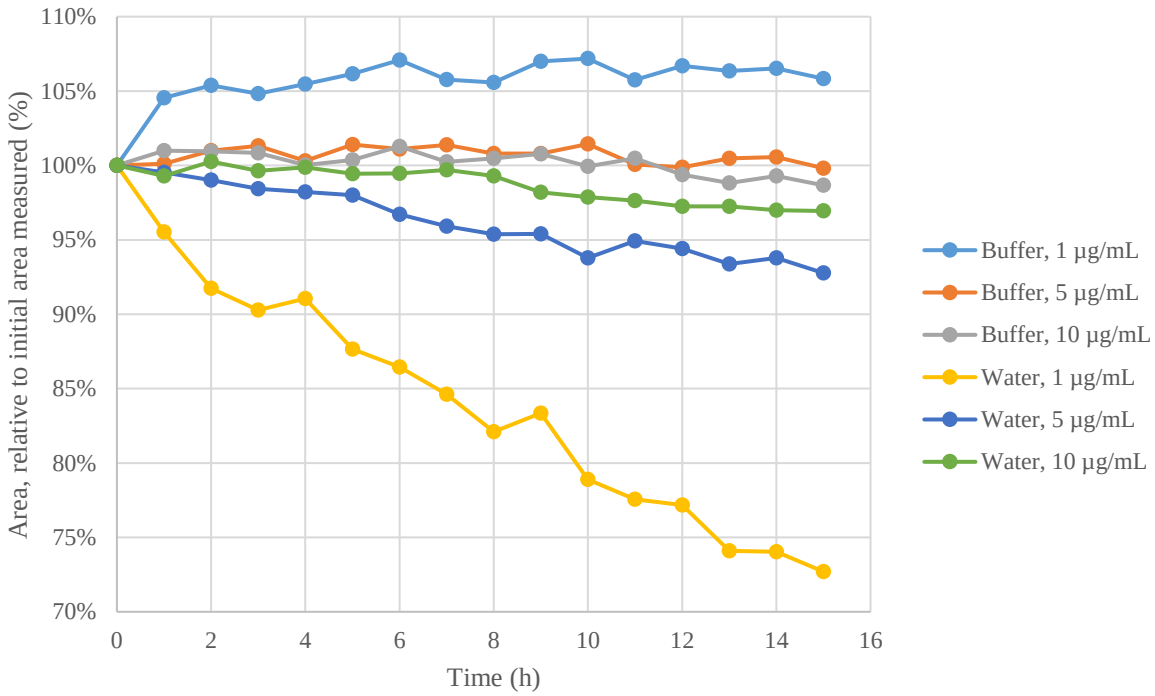

*Figure 34 Area (relative to the initial area) of aqueous solutions of polymyxin E1 at 1,5 and 10 µg/mL concentrations, both in solutions with and without 100 mM ammonium formate buffer (pH 4) of samples kept at room temperature (20 C). The graph was created using **Table 30** from **Appendix H6** - Raw data from the fourth stability/adsorption test*

The data trend in **Figure 34** shows an apparent decrease in signal in solutions without buffer use, with the relative decrease in the signal being more substantial the lower the concentration. The loss of signal may result from surface adsorption or polymyxin E1 degradation and shows a loss of up to 30% signal after 15 hours for the 1 µg/mL solution without buffer. After 15 hours, the concentrations of polymyxin E1 in the buffered solutions at 1, 5, and 10 µg/mL were 105.8%, 99.8%, and 98.7% of their initial concentrations, respectively. In contrast, polymyxin E1 concentrations in non-buffered solutions at 1, 5 and 10 µg/mL were 72.7%, 92.8%, and

96.9% of their initial concentrations, respectively. This suggests that the relative concentrations of polymyxin E1 in aqueous solutions depend upon pH and adsorption effects, the latter of which appears to depend upon the concentration itself. The adsorption and degradation mechanisms appeared more significant at lower than at higher concentrations. Extensive colistin loss at lower concentration makes sense, with common materials such as glass and plastics having colistin binding capacities of roughly 1.3 and 0.5 µg/cm^2, as previously described in this section [170].

Further research on colistin adsorption could yield critical insight into the behavior of colistin. However, this fourth stability/adsorption test confirmed that ammonium formate (100 mM, pH 4) is required to maintain stable polymyxin E1 concentrations, especially if kept at room temperature. As shown in **Figure 35**, which shows the absolute area rather than the relative area, the effect of a buffer on adsorption is readily visible. The drastic increase in signal in buffered solutions underlines the need for ammonium formate in colistin solutions to reduce adsorption.

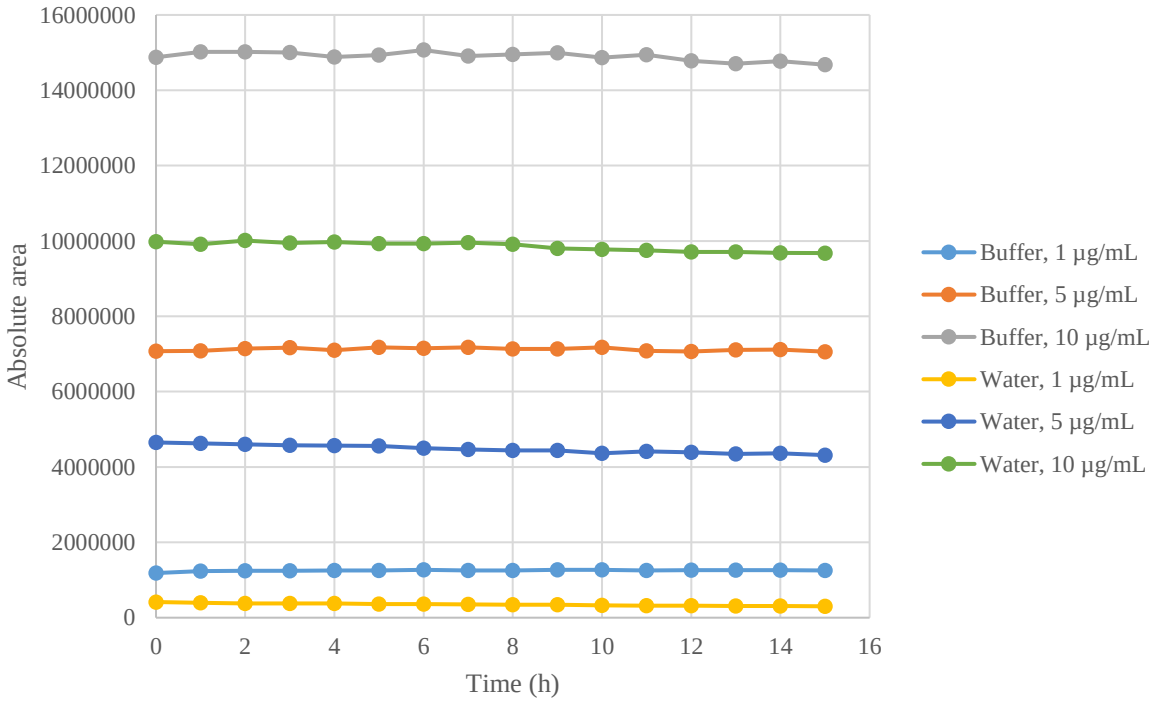

*Figure 35 Absolute area of aqueous solutions of polymyxin E1 at 1,5 and 10 µg/mL concentrations, both in solutions with and without 100 mM ammonium formate buffer (pH 4) of samples kept at room temperature (20 C). The graph was created using **Table 30** in **Appendix H6** - Raw data from the fourth stability/adsorption test.*

Method A was modified into method B, where working solutions and standard solutions used this ammonium formate buffer as a diluent rather than neat water. Method B is described in further detail in section 4.5.

In summary, various chemical modifiers were added to colistin solutions to see if concentration stability or a reduction in colistin adsorption could be achieved. Ascorbic acid, polymyxin B1, and various buffers were attempted. However, only 100 mM ammonium formate appeared able to do this, most likely through the formate counter-ions reducing the ability colistin had to interact with surfaces, a competitive surface saturation of ammonium, or a combination of these. The method initially developed (method A) was modified into method B, where 100 mM ammonium formate buffer was used as a diluent in all solutions.

5.4 METHOD B SUMMARY

Method A was equivalent to method B on all fronts apart from the method used to produce the solutions (see section 4.5 for details). Compared to other methods in **Table 15**, the method finally developed (method B) shares the product ion with many other studies. Ignoring the method using negative mode on the MS (with parent ions of 1167.7), six out of ten studies found used the same product ion. As far as the parent ion goes, only five out of ten use the same *m/z* value, with the other reporting a higher intensity for 585.6. This may be due to instrumentational differences or differences during the MS method development, for instance, as described in section 4.7.1, both polymyxins were dissolved in a 50/50 (v/v %) mixture of methanol and water during the direct injection, which might enhance the intensity of specific ions, or reduce that of others.

As previously discussed in section 5.1.3, the LOQ remained quite similar to that of other LC-MS studies of colistin A (polymyxin E1), see **Table 15**. The mLOQ remained lower than that reported in most studies; however, the signal increase originating from the use of the ammonium formate buffer, as shown in **Figure 35**, is thought to be chiefly responsible for this. More polymyxin E1 remains free in solutions when reducing adsorption, and a higher signal, and a lower mLOQ, is achieved. The method run time (7.5 min) was, on average, slightly shorter than those of the 11 methods compared.

Table 15 Summary and comparison of other LC-MS methods developed to quantify polymyxin E1 (and for some, other analytes as well). mLOQ was calculated through the LOQ and injection volume. Dashes represent information that was not applicable or could not be located (for instance, LOQs from solid samples given in µg/kg were omitted from this table). The resulting parameters obtained with method B in this thesis are highlighted in blue.

Parent ion	Product ion	Column (ID x length, particle size)	Elution	Run time (minutes)	LOQ (µg/mL)	mLOQ (pg)	Ref.
390.9	101.1	ACE C18 (2.1 x 100 mm, 3 µm)	Isocratic	7.5	0.025	500	Method B
585.6	101.1	Poroshell 120 SB-C18 (4.6 x 150 mm, 2.7 µm)	Gradient	20	-	-	[123]
585.7	101.2	Synergi Fusion-RP (200 x 2 mM, 2 µm)	Isocratic	-	0.028	1400	[124]
391	385	Phenomenex Luna C18 (2.1 x 150 mm, 5 µm)	Gradient	15	-	-	[125]
1167.7	1079.6	Ultrasphere C18 (250 x 4.6 mm, 5 µm)	Isocratic	10	0.194	9700	[126]
391	385	Acquity BEH C18 (2.1 x 50 mm, 1.7 µm)	Gradient	5.5	-	-	[127]
390.1	101.2	MC C8 (50 x 4.0 mm, 3 µm)	Isocratic	2	0.027	810	[128]
585.5	534.9	MassTox[5]	Gradient	3.5	0.1	500	[129]
585.5	101.2	C18 Xbridge (150 x 2.1 mm, 5 µm)	Isocratic	3.8	0.024	480	[130]
585.5	101	Symmetry C18 (150 x 4.6 mm, 5 µm)	Gradient	15	0.014	280	[131]
390.1	385	Acquity BEH C18 (100 x 2.1 mm, 1.7 µm)	Gradient	5	-	-	[132]
390.6	101.1	Kinetex C18 (50 x 2.1 mm, 2.6 µm)	Isocratic	10	0.13	1300	[133]
1167.8	1123.7	Acquity BEH C8 (100 x 2.1 mm, 1.7 µm)	Gradient	4.5	0.05	1000	[134]

5.5 METHOD B EVALUATION

As method B offered analyte control (in the form of concentration stability), the method was partially validated. Method B was partially validated according to the Guideline on Bioanalytical Method Validation proposed by the European Medicines Agency (EMA) in 2011 [164]. Accuracy was not addressed due to the lack of a known and validated standard. One stock solution only was used in this work (separated into aliquots of 1 mL, see section 4.4.1 for further details).

[5] Further information could not be located in the article referenced.

5.5.1 Retention times

No notable retention time shift was noticed in analytical sequences for either analyte. The average retention time for polymyxin E1 was 2.48 ± 0.11 minutes (based on data from **Appendix H1** – Raw data from the first liposome release study and **H2** – Raw data from the second liposome release study), while the average retention time for polymyxin B1 was 3.40 ± 0.05 minutes (based on data from **Appendix I9** - Retention times).

5.5.2 Limit of quantification

The limit of quantification was assessed using an extended, 15-point calibration curve, ranging from 10 µg/mL to as low as 0.001 µg/mL. The injection volume was 20 µL. Initially, the LOQ was determined using method A by the lowest point of the linear range of polymyxin E1, whose calibration curve from the LLOQ to the ULOQ remained nonlinear below 0.75 µg/mL. This assessment was done before discovering that polymyxin E1 was not particularly stable without high control of both pH and temperature and adhered to various surfaces (see section 5.3). Therefore, the LLOQ was established once more using method B, where these effects were under control.

Method B produced a far more linear curve (see **Figure 36**). The LOQ was determined to be 0.025 µg/mL when using a buffer, a vast improvement from the ~1 µg/mL LOQ determined with method A, where no ammonium formate buffer was used. With an injection volume of 20 µL, this gives a mass limit of quantification (mLOQ) of 500 pg. The improved LOQ is also due to the increased signal originating from the use of ammonium formate, as shown clearly in **Figure 35**.

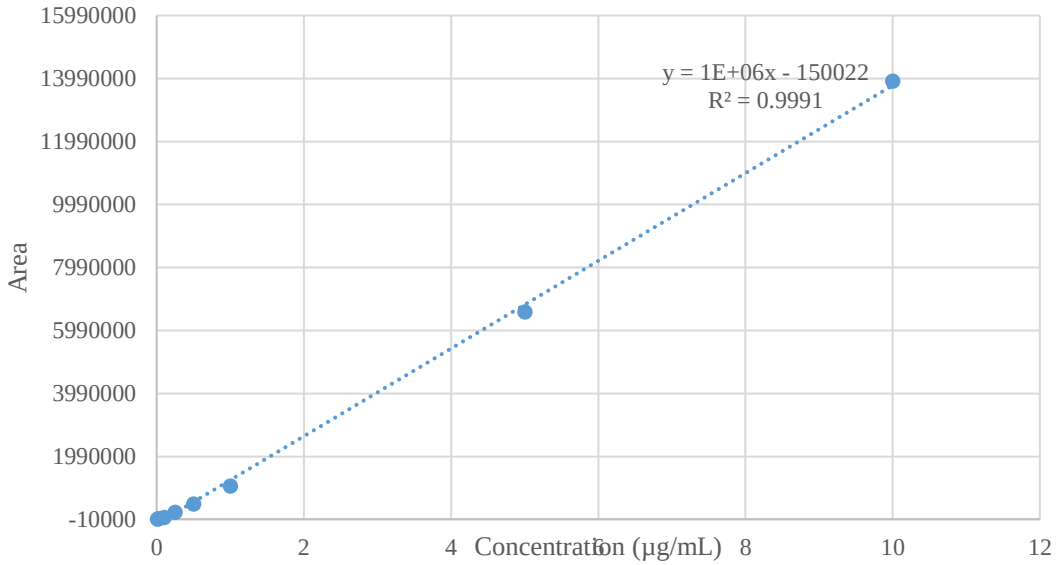

Figure 36 Area to the concentration of polymyxin E1. The linear range appears to continue down towards the LOD. No upper limit of the linear range was determined, as sample concentrations were consistently low. A fitted linear curve

*shows a correlation coefficient of 0.9991, showing a highly linear relationship within the calibration range. While samples at a lower concentration were also measured, these did not give a signal-to-noise response above three due to low sensitivity in the instrument and were therefore not used. Graph created using data from **Table 32** in **Appendix I1** – LOQ.*

5.5.3 Carry-over

Carry-over was determined by four injections of 10 µg/mL solutions, each separated by three blanks, in which the first blank was used to determine the carry-over from the 10 µg/mL solutions. A total of four replicates were used to evaluate carry over, which was found to be 0.064 ± 0.009 %, which meets the criteria presented by the EMA [164]. The raw data can be found in **Table 33** in **Appendix I2** – Carry-over.

5.5.4 Precision and repeatability

Four solutions were prepared to assess the precision of the method: one at the LLOQ (lower limit of quantification), one 20% higher than the LLOQ, 50% of the ULOQ (upper limit of quantification), and one at the ULOQ, which had the concentrations 0.025, 0.030, 5 and 10 µg/mL, respectively. However, as the MS sensitivity is liable to change day-to-day, calibration curves were also prepared each time to calculate a concentration ranging from 0 to 10 µg/mL. The exact concentrations can be seen in **Appendix I3** – Intra-day precision.

Additionally, it is worth noting that the calibration curves used were not linear relationships between signal (area) and concentration but rather linear curves with log-log transformed data. The explanation and justification for this choice can be seen in **Appendix L1** - Calibration curve fittings. The correlation coefficient for the calibration curve prepared each day remained above 0.99 for all sets.

5.5.4.1 Intra-day precision

To assess the intra-day precision, six replicates of each concentration were prepared and measured on the same day, matched against one set of calibration solutions. The precision for the solutions at 0.025, 0.030, 5, and 10 µg/mL were well within the criteria presented by the EMA guidelines (maximum 20% random standard deviation (RSD) at LLOQ, 15% otherwise), see **Table 16**. The raw data can be seen in **Appendix I3** – Intra-day precision.

Table 16 Intra-day precision for solutions at the LLOQ, 1.2LLOQ, 0.5ULOQ and ULOQ. $n = 6$. ST.DEV.: Standard deviation.

Solution	Concentration (µg/mL)	Mean back-calculated concentration (µg/mL)	ST.DEV (µg/mL)	RSD (%)
LLOQ	0.025	0.021	0.004	15.2%
1.2LLOQ	0.030	0.028	0.003	6.3%
0.5ULOQ	5.0	4.8	0.03	4.4%
ULOQ	10.0	9.6	0.1	4.5%

5.5.4.2 Inter-day precision

The inter-day precision was intentionally assessed not in a fixed rhythm of days. Instead, to reflect upon reality, the first three days were in sequence, followed by a space of inactivity for 5 days. Precision and the relative inaccuracy (error) were well within limits set by the EMA guidelines (see **Table 17)**. The raw data can be seen in **Appendix I3** – Intra-day precision.

Table 17 Inter-day precision for solutions at the LLOQ, 1.2LLOQ, 0.5ULOQ and ULOQ. The relative error is the relative difference between the nominal and back-calculated concentrations. $n = 6$.

Nominal concentration (µg/mL)	Mean back-calculated concentration (µg/mL)	ST.DEV (µg/mL)	RSD (%)	Relative error (%)
0.025	0.025	0.001	4.0%	2%
0.03	0.030	0.002	7.4%	1%
5.0	5.0	0.2	3.1%	-1%
10.0	10.1	0.4	3.7%	2%

5.5.4.3 Reinjection reproducibility

By injection of the same sample (10 µg/mL polymyxin E1, 20 µL injection volume) a total of 20 times, the reinjection reproducibility (instrumentational precision) was determined as the relative standard deviation of these 20 samples injected directly after one another. The reinjection reproducibility (presented as the RSD (%)) was equal to 0.50 % at the highest (qualifier transition) and 0.42 at the lowest (quantifier transition), see **Appendix I5** – Reinjection reproducibility.

5.5.5 Matrix effects on stability

Matrix effects relevant to this work (factors that could affect adsorption and concentration stability) were assessed by comparing the signals (areas) of polymyxin E1 solutions at varying concentrations in various buffers. Ammonium formate was used as a reference. Tris (50 mM, pH 7.2), citric acid/phosphate buffer (50 mM, pH 5.5), and PBS (50mM, pH 7.4) were examined, as these were the buffers used for the preparation of the liposomes and other nanoparticles (and would therefore be present in samples). It was found that the citric acid buffer could be of use, as it gave a better signal than ammonium formate buffered solutions at

higher concentrations (> 1 µg/mL). However, the citric acid/phosphate buffer gave a lower signal at concentrations below this, for reasons unknown. Therefore, there may be some potential in using a citric acid/phosphate buffer, but further research should be conducted before any conclusions may be drawn. It is worth noting that all buffers except ammonium formate fail to negate adsorption/degradation across the entire calibration range. The areas obtained relative to that obtained from solutions using the ammonium formate buffer can be seen in **Table 18**.

Table 18 Relative areas of polymyxin E1 solutions at varying concentrations in different buffers compared to ammonium formate buffered solutions of equal concentrations.

Area relative to the area in equally concentrated ammonium formate buffers			
Concentration (µg/mL)	Tris	Citric acid	PBS
10	61%	123%	57%
1	35%	124%	48%
0.5	9%	48%	38%
0.1	0%	33%	21%

The stability of polymyxin E1 in these various buffers was also examined, and the evidence presented in section 5.3 that polymyxin E1 concentrations remained unstable in solutions containing PBS, was supported. The only buffers that seemed to improve polymyxin E1 stability were ammonium formate and citric acid/phosphate (see **Figure 37**). Therefore, the potential citric acid holds should be investigated further. The miniature stability study was conducted by repeat injections of the same solutions.

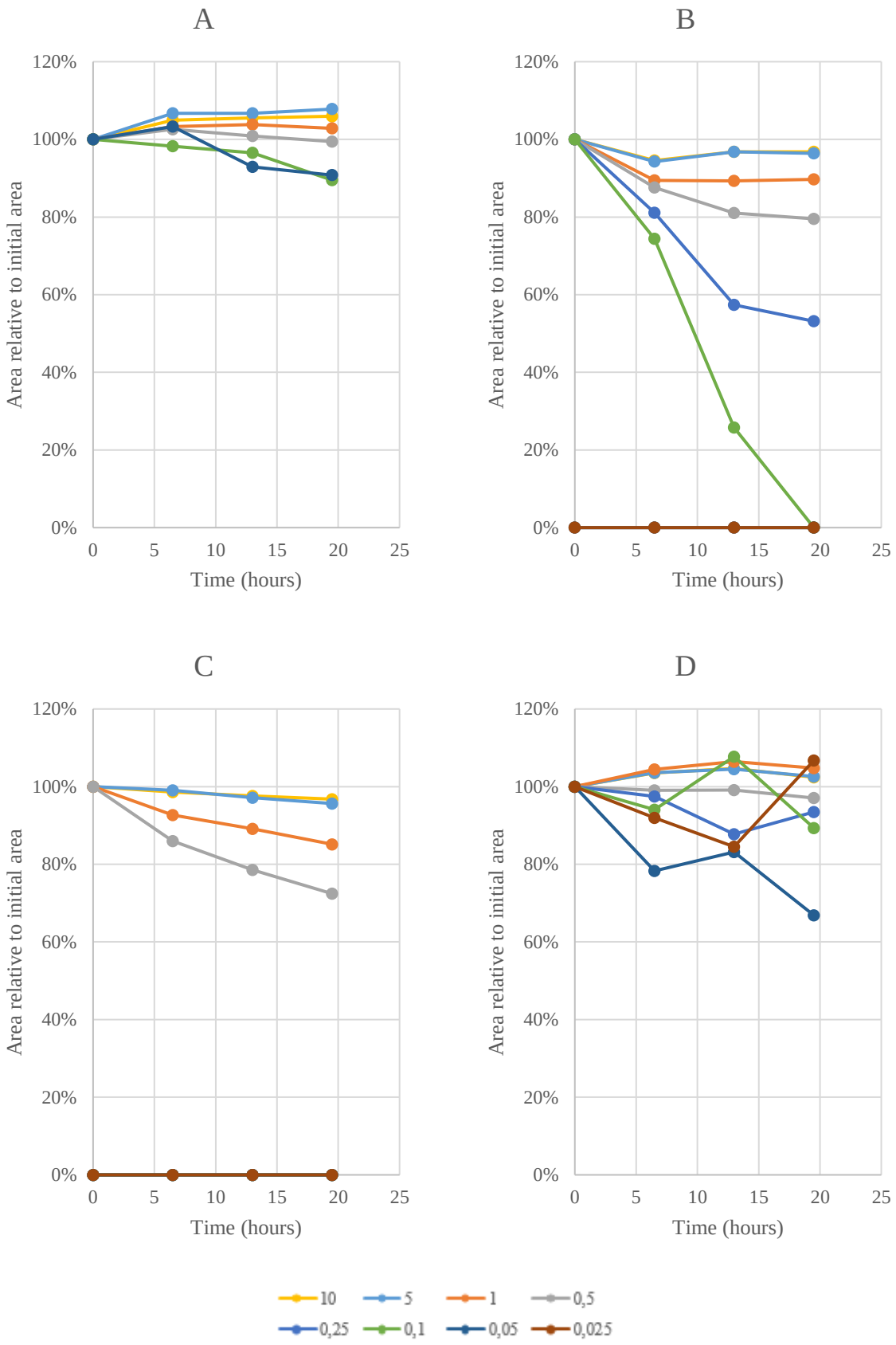

Figure 37 Area relative to the initial area (initial area not shown) for polymyxin E1 solutions at varying concentrations in different buffers, showing a concentration-dependent degradation of polymyxin E1. The concentrations of all buffers were 50 mM. A: Ammonium formate (pH apx. 3). B: PBS (pH 7.4). C: Tris (pH 7.2). D: Citric acid / Phosphate (pH 5.5)

The effect of the ammonium formate concentration was evaluated, and no significant difference was found between ammonium formate concentrations of 100, 150, and 200 mM (at pH 3). For details, see **Appendix I7** – Effect of different ammonium formate concentrations.

Ion suppression/enhancement caused by co-elution of ammonium formate and other salts was not of concern, as the retention time for both polymyxin E1 and polymyxin B1 were sufficiently higher than t_M. The lack of ion suppression/enhancement effects for polymyxin E1 can be seen clearly in **Figure 46** in **Appendix I6** – Matrix effects.

In summary, controlling the behavior of colistin with the 100 mM ammonium formate buffer enabled the partial validation of method B (according to the guidelines established by the EMA). The LOQ and calibration curve linearity was drastically improved from that achieved by using method A. Method B proved a vast superiority and should be of high relevance for further work on colistin.

6 FURTHER WORK

Further studies on the stability/adsorption of colistin should be conducted to see if other buffers or compounds can decrease the adsorption of colistin in a similar/better manner or aid in the stability of the compound. While it seems highly likely that the other subvariants of polymyxin E (2, 3, etc.) behave in a near-identical manner, extensive extrapolation should be avoided, and studies should be conducted to compare their behaviors.

While the work presented in this thesis showed that a 100 mM ammonium formate concentration reduced the adsorption of polymyxin E1, a lower concentration may be closer to the ideal. As described previously in this section, using ammonium formate during the preparation of the liposomes should also be looked at to reduce colistin adsorption at every step of the analytical pipeline that starts with the liposomal loading and culminates with the determination of the released colistin. It is worth noting that due to the high degree of structural similarity, polymyxin B1 may exhibit similar degradation/adsorption effects, which should be investigated before its use as an internal standard.

Minimizing the number of unsaturated surfaces in vials and Eppendorf tubes that colistin is free to interact with is of paramount importance when working with lower concentrations. The need to dialyze the pre-saturated mixture of liposomes and colistin could be mitigated by on-line SEC separation. In effect, this means colistin emerging from the liposomes would only interact with the LC system and the vial the fraction is collected within, before analysis, instead of requiring transfer from one container to another (increasing exposure to surfaces colistin may bind to). As the liposomes in this thesis were dissolved in a PBS/Tris buffer, adding a buffer to the SEC mobile phase should be considered to avoid osmotic shock of the liposomes. If possible, using ammonium formate in combination or instead of the PBS/Tris buffer should also be looked at for the sake of simplicity.

To assess whether liposomal encapsulation of colistin has a significant effect on nephrotoxicity, tentative studies on Human Renal Proximal Tubule Epithelial Cells (HRPTEpC) should be conducted to compare the toxicity of liposomal encapsulated versus free colistin. To do this, as presented in **Appendix A2** - Assessing colistin-induced renal damage and **B3** - The role of Kidney Injure Molecule 1 in the renal damage/repair process, concentrations of the highly viable biomarker, Kidney Injure Molecule 1 (KIM-1), should be carefully measured over time. To do this, as described in section **Appendix E** - Targeted proteomics, bottom-up proteomics should be utilized. Following this, if the results show a promising or vague effect, a more

thorough study should be conducted using the so-called organoids, highly representative micro-organs that provide a decent picture of how live human organs interact with various compounds, liposomally encapsulated or otherwise. These are described in **Appendix D** – Organoids as substitutes for *in vivo* trials.

Finally, release studies should be conducted to see if, and if so, how the released (free, aqueous) colistin relates to the nephrotoxicity that can be evaluated using the KIM-1 biomarker. In short, a bottom-up proteomics method for the detection of KIM-1 should be developed and used on renal cells (and eventually, organoids) to assess the colistin-induced nephrotoxicity and use this method to observe the actual effect of liposomal encapsulating colistin.

In summary, now that the behavior of colistin is under control and precise and accurate work with colistin can finally be conducted, further work on assessing liposomes as adequate colistin carriers should be performed, and the toxicity of colistin should be evaluated using cell cultures and organoids.

7 CONCLUDING REMARKS

While the primary goal of this thesis, to observe the release of polymyxin E1 from liposomal nanoparticles, was only partially achieved, the work presented has exposed the difficulties of working with colistin and the methods that must be used to negate these. The work conducted and presented stands as a reliable and solid platform for future research to build upon, working as a first step towards fully utilizing our dwindling last line of defense, colistin, for therapeutic use and to buy the precious time needed for alternative solutions to emerge.

Attempts to utilize UV and RI detection for the determination of polymyxin E1 and B1 rapidly revealed that these detectors had insufficient sensitivity for measuring low (< 10 µg/mL) concentrations of either polymyxin. While UV detection would be possible if a derivatization agent was used, this remained unfavorable as altering the structure of polymyxin E1 would most likely alter the release mechanics from liposomes and potentially give faulty release study indications. Mass spectrometry proved highly viable for the measurement of both polymyxins, however.

Liposome release studies were attempted but yielded inconclusive data. Additionally, while initially working with polymyxin E1, numerous attempts were made to produce and reproduce data, with a significant day-to-day variation. Solutions left on the benchtop overnight gave no signal the next day, and a literature search was promptly initiated in an attempt to discover what was happening. The literature revealed that colistin was readily adsorbed to surfaces and would readily degrade in aqueous solutions of non-acidic pH. This is what sparked the efforts to mitigate these mechanisms, as reliable quantification requires precise analyte control.

It was eventually discovered that ammonium formate (100mM, pH 3-4) was sufficient to stabilize polymyxin E1 and drastically reduce surface adsorption. Following this novel discovery, the method was validated to the extent the available resources made possible. While temporal and logistical constraints rendered it impossible to conduct a third and thorough liposome release study of polymyxin E1, the work presented here instead offers a reliable, accurate platform for further research to build upon where the unfortunate behavior of polymyxin E1 is taken into account and effectively mitigated.

Outbreaks of MDR gram-negative bacteria have already spread like wildfire. As recent as 2013, Sally Davies, the chief medical officer of the United Kingdom, described CREs as a risk as

serious as terrorism [177]. The threat is now, and as described by a CDC report from 2013, the potential consequences remain nothing short but “catastrophic” [178]. As previously stated, polymyxins are currently our very last line of defense against these gram-negative bacteria [179]. This work provides a reliable and solid foundation for analytical work with colistin and highlights some of the challenges ahead. More research is critical to prevent the joint return to the pre-antibiotic era, where even paper cuts could prove fatal.

8 SOURCES

1. Aminov, R., *A Brief History of the Antibiotic Era: Lessons Learned and Challenges for the Future.* Frontiers in Microbiology, 1 (**2010**).
2. Nikaido, H., *Antibiotic Resistance Caused by Gram-Negative Multidrug Efflux Pumps.* Clinical Infectious Diseases, 27 (**1998**) S32-S41.
3. Wright, G.D., *Resisting resistance: new chemical strategies for battling superbugs.* Chemistry & Biology, 7 (**2000**) R127-R132.
4. Nordmann, P., T. Naas, N. Fortineau, and L. Poirel, *Superbugs in the coming new decade; multidrug resistance and prospects for treatment of Staphylococcus aureus, Enterococcus spp. and Pseudomonas aeruginosa in 2010.* Current Opinion in Microbiology, 10 (**2007**) 436-440.
5. Baron, S., *Medical Microbiology*. (**1996**): University of Texas Medical Branch at Galveston.
6. Silhavy, T.J., D. Kahne, and S. Walker, *The bacterial cell envelope.* Cold Spring Harbor perspectives in biology, 2 (**2010**) a000414-a000414.
7. Lüderitz, O., M.A. Freudenberg, C. Galanos, V. Lehmann, E.T. Rietschel, and D.H. Shaw, *Lipopolysaccharides of Gram-Negative Bacteria*, in *Current Topics in Membranes and Transport*, F. Bronner and A. Kleinteller, Editors. (**1982**), Academic Press. 79-151.
8. Ulevitch, R.J. and P.S. Tobias, *Recognition of Gram-negative bacteria and endotoxin by the innate immune system.* Current Opinion in Immunology, 11 (**1999**) 19-22.
9. Breijyeh, Z., B. Jubeh, and R. Karaman, *Resistance of Gram-Negative Bacteria to Current Antibacterial Agents and Approaches to Resolve It.* Molecules, 25 (**2020**) 1340.
10. *BioRender*. (**2020**); Available from: https://biorender.com/.
11. Zhang, R., K. Eggleston, V. Rotimi, and R.J. Zeckhauser, *Antibiotic resistance as a global threat: Evidence from China, Kuwait and the United States.* Globalization and Health, 2 (**2006**) 6.
12. Falagas, M.E. and P.I. Rafailidis, *When to include polymyxins in the empirical antibiotic regimen in critically ill patients with fever? A decision analysis approach.* Shock, 27 (**2007**) 605-609.
13. Lu, T.K. and M.S. Koeris, *The next generation of bacteriophage therapy.* Current Opinion in Microbiology, 14 (**2011**) 524-531.
14. Kosikowska, P. and A. Lesner, *Antimicrobial peptides (AMPs) as drug candidates: a patent review (2003–2015).* Expert Opinion on Therapeutic Patents, 26 (**2016**) 689-702.
15. Zhang, L.-j. and R.L. Gallo, *Antimicrobial peptides.* Current Biology, 26 (**2016**) R14-R19.
16. Butaye, P. and C. Wang, *Colistin resistance, beyond the current knowledge.* EBioMedicine, 34 (**2018**) 16-17.
17. Zasloff, M., *Antimicrobial peptides of multicellular organisms.* Nature, 415 (**2002**) 389-395.
18. Velkov, T., K.D. Roberts, R.L. Nation, J. Wang, P.E. Thompson, and J. Li, *Teaching 'Old' Polymyxins New Tricks: New-Generation Lipopeptides Targeting Gram-Negative 'Superbugs'.* ACS Chemical Biology, 9 (**2014**) 1172-1177.
19. Paterson, D.L. and P.N.A. Harris, *Colistin resistance: a major breach in our last line of defence.* The Lancet Infectious Diseases, 16 (**2016**) 132-133.

20. Falagas, M.E., S.K. Kasiakou, and L.D. Saravolatz, *Colistin: The Revival of Polymyxins for the Management of Multidrug-Resistant Gram-Negative Bacterial Infections.* Clinical Infectious Diseases, 40 (**2005**) 1333-1341.
21. Conly, J.M. and B.L. Johnston, *Colistin: The phoenix Arises.* Canadian Journal of Infectious Diseases and Medical Microbiology, 17 (**2006**) 901873.
22. Sun, J., H. Zhang, Y.-H. Liu, and Y. Feng, *Towards Understanding MCR-like Colistin Resistance.* Trends in Microbiology, 26 (**2018**) 794-808.
23. Shaheen, M., J. Li, Avena C. Ross, John C. Vederas, and Susan E. Jensen, *Paenibacillus polymyxa PKB1 Produces Variants of Polymyxin B-Type Antibiotics.* Chemistry & Biology, 18 (**2011**) 1640-1648.
24. Kwa, A., S.K. Kasiakou, V.H. Tam, and M.E. Falagas, *Polymyxin B: similarities to and differences from colistin (polymyxin E).* Expert Review of Anti-infective Therapy, 5 (**2007**) 811-821.
25. Yu, Z., W. Qin, J. Lin, S. Fang, and J. Qiu, *Antibacterial Mechanisms of Polymyxin and Bacterial Resistance.* BioMed Research International, 2015 (**2015**) 679109.
26. Vogler, K. and R.O. Studer, *The chemistry of the polymyxin antibiotics.* Experientia, 22 (**1966**) 345-354.
27. Martin, N.I., H. Hu, M.M. Moake, J.J. Churey, R. Whittal, R.W. Worobo, and J.C. Vederas, *Isolation, Structural Characterization, and Properties of Mattacin (Polymyxin M), a Cyclic Peptide Antibiotic Produced by Paenibacillus kobensis M*.* Journal of Biological Chemistry, 278 (**2003**) 13124-13132.
28. Bibi, M., S. Murphy, R.I. Benhamou, A. Rosenberg, A. Ulman, T. Bicanic, M. Fridman, and J. Berman, *Combining Colistin and Fluconazole Synergistically Increases Fungal Membrane Permeability and Antifungal Cidality.* ACS Infectious Diseases, 7 (**2021**) 377-389.
29. Lewis, J.R. and S.A. Lewis, *Colistin interactions with the mammalian urothelium.* American Journal of Physiology-Cell Physiology, 286 (**2004**) C913-C922.
30. van der Voort, P.H.J. and H.K.F. van Saene, *Selective Digestive Tract Decontamination in Intensive Care Medicine: a Practical Guide to Controlling Infection*. (**2008**): Springer Milan.
31. Azzopardi, E.A., E.L. Ferguson, and D.W. Thomas, *Colistin past and future: A bibliographic analysis.* Journal of Critical Care, 28 (**2013**) 219.e13-219.e19.
32. Gupta, S., D. Govil, P.N. Kakar, O. Prakash, D. Arora, S. Das, P. Govil, and A. Malhotra, *Colistin and polymyxin B: a re-emergence.* Indian Journal of Critical Care Medicine, 13 (**2009**) 49-53.
33. Gai, Z., S.L. Samodelov, G.A. Kullak-Ublick, and M. Visentin, *Molecular Mechanisms of Colistin-Induced Nephrotoxicity.* Molecules, 24 (**2019**).
34. Nation, R.L. and J. Li, *Colistin in the 21st century.* Current Opinion in Infectious Diseases, 22 (**2009**) 535-543.
35. WHO, *Critically Important Antimicrobials For Human Medicine—3rd Revision 2011*. (**2012**), World Health Organization Geneva, Switzerland.
36. *Salvage Therapy (n.d.)*, in *Gale Encyclopedia of Medicine*. (**2008**).
37. Kallel, H., M. Bahloul, L. Hergafi, M. Akrout, W. Ketata, H. Chelly, C.B. Hamida, N. Rekik, A. Hammami, and M. Bouaziz, *Colistin as a salvage therapy for nosocomial infections caused by multidrug-resistant bacteria in the ICU.* International Journal of Antimicrobial Agents, 28 (**2006**) 366-369.
38. Landman, D., C. Georgescu, D.A. Martin, and J. Quale, *Polymyxins Revisited.* Clinical Microbiology Reviews, 21 (**2008**) 449-465.

39. Wallace, S.J., J. Li, R.L. Nation, R.J. Prankerd, and B.J. Boyd, *Interaction of Colistin and Colistin Methanesulfonate with Liposomes: Colloidal Aspects and Implications for Formulation.* Journal of Pharmaceutical Sciences, 101 (**2012**) 3347-3359.
40. Cai, Y., W. Lee, and A.L. Kwa, *Polymyxin B versus colistin: an update.* Expert Review of Anti-infective Therapy, 13 (**2015**) 1481-1497.
41. Jennifer A. Orwa, C.G., Roger Busson, Eugene Roets, Ann Van Schepdael, Jos Hoogmartens, *Isolation and Structural Characterization of Colistin Components.* The Journal of Antibiotics, 54 (**2001**) 595-599.
42. Nation, R.L. and J. Li, *Polymyxins*, in *Kucers the Use of Antibiotics: A Clinical Review of Antibacterial, Antifungal, Antiparasitic, and Antiviral Drugs*. (**2017**), CRC Press. 1420-1449.
43. Bergen, P.J., J. Li, C.R. Rayner, and R.L. Nation, *Colistin Methanesulfonate Is an Inactive Prodrug of Colistin against Pseudomonas aeruginosa.* Antimicrobial Agents and Chemotherapy, 50 (**2006**) 1953-1958.
44. Lim, L.M., N. Ly, D. Anderson, J.C. Yang, L. Macander, A. Jarkowski III, A. Forrest, J.B. Bulitta, and B.T. Tsuji, *Resurgence of Colistin: A Review of Resistance, Toxicity, Pharmacodynamics, and Dosing.* Pharmacotherapy: The Journal of Human Pharmacology and Drug Therapy, 30 (**2010**) 1279-1291.
45. Spapen, H., R. Jacobs, V. Van Gorp, J. Troubleyn, and P.M. Honoré, *Renal and neurological side effects of colistin in critically ill patients.* Annals of intensive care, 1 (**2011**) 14-14.
46. Paterson, D.L., *Serious Infections in the Intensive Care Unit: Pseudomonas aeruginosa and Acinetobacter baumannii.* Clinical Infectious Diseases, 43 (**2006**) S41-S42.
47. Nation, R.L., S.M. Garonzik, V. Thamlikitkul, E.J. Giamarellos-Bourboulis, A. Forrest, D.L. Paterson, J. Li, and F.P. Silveira, *Dosing guidance for intravenous colistin in critically-ill patients.* Clin Infect Dis, 64 (**2017**) 565-571.
48. Tsuji, B.T., J.M. Pogue, A.P. Zavascki, M. Paul, G.L. Daikos, A. Forrest, D.R. Giacobbe, C. Viscoli, H. Giamarellou, I. Karaiskos, D. Kaye, J.W. Mouton, V.H. Tam, V. Thamlikitkul, R.G. Wunderink, J. Li, R.L. Nation, and K.S. Kaye, *International Consensus Guidelines for the Optimal Use of the Polymyxins: Endorsed by the American College of Clinical Pharmacy (ACCP), European Society of Clinical Microbiology and Infectious Diseases (ESCMID), Infectious Diseases Society of America (IDSA), International Society for Anti-infective Pharmacology (ISAP), Society of Critical Care Medicine (SCCM), and Society of Infectious Diseases Pharmacists (SIDP).* Pharmacotherapy: The Journal of Human Pharmacology and Drug Therapy, 39 (**2019**) 10-39.
49. Li, J., R.L. Nation, J.D. Turnidge, R.W. Milne, K. Coulthard, C.R. Rayner, and D.L. Paterson, *Colistin: the re-emerging antibiotic for multidrug-resistant Gram-negative bacterial infections.* The Lancet Infectious Diseases, 6 (**2006**) 589-601.
50. Biswas, S., J.-M. Brunel, J.-C. Dubus, M. Reynaud-Gaubert, and J.-M. Rolain, *Colistin: an update on the antibiotic of the 21st century.* Expert Review of Anti-infective Therapy, 10 (**2012**) 917-934.
51. Weterings, V., K. Zhou, J.W. Rossen, D. van Stenis, E. Thewessen, J. Kluytmans, and J. Veenemans, *An outbreak of colistin-resistant Klebsiella pneumoniae carbapenemase-producing Klebsiella pneumoniae in the Netherlands (July to December 2013), with inter-institutional spread.* European Journal of Clinical Microbiology & Infectious Diseases, 34 (**2015**) 1647-1655.

52. Ebrahimi, S., B. Sisakhtpour, A. Mirzaei, V. Karbasizadeh, and S. Moghim, *Efficacy of isolated bacteriophage against biofilm embedded colistin-resistant Acinetobacter baumannii.* Gene Reports, 22 (**2021**) 100984.
53. Shen, Y., R. Zhang, S. Schwarz, C. Wu, J. Shen, T.R. Walsh, and Y. Wang, *Farm animals and aquaculture: significant reservoirs of mobile colistin resistance genes.* Environmental Microbiology, 22 (**2020**) 2469-2484.
54. Huang, X., L. Yu, X. Chen, C. Zhi, X. Yao, Y. Liu, S. Wu, Z. Guo, L. Yi, Z. Zeng, and J.-H. Liu, *High Prevalence of Colistin Resistance and mcr-1 Gene in Escherichia coli Isolated from Food Animals in China.* Frontiers in Microbiology, 8 (**2017**).
55. Liu, Y.-Y., Y. Wang, T.R. Walsh, L.-X. Yi, R. Zhang, J. Spencer, Y. Doi, G. Tian, B. Dong, X. Huang, L.-F. Yu, D. Gu, H. Ren, X. Chen, L. Lv, D. He, H. Zhou, Z. Liang, J.-H. Liu, and J. Shen, *Emergence of plasmid-mediated colistin resistance mechanism MCR-1 in animals and human beings in China: a microbiological and molecular biological study.* The Lancet Infectious Diseases, 16 (**2016**) 161-168.
56. Walsh, T.R. and Y. Wu, *China bans colistin as a feed additive for animals.* The Lancet Infectious Diseases, 16 (**2016**) 1102-1103.
57. Reardon, S., *Resistance to last-ditch antibiotic has spread farther than anticipated.* Nature news, (**2017**).
58. Olaitan, A.O., I. Dandachi, S.A. Baron, Z. Daoud, S. Morand, and J.-M. Rolain, *Banning colistin in feed additives: a small step in the right direction.* The Lancet Infectious Diseases, 21 (**2021**) 29-30.
59. Schwarz, S. and A.P. Johnson, *Transferable resistance to colistin: a new but old threat.* Journal of Antimicrobial Chemotherapy, 71 (**2016**) 2066-2070.
60. Ma, G., Y. Zhu, Z. Yu, A. Ahmad, and H. Zhang, *High resolution crystal structure of the catalytic domain of MCR-1.* Scientific reports, 6 (**2016**) 39540-39540.
61. Zhang, J., J. Wang, L. Chen, A.K. Yassin, P. Kelly, P. Butaye, J. Li, J. Gong, R. Cattley, K. Qi, and C. Wang, *Housefly (Musca domestica) and Blow Fly (Protophormia terraenovae) as Vectors of Bacteria Carrying Colistin Resistance Genes.* Applied and Environmental Microbiology, 84 (**2018**) e01736-17.
62. Franklin, A.B., A.M. Ramey, K.T. Bentler, N.L. Barrett, L.M. McCurdy, C.A. Ahlstrom, J. Bonnedahl, S.A. Shriner, and J.C. Chandler, *Gulls as Sources of Environmental Contamination by Colistin-resistant Bacteria.* Scientific Reports, 10 (**2020**) 4408.
63. Janssen, A.B. and W. van Schaik, *Harder, better, faster, stronger: Colistin resistance mechanisms in Escherichia coli.* PLOS Genetics, 17 (**2021**) e1009262.
64. Dijkmans, A.C., E.B. Wilms, I.M.C. Kamerling, W. Birkhoff, N.V. Ortiz-Zacarías, C. van Nieuwkoop, H.A. Verbrugh, and D.J. Touw, *Colistin: Revival of an Old Polymyxin Antibiotic.* Therapeutic Drug Monitoring, 37 (**2015**) 419-427.
65. Hancock, R.E.W., *Cationic antimicrobial peptides: towards clinical applications.* Expert Opinion on Investigational Drugs, 9 (**2000**) 1723-1729.
66. ŞENTÜRK, S., *Evaluation of the anti-endotoxic effects of polymyxin-E (colistin) in dogs with naturally occurred endotoxic shock.* Journal of Veterinary Pharmacology and Therapeutics, 28 (**2005**) 57-63.
67. Matzneller, P., S. Strommer, C. Drucker, K. Petroczi, C. Schörgenhofer, E. Lackner, B. Jilma, and M. Zeitlinger, *Colistin Reduces LPS-Triggered Inflammation in a Human Sepsis Model In Vivo: A Randomized Controlled Trial.* Clinical Pharmacology & Therapeutics, 101 (**2017**) 773-781.
68. Gough, M., R.E. Hancock, and N.M. Kelly, *Antiendotoxin activity of cationic peptide antimicrobial agents.* Infection and Immunity, 64 (**1996**) 4922-4927.

69. Ordooei Javan, A., S. Shokouhi, and Z. Sahraei, *A review on colistin nephrotoxicity.* European Journal of Clinical Pharmacology, 71 (**2015**) 801-810.
70. Pajouhesh, H. and G.R. Lenz, *Medicinal chemical properties of successful central nervous system drugs.* NeuroRX, 2 (**2005**) 541-553.
71. Sweet, D.H. and J.B. Pritchard, *The molecular biology of renal organic anion and organic cation transporters.* Cell Biochemistry and Biophysics, 31 (**1999**) 89-118.
72. Hancock, R.E.W., *Peptide antibiotics.* The Lancet, 349 (**1997**) 418-422.
73. Eadon, M.T., B.K. Hack, J.J. Alexander, C. Xu, M.E. Dolan, and P.N. Cunningham, *Cell cycle arrest in a model of colistin nephrotoxicity.* Physiological Genomics, 45 (**2013**) 877-888.
74. Henry, S., S. Kohlwein, and G. Carman, *Metabolism and Regulation of Glycerolipids in the Yeast Saccharomyces cerevisiae.* Genetics, 190 (**2012**) 317-49.
75. Bretscher, M.S., *The Molecules of the Cell Membrane.* Scientific American, 253 (**1985**) 100-109.
76. Lee, A. and A.P. Moran, *Lipopolysaccharide (LPS)-related damage by H. pylori*, in *Helicobacter pylori: Basic Mechanisms to Clinical Cure*, R.H. Hunt and G.N.J. Tytgat, Editors. (**1994**), Springer Netherlands: Dordrecht. 169-179.
77. Hermsen, E.D., C.J. Sullivan, and J.C. Rotschafer, *Polymyxins:: Pharmacology, pharmacokinetics, pharmacodynamics, and clinical applications.* Infectious Disease Clinics of North America, 17 (**2003**) 545-562.
78. Mohamed, Y.F., H.M. Abou-Shleib, A.M. Khalil, N.M. El-Guink, and M.A. El-Nakeeb, *Membrane permeabilization of colistin toward pan-drug resistant Gram-negative isolates.* Brazilian Journal of Microbiology, 47 (**2016**) 381-388.
79. Yahav, D., L. Farbman, L. Leibovici, and M. Paul, *Colistin: new lessons on an old antibiotic.* Clinical Microbiology and Infection, 18 (**2012**) 18-29.
80. Witherell, K.S., J. Price, A.D. Bandaranayake, J. Olson, and D.R. Call, *In vitro activity of antimicrobial peptide CDP-B11 alone and in combination with colistin against colistin-resistant and multidrug-resistant Escherichia coli.* Scientific Reports, 11 (**2021**) 2151.
81. Zavascki, A.P., L.Z. Goldani, J. Li, and R.L. Nation, *Polymyxin B for the treatment of multidrug-resistant pathogens: a critical review.* Journal of Antimicrobial Chemotherapy, 60 (**2007**) 1206-1215.
82. Dupuy, F.G., I. Pagano, K. Andenoro, M.F. Peralta, Y. Elhady, F. Heinrich, and S. Tristram-Nagle, *Selective Interaction of Colistin with Lipid Model Membranes.* Biophysical Journal, 114 (**2018**) 919-928.
83. Knopp, M., A.M. Babina, J.S. Gudmundsdóttir, M.V. Douglass, M.S. Trent, and D.I. Andersson, *A novel type of colistin resistance genes selected from random sequence space.* PLOS Genetics, 17 (**2021**) e1009227.
84. Mouritsen, O.G. and M.J. Zuckermann, *What's so special about cholesterol?* Lipids, 39 (**2004**) 1101-13.
85. Dai, C., J. Li, and J. Li, *New insight in colistin induced neurotoxicity with the mitochondrial dysfunction in mice central nervous tissues.* Experimental and Toxicologic Pathology, 65 (**2013**) 941-948.
86. Dai, C., J. Li, S. Tang, J. Li, and X. Xiao, *Colistin-Induced Nephrotoxicity in Mice Involves the Mitochondrial, Death Receptor, and Endoplasmic Reticulum Pathways.* Antimicrobial Agents and Chemotherapy, 58 (**2014**) 4075-4085.
87. Lee, B.K., Y.H. Yun, and K. Park, *Smart Nanoparticles for Drug Delivery: Boundaries and Opportunities.* Chem Eng Sci, 125 (**2015**) 158-164.

88. Abed, N. and P. Couvreur, *Nanocarriers for antibiotics: A promising solution to treat intracellular bacterial infections.* International Journal of Antimicrobial Agents, 43 (**2014**) 485-496.
89. Kataria, S., P. Sandhu, A. Bilandi, M. Akanksha, and B. Kapoor, *Stealth liposomes: a review.* International Journal of Research in Ayurveda & Pharmacy, 2 (**2011**).
90. Cattel, L., M. Ceruti, and F. Dosio, *From Conventional to Stealth Liposomes: a New Frontier in Cancer Chemotherapy.* Journal of Chemotherapy, 16 (**2004**) 94-97.
91. Barenholz, Y., D. Gibbes, B.J. Litman, J. Goll, T.E. Thompson, and F.D. Carlson, *A simple method for the preparation of homogeneous phospholipid vesicles.* Biochemistry, 16 (**1977**) 2806-2810.
92. Huang, C., *Studies on phosphatidylcholine vesicles. Formation and physical characteristics.* Biochemistry, 8 (**1969**) 344-352.
93. Szoka, F. and D. Papahadjopoulos, *Procedure for preparation of liposomes with large internal aqueous space and high capture by reverse-phase evaporation.* Proceedings of the National Academy of Sciences, 75 (**1978**) 4194-4198.
94. Vemuri, S. and C.T. Rhodes, *Preparation and characterization of liposomes as therapeutic delivery systems: a review.* Pharmaceutica Acta Helvetiae, 70 (**1995**) 95-111.
95. Hunt, C.A. and D.P. Papahadjopoulous, *Method for producing liposomes in selected size range*. (**1985**), Google Patents.
96. Mayer, L.D., M.J. Hope, and P.R. Cullis, *Vesicles of variable sizes produced by a rapid extrusion procedure.* Biochimica et Biophysica Acta (BBA) - Biomembranes, 858 (**1986**) 161-168.
97. Morano, F.J.M.K., *Liposome extrusion method*, L.T. Inc, Editor. (**1986**), Liposome Technology Inc: United States.
98. Olson, F., C.A. Hunt, F.C. Szoka, W.J. Vail, and D. Papahadjopoulos, *Preparation of liposomes of defined size distribution by extrusion through polycarbonate membranes.* Biochimica et Biophysica Acta (BBA) - Biomembranes, 557 (**1979**) 9-23.
99. Ruf, H., Y. Georgalis, and E. Grell, *Dynamic laser light scattering to determine size distributions of vesicles*, in *Methods in Enzymology*. (**1989**), Academic Press. 364-390.
100. Ruozi, B., G. Tosi, F. Forni, M. Fresta, and M.A. Vandelli, *Atomic force microscopy and photon correlation spectroscopy: Two techniques for rapid characterization of liposomes.* European Journal of Pharmaceutical Sciences, 25 (**2005**) 81-89.
101. Frederik, P.M. and D.H.W. Hubert, *Cryoelectron Microscopy of Liposomes*, in *Methods in Enzymology*. (**2005**), Academic Press. 431-448.
102. Jass, J., T. Tjärnhage, and G. Puu, *Atomic Force Microscopy Imaging of Liposomes*, in *Methods in Enzymology*. (**2003**), Academic Press. 199-213.
103. Edwards, K.A. and A.J. Baeumner, *Analysis of liposomes.* Talanta, 68 (**2006**) 1432-1441.
104. McCracken, M.S. and M.C. Sammons, *Sizing of a Vesicle Drug Formulation by Quasi-Elastic Light Scattering and Comparison with Electron Microscopy and Ultracentrifugation.* Journal of Pharmaceutical Sciences, 76 (**1987**) 56-59.
105. Arifin, D.R. and A.F. Palmer, *Determination of Size Distribution and Encapsulation Efficiency of Liposome-Encapsulated Hemoglobin Blood Substitutes Using Asymmetric Flow Field-Flow Fractionation Coupled with Multi-Angle Static Light Scattering.* Biotechnology Progress, 19 (**2003**) 1798-1811.
106. Korgel, B.A., J.H. van Zanten, and H.G. Monbouquette, *Vesicle Size Distributions Measured by Flow Field-Flow Fractionation Coupled with Multiangle Light Scattering.* Biophysical Journal, 74 (**1998**) 3264-3272.

107. Jose Chirayil, C., J. Abraham, R. Kumar Mishra, S.C. George, and S. Thomas, *Chapter 1 - Instrumental Techniques for the Characterization of Nanoparticles*, in *Thermal and Rheological Measurement Techniques for Nanomaterials Characterization*, S. Thomas, et al., Editors. (**2017**), Elsevier. 1-36.
108. Grabielle-Madelmont, C., S. Lesieur, and M. Ollivon, *Characterization of loaded liposomes by size exclusion chromatography.* Journal of Biochemical and Biophysical Methods, 56 (**2003**) 189-217.
109. Lundahl, P., C.-M. Zeng, C. Lagerquist Hägglund, I. Gottschalk, and E. Greijer, *Chromatographic approaches to liposomes, proteoliposomes and biomembrane vesicles.* Journal of Chromatography B: Biomedical Sciences and Applications, 722 (**1999**) 103-120.
110. Lesieur, S., C. Grabielle-Madelmont, M. Paternostre, and M. Ollivon, *Study of size distribution and stability of liposomes by high performance gel exclusion chromatography.* Chemistry and Physics of Lipids, 64 (**1993**) 57-82.
111. Nguyen, D.T.-T., D. Guillarme, S. Rudaz, and J.-L. Veuthey, *Fast analysis in liquid chromatography using small particle size and high pressure.* Journal of Separation Science, 29 (**2006**) 1836-1848.
112. Fekete, S., J. Schappler, J.-L. Veuthey, and D. Guillarme, *Current and future trends in UHPLC.* TrAC Trends in Analytical Chemistry, 63 (**2014**) 2-13.
113. Altmaier, S. and K. Cabrera, *Structure and performance of silica-based monolithic HPLC columns.* Journal of Separation Science, 31 (**2008**) 2551-2559.
114. Tanaka, N., H. Kobayashi, N. Ishizuka, H. Minakuchi, K. Nakanishi, K. Hosoya, and T. Ikegami, *Monolithic silica columns for high-efficiency chromatographic separations.* Journal of Chromatography A, 965 (**2002**) 35-49.
115. Lam, S.C., E. Sanz Rodriguez, P.R. Haddad, and B. Paull, *Recent advances in open tubular capillary liquid chromatography.* Analyst, 144 (**2019**) 3464-3482.
116. Mori, S. and H.G. Barth, *Size Exclusion Chromatography*. (**2013**): Springer Berlin Heidelberg.
117. Daniel C. Harris, C.A.L., *Quantitative Chemical Analysis*. 9 ed. (**2016**): W.H. Freeman and Company.
118. Snyder, L.R., J.J. Kirkland, and J.W. Dolan, *Introduction to Modern Liquid Chromatography*. (**2011**): Wiley.
119. Moldoveanu, S.C. and V. David, *Essentials in Modern HPLC Separations*. (**2012**): Elsevier Science.
120. Buszewski, B. and S. Noga, *Hydrophilic interaction liquid chromatography (HILIC)—a powerful separation technique.* Analytical and Bioanalytical Chemistry, 402 (**2012**) 231-247.
121. Yang, Y., H. Li, Z. Li, Y. Zhang, S. Zhang, Y. Chen, M. Yu, G. Ma, and Z. Su, *Size-exclusion HPLC provides a simple, rapid, and versatile alternative method for quality control of vaccines by characterizing the assembly of antigens.* Vaccine, 33 (**2015**) 1143-1150.
122. Zabidi, M.S., R. Abu Bakar, N. Musa, and W.N. Wan Yusuf, *Analytical methodologies for measuring colistin levels in pharmacokinetic studies.* Journal of Liquid Chromatography & Related Technologies, 43 (**2020**) 671-686.
123. Liu, T., C. Zhang, F. Zhang, B. Nie, F. Yuan, H. Huang, and H. Li, *Sensitive Determination of Four Polypeptide Antibiotic Residues in Milk Powder by High Performance Liquid Chromatography–Electrospray Tandem Mass Spectrometry.* Chromatographia, 82 (**2019**) 1479-1487.

124. Ma, Z., J. Wang, J.P. Gerber, and R.W. Milne, *Determination of colistin in human plasma, urine and other biological samples using LC–MS/MS.* Journal of Chromatography B, 862 (**2008**) 205-212.
125. Wan, E.C.-h., C. Ho, D.W.-m. Sin, and Y.-c. Wong, *Detection of residual bacitracin A, colistin A, and colistin B in milk and animal tissues by liquid chromatography tandem mass spectrometry.* Analytical and Bioanalytical Chemistry, 385 (**2006**) 181-188.
126. Jansson, B., M. Karvanen, O. Cars, D. Plachouras, and L.E. Friberg, *Quantitative analysis of colistin A and colistin B in plasma and culture medium using a simple precipitation step followed by LC/MS/MS.* Journal of Pharmaceutical and Biomedical Analysis, 49 (**2009**) 760-767.
127. Fu, Q., X. Li, K. Zheng, Y. Ke, Y. Wang, L. Wang, F. Yu, and X. Xia, *Determination of colistin in animal tissues, egg, milk, and feed by ultra-high performance liquid chromatography-tandem mass spectrometry.* Food Chemistry, 248 (**2018**) 166-172.
128. Dotsikas, Y., C.K. Markopoulou, J.E. Koundourellis, and Y.L. Loukas, *Validation of a novel LC-MS/MS method for the quantitation of colistin A and B in human plasma.* Journal of Separation Science, 34 (**2011**) 37-45.
129. Cangemi, G., S. Barco, E. Castagnola, G. Tripodi, F. Favata, and A. D'Avolio, *Development and validation of UHPLC–MS/MS methods for the quantification of colistin in plasma and dried plasma spots.* Journal of Pharmaceutical and Biomedical Analysis, 129 (**2016**) 551-557.
130. Gobin, P., F. Lemaître, S. Marchand, W. Couet, and J.-C. Olivier, *Assay of Colistin and Colistin Methanesulfonate in Plasma and Urine by Liquid Chromatography-Tandem Mass Spectrometry.* Antimicrobial Agents and Chemotherapy, 54 (**2010**) 1941-1948.
131. Mercier, T., F. Tissot, C. Gardiol, N. Corti, S. Wehrli, M. Guidi, C. Csajka, T. Buclin, W. Couet, O. Marchetti, and L.A. Decosterd, *High-throughput hydrophilic interaction chromatography coupled to tandem mass spectrometry for the optimized quantification of the anti-Gram-negatives antibiotic colistin A/B and its pro-drug colistimethate.* Journal of Chromatography A, 1369 (**2014**) 52-63.
132. Xu, Y., X. Tian, C. Ren, H. Huang, X. Zhang, X. Gong, H. Liu, Z. Yu, and L. Zhang, *Analysis of colistin A and B in fishery products by ultra performance liquid chromatography with positive electrospray ionization tandem mass spectrometry.* Journal of Chromatography B, 899 (**2012**) 14-20.
133. Tsai, I.L., H.-Y. Sun, G.-Y. Chen, S.-W. Lin, and C.-H. Kuo, *Simultaneous quantification of antimicrobial agents for multidrug-resistant bacterial infections in human plasma by ultra-high-pressure liquid chromatography–tandem mass spectrometry.* Talanta, 116 (**2013**) 593-603.
134. Gikas, E., F.N. Bazoti, M. Katsimardou, D. Anagnostopoulos, K. Papanikolaou, I. Inglezos, A. Skoutelis, G.L. Daikos, and A. Tsarbopoulos, *Determination of colistin A and colistin B in human plasma by UPLC–ESI high resolution tandem MS: Application to a pharmacokinetic study.* Journal of Pharmaceutical and Biomedical Analysis, 83 (**2013**) 228-236.
135. Mann, M., C.K. Meng, and J.B. Fenn, *Interpreting mass spectra of multiply charged ions.* Analytical Chemistry, 61 (**1989**) 1702-1708.
136. Loo, J.A., C.G. Edmonds, and R.D. Smith, *Tandem mass spectrometry of very large molecules: serum albumin sequence information from multiply charged ions formed by electrospray ionization.* Analytical chemistry, 63 (**1991**) 2488-2499.
137. Pitt, J.J., *Principles and applications of liquid chromatography-mass spectrometry in clinical biochemistry.* The Clinical biochemist. Reviews, 30 (**2009**) 19-34.

138. Fenn, J.B., *Electrospray Wings for Molecular Elephants (Nobel Lecture).* Angewandte Chemie International Edition, 42 (**2003**) 3871-3894.
139. Kebarle, P. and U.H. Verkerk, *Electrospray: From ions in solution to ions in the gas phase, what we know now.* Mass Spectrometry Reviews, 28 (**2009**) 898-917.
140. Cech, N.B. and C.G. Enke, *Practical implications of some recent studies in electrospray ionization fundamentals.* Mass Spectrometry Reviews, 20 (**2001**) 362-387.
141. Loo, J.A., *Electrospray ionization mass spectrometry: a technology for studying noncovalent macromolecular complexes.* International Journal of Mass Spectrometry, 200 (**2000**) 175-186.
142. Van Berkel, G.J., G.E. Giles, Bullock, and L.J. Gray, *Computational Simulation of Redox Reactions within a Metal Electrospray Emitter.* Analytical Chemistry, 71 (**1999**) 5288-5296.
143. Van Berkel, G.J. and F. Zhou, *Characterization of an Electrospray Ion Source as a Controlled-Current Electrolytic Cell.* Analytical Chemistry, 67 (**1995**) 2916-2923.
144. Benassi, M., C. Wu, M. Nefliu, D.R. Ifa, M. Volný, and R.G. Cooks, *Redox transformations in desorption electrospray ionization.* International Journal of Mass Spectrometry, 280 (**2009**) 235-240.
145. Amad, M.a.H., N.B. Cech, G.S. Jackson, and C.G. Enke, *Importance of gas-phase proton affinities in determining the electrospray ionization response for analytes and solvents.* Journal of Mass Spectrometry, 35 (**2000**) 784-789.
146. Schmidt, A., M. Karas, and T. Dülcks, *Effect of different solution flow rates on analyte ion signals in nano-ESI MS, or: when does ESI turn into nano-ESI?* Journal of the American Society for Mass Spectrometry, 14 (**2003**) 492-500.
147. Matthiesen, R., *Mass Spectrometry Data Analysis in Proteomics*. (**2007**): Humana Press.
148. Chernushevich, I.V., A.V. Loboda, and B.A. Thomson, *An introduction to quadrupole–time-of-flight mass spectrometry.* Journal of Mass Spectrometry, 36 (**2001**) 849-865.
149. Henry, H., H.R. Sobhi, O. Scheibner, M. Bromirski, S.B. Nimkar, and B. Rochat, *Comparison between a high-resolution single-stage Orbitrap and a triple quadrupole mass spectrometer for quantitative analyses of drugs.* Rapid Communications in Mass Spectrometry, 26 (**2012**) 499-509.
150. Lu, W., B.D. Bennett, and J.D. Rabinowitz, *Analytical strategies for LC–MS-based targeted metabolomics.* Journal of Chromatography B, 871 (**2008**) 236-242.
151. Wells, G. and C. Huston, *High-resolution selected ion monitoring in a quadrupole ion trap mass spectrometer.* Analytical Chemistry, 67 (**1995**) 3650-3655.
152. Xian, F., C.L. Hendrickson, and A.G. Marshall, *High Resolution Mass Spectrometry.* Analytical Chemistry, 84 (**2012**) 708-719.
153. Orwa, J.A., C. Govaerts, K. Gevers, E. Roets, A. Van Schepdael, and J. Hoogmartens, *Study of the stability of polymyxins B1, E1 and E2 in aqueous solution using liquid chromatography and mass spectrometry.* Journal of Pharmaceutical and Biomedical Analysis, 29 (**2002**) 203-212.
154. Sarkar, S., E.R.H. DeSantis, and J. Kuper, *Resurgence of colistin use.* American Journal of Health-System Pharmacy, 64 (**2007**) 2462-2466.
155. Chepyala, D., I.L. Tsai, H.-Y. Sun, S.-W. Lin, and C.-H. Kuo, *Development and validation of a high-performance liquid chromatography-fluorescence detection method for the accurate quantification of colistin in human plasma.* Journal of Chromatography B, 980 (**2015**) 48-54.

156. Bihan, K., Q. Lu, M. Enjalbert, M. Apparuit, O. Langeron, J.-J. Rouby, C. Funck-Brentano, and N. Zahr, *Determination of Colistin and Colistimethate Levels in Human Plasma and Urine by High-Performance Liquid Chromatography–Tandem Mass Spectrometry.* Therapeutic Drug Monitoring, 38 (**2016**) 796-803.
157. Zhao, M., X.-J. Wu, Y.-X. Fan, B.-N. Guo, and J. Zhang, *Development and validation of a UHPLC–MS/MS assay for colistin methanesulphonate (CMS) and colistin in human plasma and urine using weak-cation exchange solid-phase extraction.* Journal of Pharmaceutical and Biomedical Analysis, 124 (**2016**) 303-308.
158. Swartz, M., *HPLC Detectors: A brief review.* Journal of Liquid Chromatography & Related Technologies, 33 (**2010**) 1130-1150.
159. Leporati, M., R.O. Bua, F. Mariano, P. Carignano, M. Stella, L. Biancone, and M. Vincenti, *Determination by LC–MS/MS of Colistins A and B in Plasma and Ultrafiltrate From Critically Ill Patients Undergoing Continuous Venovenous Hemodiafiltration.* Therapeutic Drug Monitoring, 36 (**2014**).
160. Cheng, C., S. Liu, D. Xiao, J. Hollembaek, L. Yao, J. Lin, and S. Hansel, *LC–MS/MS method development and validation for the determination of polymyxins and vancomycin in rat plasma.* Journal of Chromatography B, 878 (**2010**) 2831-2838.
161. Barco, S., A. Mesini, L. Barbagallo, A. Maffia, G. Tripodi, F. Pea, C. Saffioti, E. Castagnola, and G. Cangemi, *A liquid chromatography-tandem mass spectrometry platform for the routine therapeutic drug monitoring of 14 antibiotics: Application to critically ill pediatric patients.* Journal of Pharmaceutical and Biomedical Analysis, 186 (**2020**) 113273.
162. Boison, J.O., S. Lee, and J. Matus, *A multi-residue method for the determination of seven polypeptide drug residues in chicken muscle tissues by LC-MS/MS.* Analytical and Bioanalytical Chemistry, 407 (**2015**) 4065-4078.
163. Balogh, M. *Debating Resolution and Mass Accuracy in Mass Spectrometry* Spectroscopy Online, 2004, 34-40.
164. Agency, E.M., *Guideline on bioanalytical method validation.* European Medicines Agency, (**2011**).
165. Mutasim Elimam, M., S. Wagiealla Shantier, E. Ahmed Gadkariem, and M. Awadalla Mohamed, *Derivative Spectrophotometric Methods for the Analysis and Stability Studies of Colistin Sulphate.* Journal of Chemistry, 2015 (**2015**) 624316.
166. Matar, K.M. and B. Al-Refai, *Quantification of Colistin in Plasma by Liquid Chromatography-Tandem Mass Spectrometry: Application to a Pharmacokinetic Study.* Scientific Reports, 10 (**2020**) 8198.
167. Li, J., R.W. Milne, R.L. Nation, J.D. Turnidge, and K. Coulthard, *Stability of Colistin and Colistin Methanesulfonate in Aqueous Media and Plasma as Determined by High-Performance Liquid Chromatography.* Antimicrobial Agents and Chemotherapy, 47 (**2003**) 1364-1370.
168. Wishart, D.S., Y.D. Feunang, A.C. Guo, E.J. Lo, A. Marcu, J.R. Grant, T. Sajed, D. Johnson, C. Li, Z. Sayeeda, N. Assempour, I. Iynkkaran, Y. Liu, A. Maciejewski, N. Gale, A. Wilson, L. Chin, R. Cummings, D. Le, A. Pon, C. Knox, and M. Wilson, *DrugBank 5.0: a major update to the DrugBank database for 2018.* Nucleic Acids Residues, 46 (**2018**) D1074-d1082.
169. Grzeskowiak, R., S. Hamels, and E. Gancarek, *Comparative Analysis of Protein Recovery Rates in Eppendorf LoBind® and Other "Low Binding" Tubes.*
170. Karvanen, M., C. Malmberg, P. Lagerbäck, L.E. Friberg, and O. Cars, *Colistin Is Extensively Lost during Standard In Vitro Experimental Conditions.* Antimicrobial Agents and Chemotherapy, 61 (**2017**) e00857-17.

171. Li, J., R.L. Nation, and K.S. Kaye, *Polymyxin antibiotics: from laboratory bench to bedside*. Vol. 1145. (**2019**): Springer. ISBN: 978-3-030-16371-6
172. Sader, H.S., P.R. Rhomberg, R.K. Flamm, and R.N. Jones, *Use of a surfactant (polysorbate 80) to improve MIC susceptibility testing results for polymyxin B and colistin.* Diagnostic Microbiology and Infectious Disease, 74 (**2012**) 412-414.
173. Turlej-Rogacka, A., B.B. Xavier, L. Janssens, C. Lammens, O. Zarkotou, S. Pournaras, H. Goossens, and S. Malhotra-Kumar, *Evaluation of colistin stability in agar and comparison of four methods for MIC testing of colistin.* European Journal of Clinical Microbiology & Infectious Diseases, 37 (**2018**) 345-353.
174. Wallace, S.J., J. Li, R.L. Nation, R.J. Prankerd, T. Velkov, and B.J. Boyd, *Self-assembly behavior of colistin and its prodrug colistin methanesulfonate: implications for solution stability and solubilization.* The journal of physical chemistry. B, 114 (**2010**) 4836-4840.
175. Mestres, C., M.A. Alsina, M.A. Busquets, I. Murányi, and F. Reig, *Interaction of colistin with lipids in liposomes and monolayers.* International Journal of Pharmaceutics, 160 (**1998**) 99-107.
176. Sutherland, C.A. and D.P. Nicolau, *To Add or Not To Add Polysorbate 80: Impact on Colistin MICs for Clinical Strains of Enterobacteriaceae and Pseudomonas aeruginosa and Quality Controls.* Journal of Clinical Microbiology, 52 (**2014**) 3810-3810.
177. McKenna, M., *Antibiotic resistance: the last resort.* Nature News, 499 (**2013**) 394.
178. CDC, *Antibiotic resistance threats in the United States, 2013*. (**2013**), US Department of Health and Human Services Atlanta.
179. Haeili, M. and M.M. Feizabadi, *The threat of colistin resistance among carbapenem-resistant Klebsiella pneumoniae isolates in Iran.* Iranian Journal of Microbiology, 10 (**2018**) 72-73.

9 APPENDICES

Appendices **A** through **E** contain further reading on kidney biology, colistin toxicity, liquid chromatography, organoids, and targeted proteomics, respectively. Reports of instances of the Mobilized Colistin Resistance gene 1 (MCR-1) can be found in **Appendix F**. The method used to prepare the liposomes used in this work can be found in **Appendix G**. Raw data can be found in appendices **H** and **I**. Absorption spectra from the attempted LC-UV-RI system can be found in **Appendix J**. An estimation of the pH of a solution of colistin can be found in **Appendix K**. Statistics can be found in **Appendix L**. Sources for references used in these appendices can be found in **Appendix M**.

9.1 APPENDIX A – KIDNEY BIOLOGY

9.1.1 A1 - The kidneys: Function and interactions with colistin

Chiefly responsible for filtering blood in the human body, the kidneys play a vital role in maintaining homeostasis through salt concentration regulations, metabolite excretion, and more. Each kidney contains more than a million nephrons, complex microstructures that filter the blood into a crude filtrate, adjusting this through a long, winding tube to produce urine, excreting and absorbing metabolites, nutrients, salts, and other compounds as needed. Each nephron consists of two main parts: the glomerulus and a long, winded tubule (see **Figure 38**). The glomerulus is a large bundle of highly permeable blood vessels surrounded by a filter that retains only very large proteins and entire cells. The filtrate then enters the tubules, divided into three main parts: the proximal tubule, the loop of Henle, and the distal tubule. These tubules are the part of the nephron responsible for the uptake and excretion of water, nutrients, ions, xenobiotics, metabolites, and more [1].

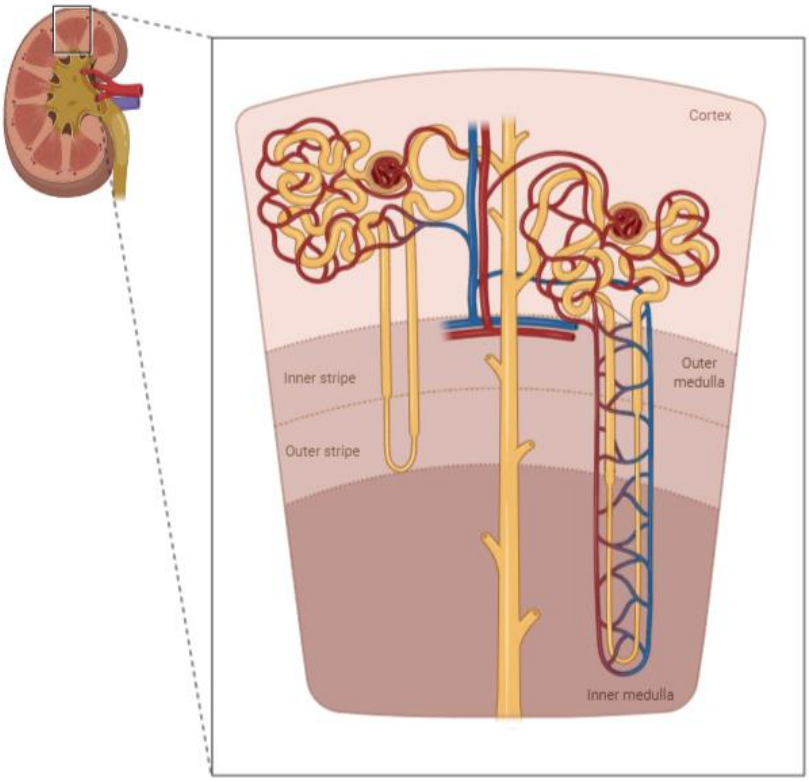

Figure 38 Illustration of the nephrons contained within the kidneys. The collecting duct (shown in yellow, center) transports the produced urine to the bladder. Blood vessels colored red/blue. Obtained from [2].

9.1.2 **A2 - Assessing colistin-induced renal damage**

The different regions of the tubules serve different functions and contain slightly different proteins embedded in their cellular membrane to interact with the extracellular blood filtrate appropriately. Colistin-induced nephrotoxicity is thought to be enabled through heavy reabsorption of colistin, thought to result in cellular swelling and lysis [3]. With the renal clearance of colistin having been proven minimal, it is implied that colistin elimination is chiefly performed by other organs [4]. As previously described in section 9.2.2, absorption is primarily thought to be mediated by OCTN1 and PEPT, causing damage to the epithelial cells in the interior of the tubules, specifically, the proximal tubule [5].

When looking for induced tissue damage or chemical effects, it is common to look for one or more specific compounds that can be used as quantitative indicators of the impact in question. These compounds are typically referred to as biomarkers, alongside other biological processes that can be objectively, repeatedly, and accurately measured [6, 7]. Several candidates have been proposed and compared for the specific colistin-induced injury of renal epithelial cells in the proximal tubule. A study published in 2013 by Keirstead et al. [8] compared the

nephrotoxicity of an *in vivo* rat model with that of an *in vitro* kidney organoid, intending to identify potential biomarkers specific for the renal damage caused by colistin. The two biomarkers that came out best were Kidney Injure Molecule 1 (KIM-1) and α-glutathione-S-transferase (α-GST) and were concluded to be the ideal biomarkers for the detection and measurement of the induced nephrotoxicity. These biomarkers were also specific for damage caused to the proximal tubule, effectively rendering them prime biomarkers for the renal injury induced by colistin. They, relative to other biomarkers, also possessed a relatively high selectivity compared to other potential biomarkers.

Another presented candidate is Cystain C, a cysteine protease inhibitor synthesized by most cells in the body. It is filtered by the glomerulus and completely reabsorbed in a healthy proximal tubule. The levels of Cystain C are independent of traits such as age, race, muscle mass, and sex, making it a promising candidate as a biomarker for colistin-induced nephrotoxicity [9-11].

A study conducted by Ghlissi et al. in 2013 [9] on live rats found that Neutrophil Gelatinase-Associated Lipocalin (NGAL) came out on top, as its presence correlated to the concentration administered colistin. However, this study did not consider KIM-1 or α-GST.

Studies looking for biomarkers specific for colistin-induced renal damage otherwise remain sparse, and more studies examining this are required. While strong candidates have been presented, further research should be conducted to compare these candidates against one another [10]. In summary, KIM-1 appears to be the biomarker most specific and sensitive to colistin-induced renal damage and should be used in tandem with organoids (micro-representations of actual tissue) to evaluate colistin toxicity. Further reading on KIM-1 can be found in B3 - The role of Kidney Injure Molecule 1 in the renal damage/repair process. Additionally, further reading on organoids can be found in Appendix D – Organoids as substitutes for *in vivo* trials.

As of late, there has been mounting research in damage mitigation. Specifically, ways to reduce the toxic side effects of drugs are being looked into. One of these is to encapsulate the drug(s) in liposomes; spherical, hollow bilayer ‘bubbles’ release the drug gradually, reducing toxicity.

9.2 APPENDIX B – COLISTIN TOXICITY

9.2.1 B1 - Neurotoxicity

The symptoms and signs of colistin-induced neural damage are relatively well understood, with common symptoms including ataxia, myopathy, facial and peripheral paresthesia, and more [12, 13]. Observations of colistin accumulation in mice's brains after multiple administrations prove the compound can pass through the blood-brain barrier. However, single-dose administrations yield negligible concentrations, suggesting the uptake of colistin remains relatively low [14, 15].

The blood-brain barrier, responsible for controlling the flow of substances in and out of the central nervous system, is equipped with organic cation transporters. Two of these, strongly suspected to be the primary mediators of colistin uptake, are OCTN1 [16] and PEPT [3, 17] (see section 9.2.2). These are expressed in both the kidneys and the blood-brain barrier, supporting the suspicion that these two proteins play a significant role in the side effects colistin produces. However, these are still only suspicions and warrant verification through further research [15, 18].

The mode of action colistin enacts on neural cells is not entirely understood, however, as neurological symptoms typically appear only to remain temporary. While many theories of the mode of action exhibited by colistin towards neural cells have been proposed, a consensus has not yet been reached. A study from 2013 by Dai et al. [19] gave new insight into the field, suggesting a mitochondrial dysfunction resulting from membrane fission and a mitochondrial vacuolization in the central nerve tissue. However, further research is required to understand the neurotoxic side effects of colistin [15].

9.2.2 B2 - Nephrotoxicity

Colistin-induced renal damage is a more frequent [20] and potentially more harmful side effect of colistin when compared to the neurotoxic side effects. Cells located in the kidney contain many membrane-bound transport proteins responsible for mediating the movement of metabolites, xenobiotics, buffers, and more [21]. Like the blood-brain barrier, these cells are also equipped with many organic cation transporters, such as OCTN1 and PEPT, as mentioned in section 9.2.1. Because of this, renal elimination of colistin is almost not observed due to the high rate of renal reabsorption, up to 80%, by the epithelial cells located in the nephrons of the kidneys [3, 4, 10, 22].

It is thought that intracellular damage in renal epithelial cells occurs through a similar mechanism as in nerve cells, damaging the mitochondria and endoplasmic reticulum in particular [5]. As most studies on colistin-induced nephrotoxicity originate from several decades ago without proper universal guidelines on classifications, more contemporary studies suggest that the incidence of nephrotoxicity is lower than initially thought [23]. Interestingly, some evidence exists that antioxidants such as melatonin could reduce the incidence of colistin-induced nephrotoxicity [24]. However, this remains far from conclusive, with another preliminary study finding that co-administration of ascorbic acid had no notable effect on the incidence of nephrotoxicity [25]. However, evidence countering this finding has been recently presented [26]: further research is required on ascorbic acid effects [3]. Furthermore, a recent meta-analysis conducted by Khalid et al. [27] looked through five randomized control trials with a total of 371 patients and found a rate of colistin-associated nephrotoxicity of about 36%. Further research is required to reach a scientific consensus about the dangers of colistin and the various ways these can be mitigated.

9.2.3 B3 - The role of Kidney Injure Molecule 1 in the renal damage/repair process

Kidney Injure Molecule 1, or KIM-1, is a type 1 membrane protein that exhibits immunoglobulin-like domains and a mucin-like domain. It is a phosphatidylserine receptor protein; phosphatidylserine acts as an ‘eat me’ signaling molecule by apoptotic cells for phagocytes [28]. KIM-1 is expressed at very low levels in a normal kidney, which becomes highly elevated in the proximal tubule following significant stress or damage to renal tissue by cleavage of the extracellular region and subsequent release into the renal tube cavity and urine [29-32].

KIM-1 has proved itself as a viable biomarker for renal injury, as described in section 9.1.2.

When expressed on cellular membranes, the extracellular portion of KIM-1 is shed constitutively by cleavage close to the intermembrane region. This shedding is thought to occur by the mechanism of a metalloproteinase [33-35]. In one study conducted by Ichimura et al., renal injury by administration of folic acid and cisplatin resulted in a significant rise of KIM-1 levels before serum creatinine levels rose to a considerable extent [30]. Other studies finding similar trends are numerous [32, 35-40], strengthening the idea that KIM-1 may be a more sensitive biomarker than those traditionally and currently in use.

The protein has been ‘discovered’ three times in three different contexts: The hepatitis A Virus cell receptor 1 (HAVcr-1) gene in green monkeys, and subsequently the human equivalent. Structurally, these differ only in the cytoplasmic tail, the implications of which remain unknown. Finally, the protein was ‘discovered’ during another independent search for proteins expressed differentially in lymphocyte membranes – where it was named T-cell immunoglobulin 1, or TIM-1 [31, 32, 34, 35, 41, 42]. As such, KIM-1/TIM-1/HAVcr-1 is a protein with many names. KIM-1/TIM-1 should not be mistaken for Kim-1/Tim-1, as Kim-1/Tim-1 is the equivalent protein in rats, whereas KIM-1/TIM-1 can be found in humans [39].

As a response to a toxic or ischemic insult to renal tissue in the proximal tubule, a complex and temporally separated series of events occurs (see **Figure 39**). Initially, cytoskeletal integrity and polarity are lost, followed by necrosis and apoptosis. Surviving epithelial cells then undergo dedifferentiation, after which they migrate to denuded regions formerly occupied by healthy epithelial cells. These surviving proximal tubule epithelial cells then proliferate and finally differentiate to form a fully functional proximal tubule epithelium [30, 33, 43-47].

Recent studies suggest that the story does not end there; the evidence mounts that KIM-1 functions as a recruitment protein, capable of promoting renal tubular epithelial cells into pseudo-professional phagocytes, cleaning up surrounding apoptotic cells by phagocytosis. Thus, these recruited facilitate proximal tubule repair by removing apoptotic cells and other debris. This process is illustrated in **Figure 39**. For this reason, KIM-1 may also hold potential therapeutic use to mitigate renal damage or to accelerate tissue repair following injury [32, 34, 35, 37, 48-50]. As one article by Kobayashi et al. stated quite aptly regarding the structure of TIM-1/KIM-1:

> *“In summary, TIM-1 and TIM-4 have unique structures that let them look death in the eye and give it a molecular kiss.”* [48], page 8.

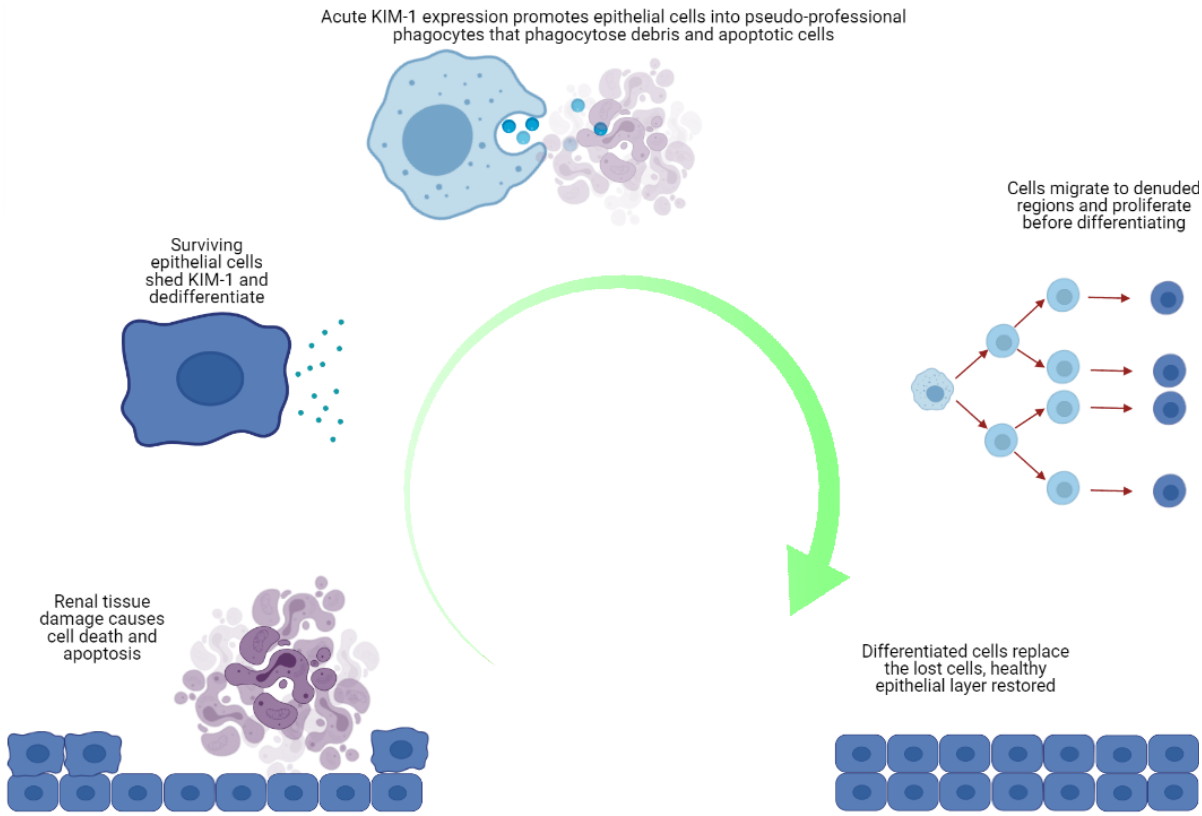

Figure 39 Simplified repair process of renal proximal tubule epithelial cells following acute damage. Following renal damage to epithelial cells (pink), KIM-1 expression skyrockets, prompting the surviving epithelial cells to dedifferentiate and assume the role of efficient, if pseudo-professional phagocytes that clear debris and apoptotic cells. These cells then migrate to the denuded regions, where they rapidly proliferate and differentiate, replacing the lost tissue. Illustration created using BioRender [2].

9.3 Appendix C – Liquid Chromatography

9.3.1 C1 - Column efficiency parameters

In chromatography, efficiency is defined as the plate height, *H*. This plate height is the constant defined as the ratio between the variance, σ^2 of a band (peak), and the distance this band has traveled, *x*. A higher plate height implies a lesser separation of closely eluting analytes, see Formula 2.

$$H = \frac{\sigma^2}{x}$$

Formula 2. Plate height is a proportionality function between the variance of a band, σ^2 , and the distance the band has traveled, x.

In an idealized example, a chromatographic peak follows a simple gaussian curve. This curve has a width at half height ($w_{0.5}$) equal to 2.35σ. The distance, *x*, is equal to the length of the column. In practice, this means that a column is more efficient if (1) the chromatographic peak (the band) is narrower or (2) the column is longer.

9.3.1.1 C1.1 Column properties

Column dimensions play a significant role in determining the efficiency of a given separation. The length of the column is not only a contributing factor in how long the injected sample spends in it, but it also determines the amount of stationary phase available for interaction with analyte molecules. A longer time spent in the column will increase the longitudinal diffusion (see section 9.3.2.1 for more details). At the same time, however, the increased amount of interactions with the stationary phase will have an opposite effect on the band width, producing a tradeoff with a balancing point that varies for different solutions [51].

The ID of the column does not affect band broadening unless the column has an open tubular structure. A wider ID will cause more radial dilution of the injected sample, causing a lower signal for concentration-sensitive detectors (UV, ESI-MS, and more). However, the upside of using a larger ID is that the capacity of the column, the volume of sample that may be injected increases [51].

9.3.1.2 C1.2 Particle properties

In packed columns, particle properties such as their overall size affect the backpressure of the LC system. Smaller particles provide higher backpressure but increased efficiency. This increase in efficiency partially originates from reducing the random flow path effect described in section 9.3.2.3 [51].

As previously described in section 2.5.1, smaller particle sizes are typically utilized for UHPLC instrumentation. These provide better efficiency at increased flow rates, as opposed to larger particles. This relationship goes per Formula 3 (Van Deemter), see **Figure 40** for an illustration of how larger/smaller particle sizes affect plate height per this relationship.

$$H = A + \frac{B}{u} + C * u$$

Formula 3 The relationship between plate height (H), linear flow rate (u), eddy diffusion(A – see section 9.3.2.3), longitudinal diffusion (B – see section 9.3.2.1), and mass transfer resistance (C – see section 9.3.2.2)

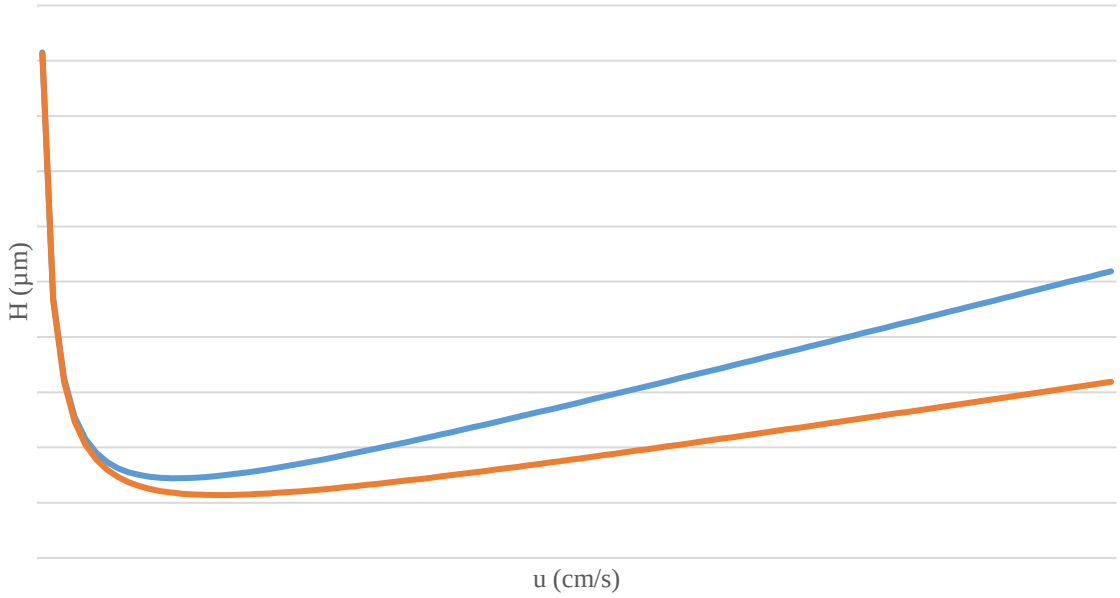

Figure 40. The typical shape of a Van-Deemter plot illustrating the relationship between particle size, flow rate (u), and plate height (H). Smaller particles (orange) provide better efficiency at higher flow rates when compared to their larger equivalents (blue).

9.3.1.3 C1.3 Band broadening effects

Band broadening in chromatography is where a chromatographic peak becomes less sharp, wider, and more a 'bulge' than a peak (see **Figure 41**). Sharper peaks are generally more desirable as they provide better identification, quantification, and separation of the compounds present in a solution. Less defined peaks with a larger width have an increased tendency to merge with surrounding peaks (see **Figure 42**), rendering quantification difficult [51].

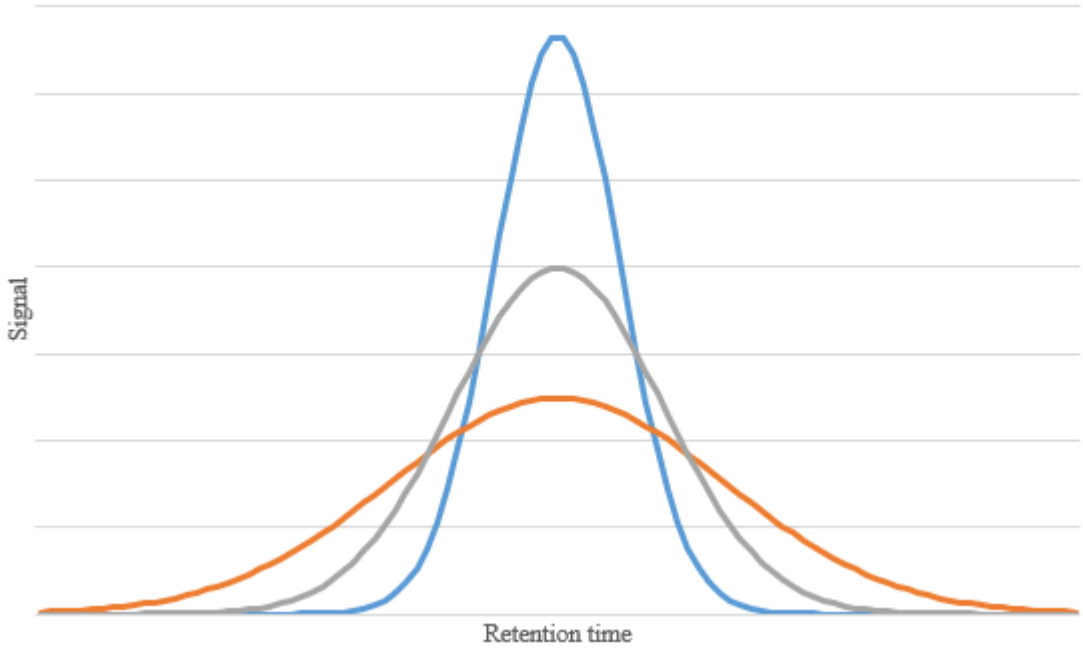

Figure 41. Illustration of (idealized) Gaussian functions, illustrating how a difference in σ^2 changes the shape of the peak. A low variance (blue) yields a relatively sharp peak, whereas a higher variance (grey) gives a broader peak. A very high variance gives a very broad peak (orange)

Chromatographic peaks broaden for a multitude of reasons. Column packing, stationary and mobile phase, temperature, particle size (if applicable), pore sizes, laminar flow velocity, dead volumes, and more are factors that come into play to varying degrees [51, 52].

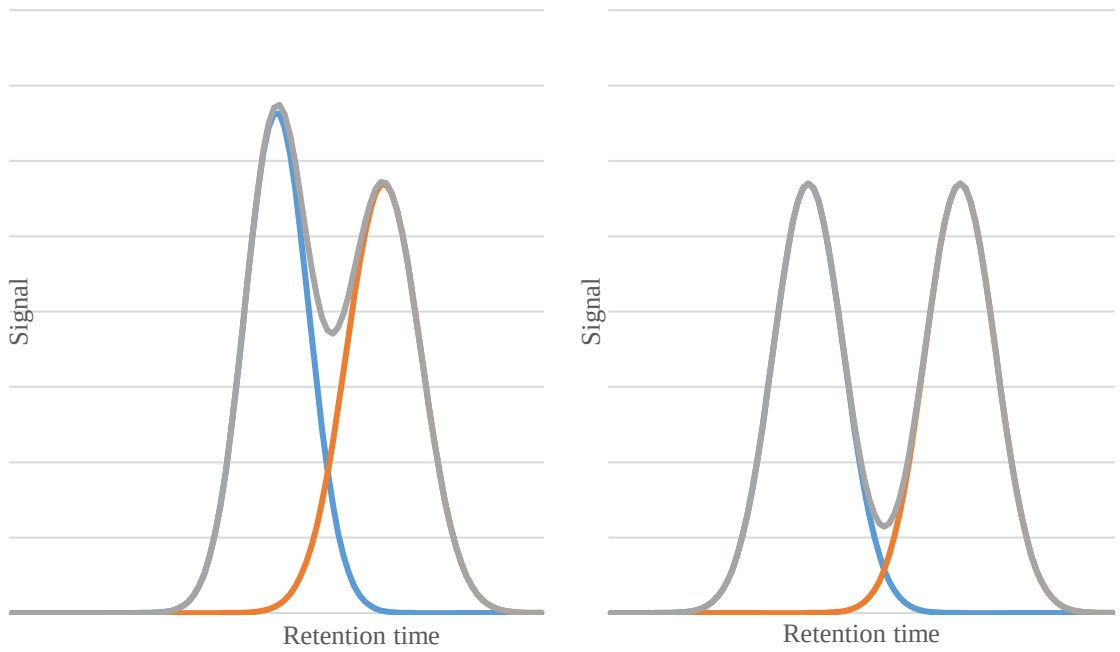

Figure 42. Illustration of what happens when peaks in a chromatographic system overlap (shown in grey). The blue and orange peaks are separate peaks that elute closely to one another. With higher efficiency, peaks are separated better, making quantification easier as the overlap is reduced.

9.3.2 C2 - Band broadening inside the column

Band broadening inside the column is caused by physical processes, such as diffusion and mass transfer reactions, described in detail below.

9.3.2.1 Band broadening due to longitudinal diffusion

At any temperature beyond 0K, molecules remain in continuous Brownian motion, causing a natural diffusion over time. When a sample solution is injected into the column, diffusion will occur at both the front and back over time, widening the column. This is why slower linear velocity of the mobile phase, which causes a more extended time spent in the column, contributes to band broadening [51, 52].

9.3.2.2 Band broadening due to resistance to mass transfer

The process of a molecule binding to and releasing itself from the stationary phase is not instantaneous. Because it requires a certain amount of time, which causes molecules interacting with the stationary phase to be retarded more so than those who, by chance, interact less with the stationary phase. This mass transfer reaction comes in two primary forms: mass transfer in the mobile phase and mass transfer in the stationary phase. The former describes the process in which a molecule moves from the mobile phase to the stationary phase. In contrast, the latter describes the inverse process, in which a molecule must diffuse through and out of the stationary phase back into the mobile phase. The rate at which this happens depends on the flow, temperature, rate of diffusion, and more [51, 52].

9.3.2.3 Band broadening due to various flow paths (eddy dispersion)

In a packed or monolithic column, the mobile phase may follow different paths of different sizes, causing different velocities through these. More narrow flow paths warrant a higher flow rate, whereas wider flow paths do the opposite. For this reason, the many flow paths molecules may follow cause them to move through the column at slightly different rates, causing band broadening [51, 52].

9.3.3 C3 - Band broadening outside the column

There are two primary causes for band broadening outside the column, the injection volume, and the connection tubing. Since the injection volume of a sample solution cannot be zero, the injected sample will take up a volume in the tubing with an internal volume of a certain width. Detector volume and response time also play a role in band broadening outside the column [53].

In addition to this, the flow of liquid through the tubing – the laminar flow (uniform, non-turbulent flow of a fluid) moves unevenly through as cylindrical tubing. The fluid will have a velocity near, but not identical to, zero at the tubing walls while maintaining the intended flow speed at the center. This uneven fluid velocity will cause the flow of fluid to 'bulge,' with the centermost fluid ahead, with the fluid nearer the walls following behind [51, 52, 54].

9.4 APPENDIX D – ORGANOIDS AS SUBSTITUTES FOR *IN VIVO* TRIALS

The development of new drugs is generally known to be quite costly. This cost is, in part, a result of the numerous and extensive tests and validations that must be performed to assess the efficiency and side effects of a drug. This process takes place in a series of stages, or phases, typically starting by testing the drug on simple cell cultures, then animals, and finally humans. However, due to the inherent differences between cells on a petri dish and living human beings, many drugs that do well on the cellular and animal-based trials fail at the human stage [55, 56]. While human cell lines are also used to obtain data more representative of human biology during the first phase of cell-based trials, these fail to provide an accurate picture of the physiological responses and interactions that can take place within a human body. Therefore, an increasingly popular option for these cell lines, and a present-day buzzword in analytical, biological, and pharmaceutical science, is *organoids* [57].

Organoids, derived from pluripotent stem cells, are effectively miniature organs that may be cultured while cellular differentiation is induced. These cells readily self-assemble and organize themselves into a three-dimensional, microscopic representation of a live human organ, with most, if not all, the fine structure required to reflect that present in the equivalent live organism. Many types of organoids may be prepared, producing accurate representations of real organs, such as lungs [58], livers [59], muscles [60], and even neural tissue [61]. These organoids may be readily implemented in on-chip designs to be used in studies of both scientific and pharmaceutical nature. In the interest of examining colistin-induced nephrotoxicity, kidney organoids may prove significantly helpful and can be readily created [62].

When compared to animal-based testing models, organoids possess numerous advantages. They provide a better representation of the complex physiology of a given organ and significantly aid in the cost reduction of future drug development [63]. Additionally, more elaborate setups may be produced by interconnecting organoids to create multi-organoid systems, giving a vastly more realistic, multi-organ encompassing view and data to reflect the live human body [64].

9.5 APPENDIX E - TARGETED PROTEOMICS

Targeted proteomics is an MS-based protein quantification approach, where intact or digested proteins (peptides) are measured to give quantitative data. There are two main approaches to this; top-down and bottom-up (though other approaches also exist). One of the significant perks of targeted proteomics is how readily a developed method can be tailored to include other proteins, which allows for rapid and reliable detection of various protein isoforms. In the case of the top-down approach, insight into the various post-translational modifications (PTM) present. However, when applying targeted proteomics to a biological sample, sample clean-up or analyte separation is usually required to the inherent complexity of biological samples; measurements are therefore typically preceded by a separation step (LC or electrophoresis) to separate proteins/peptides [65].

9.5.1 E1 - Top-down

The top-down approach does not involve proteolysis, unlike the bottom-up approach described in section 9.5.2. Instead, entire, intact proteins are sent to the MS – ideally pre-separated on a multidimensional LC system – before being broken apart into fragments in the MS ion source, which add up to the total mass of the initial protein. The main advantage of this approach is that information regarding PTM and isoform differentiation is preserved [66]. However, adequate ionization and fragmentation remain a challenge for complex samples and whole-proteome detection, and the underdevelopment of data processing software makes quantitative work challenging [66].

Proteome-wide detection and measurements require high mass resolution (mass resolving power, see section 2.6.3) to differentiate minor PTM and structural variations (such as disulfide bridges). Additionally, larger proteins will have more significant isotopic variations, distributing the ideal signal over many *m/z* values, reducing the effective signal obtained at the monoisotopic *m/z* value. Furthermore, in ESI, a population of proteins will assume a distribution of charge states due to different degrees of ionization of the various proteins. The result is splitting the signal of a single protein into numerous peaks, reducing the signal at the ideal *m/z*-ratios. This effect becomes more significant at higher protein masses as the number of isotope peaks and potential charge states increases [65, 67].

Ionization is typically achieved through the use of ESI or matrix-assisted laser desorption ionization (MALDI). MALDI primarily produces singly protonated protein ions with limited detector use to time of flight (TOF) mass analyzers. Therefore, MALDI has been limited due

to the low resolution, lacking dynamic mass range obtained by the TOF mass analyzer, and the relatively poor fragmentation achieved by MALDI [65, 68]. For this reason, ESI-based top-down proteomics is usually performed with Orbitrap or Fourier transform ion cyclotron resonance (FT-ICR) mass analyzers, which deliver a better dynamic mass range, mass accuracy, and resolution [67-69].

9.5.2 **E2 - Bottom-up**

Unlike the top-down approach described in section 9.5.1, the bottom-up approach involves the enzymatic digestion of proteins into peptides before MS measurements. This approach is also referred to as 'shotgun proteomics,' a term adapted from shotgun genomic sequencing, which in turn was adapted from a shotgun blast, in which many fragments originate from a larger shell [69-71].

The mass spectra generated are identified by comparing tandem mass spectra of *in silico* digests of a protein database. While many peptides are unique to specific proteins, many are also shared, and protein identification is also achieved by scoring and grouping the identified peptides. As peptides are more readily fragmented, have fewer isotopic peaks and fewer potential charge states, the bottom-up approach is typically preferred, despite the loss of information and increased sample complexity resulting from enzymatic digestion [69].

The most common protease used for enzymatic digestion is trypsin [72-75], an endopeptidase that breaks peptide bonds of nonterminal amino acids. Trypsin is a serine protease, generally cleaving at the C-terminal of arginine and lysine [76, 77]. However, other proteases are also used to achieve different peptides [73, 74].

Bottom-up sample preparation conditions have to be carefully controlled to maximize digestion yield. The type of protease used, pH during incubation, incubation temperature, and enzyme-to-substrate ratio are crucial parameters that need careful control to ensure optimal conditions and experiment repeatability [78].

Other approaches in proteomics also exist beyond the top-down and bottom-up approaches, such as the 'middle-down' approach, in which proteins are digested into significantly larger peptides (apx. 3-10 kDa) than those typically used in the bottom-up approach (apx. 0.7-3 kDa) [79]

9.6 APPENDIX F – COUNTRIES THAT HAVE REPORTED INSTANCES OF THE MOBILIZED COLISTIN RESISTANCE 1 GENE

Table 19 summarizes countries with reported observations of the MCR-1 gene in colistin-resistant bacteria from their own country.

Table 19 List of countries or islands (New Caledonia) that have reported instances of the MCR-1 gene from samples taken from their population, livestock, or environment.

Country	Source
Algeria	[80]
Argentina	[81]
Australia	[82]
Austria	[83]
Bahrain	[84]
Belgium	[85]
Brazil	[86]
Cambodia	[87]
Canada	[80]
China	[88]
Colombia	[89]
Denmark	[90]
Ecuador	[91]
Egypt	[92]
Estonia	[93]
France	[80]
Germany	[94]
Hungary	[95]
Italy	[96]
Japan	[97]
Laos	[80]
Lithuania	[98]
Malaysia	[99]
Morocco	[100]

Netherlands	[101]
New Caledonia	[102]
Norway	[103]
Poland	[104]
Portugal	[105]
Russia	[104]
Saudi Arabia	[84]
South Africa	[106]
South Korea	[107]
Spain	[108]
Sweden	[109]
Switzerland	[110]
Taiwan	[111]
Thailand	[112]
Tunisia	[113]
United Kingdom	[114]
United Arab Emirates	[84]
United States of America	[115]
Vietnam	[116]

9.7 APPENDIX G – LIPOSOME PREPARATION METHOD

The following procedure describes the method used to produce the liposomes used in this work. These were produced by Andersen Nahm (Bio3 – Chemical life sciences, Department of Chemistry, University of Oslo, Norway).

1. Turn on the water bath. The temperature should be 10 degrees Celsius above the melting point of lipids.
2. Clean a round flask with methanol and type 1 water.
3. Weigh lipids and transfer them to the round flask.
4. Prepare a mixture of dichloromethane (DCM) and methanol (3:1 ratio DCM: MeOH)
5. Add the DCM/MeOH mixture to the round flask.

6. Connect the round flask to the rotor evaporator using Teflon tape to ensure tightness.
7. Check system integrity and turn on the vacuum pump. Lower the pressure to 550 mbar, then slowly down to 40 mbar.
8. Let all the fluids evaporate until there is only a thin film coating the flask bottom.
9. Add buffer solution and attach the round flask to the rotor evaporator once more. Use the water bath, but do not use the vacuum pump. Let the film hydrate for a minimum of 1 hour.
10. Turn the ultrasonic feature on the water bath on. Sonicate the hydrated film for 15 minutes.
11. Assemble the extruder, drenching filter supports, and membrane with buffer solution. Push 0.5-1 mL buffer through the extruder to ensure filter saturation.
12. Directly after sonication, extrude the solution an odd number of times, minimum 21.
13. Wash the extruder with water and ethanol, let dry.
14. Store the solution of liposomes in a fridge.

9.8 APPENDIX H – RAW DATA FROM METHOD A AND METHOD B DEVELOPMENT

9.8.1 H1 – Raw data from the first liposome release study

The raw data from the first liposome release study can be found in **Table 20** and **Table 21**.

Table 20 Calibration solutions, their concentrations, and the integrated areas for the pseudoquantitative determination of colistin.

Calibration solution #	Concentration (µg/mL)	Area
1	0,008	677
2	0,01	1042
3	0,05	1941
4	0,19	1048040
5	0,5	2375284
6	1	5313821

*Table 21 Sample solutions, calculated concentrations, and their area. Calculations were performed using the equation area-concentration relationship illustrated in **Figure 25**.*

Sample #	Calculated concentration (µg/mL)	Calculated concentration (ng/mL)	Area
1	< LOD	< LOD	50
2	0,001853	1,853	9634
3	0,002397	2,397	12463
4	0,002783	2,783	14469

9.8.2 H2 – Raw data from the second liposome release study

As described in section 5.2.2, the measurements were performed across two days due to instrument failure. Separate calibration curves were used for separate days. The calibration curve used for day 1 can be seen in **Figure 43**. The calibration curve for day 2 can be seen in **Figure 44**.

Raw data used for the creation of the calibration curves can be seen in **Table 23**.

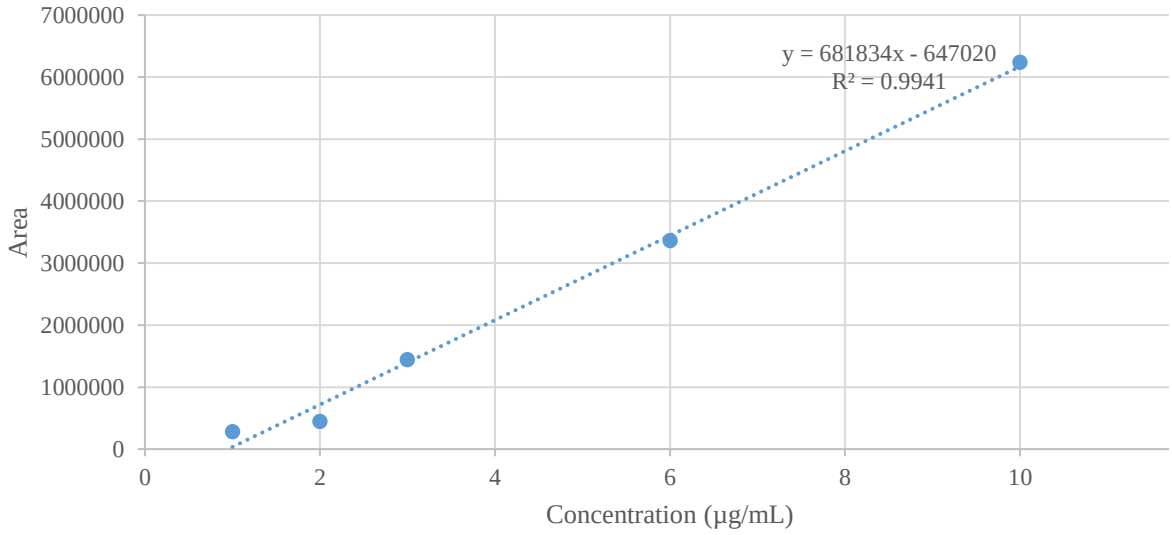

*Figure 43. Calibration curve used for samples measured on day 1. The calibration curve was originally longer, but for unknown reasons, there was a sharp drop in signal below 1 µg/mL, and the range 1-10 µg/mL was therefore used, and samples with a concentration < 1 µg/mL were therefore extrapolated on the assumption the linear range continued to the range of the lowest concentration, determined to be approximately 0.95 µg/mL. The graph was produced using data from **Table 23**.*

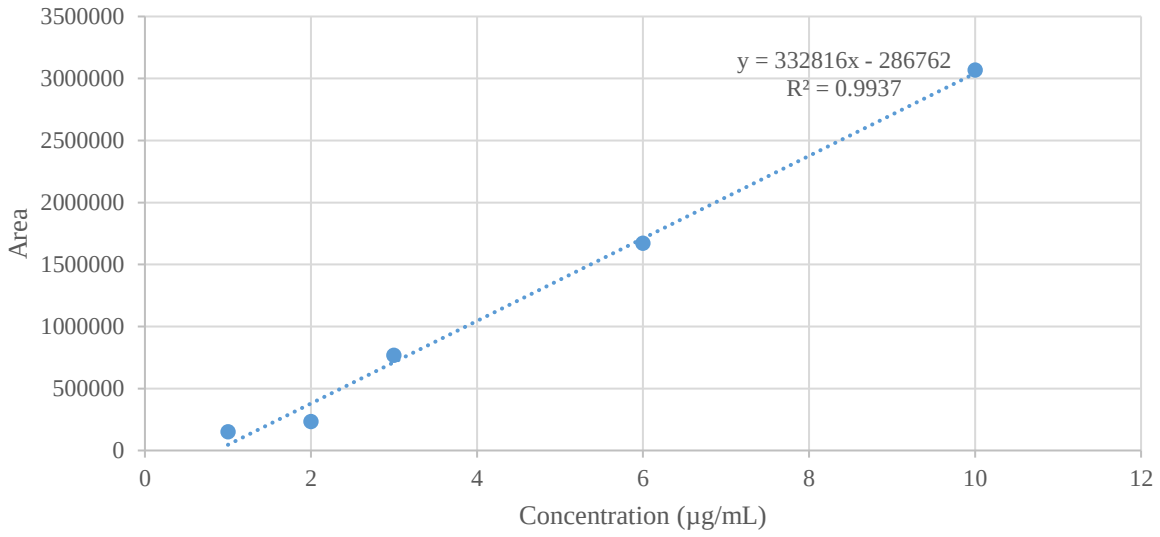

Figure 44. Calibration curve used for samples measured on day 2. The calibration curve was originally longer, but for unknown reasons, there was a sharp drop in signal below 1 µg/mL, and the range 1-10 µg/mL was therefore used, and samples with a concentration < 1 µg/mL were therefore extrapolated on the assumption the linear range continued to the range of the lowest concentration, determined to be approximately 0.95 µg/mL. The graph was produced using data from ***Table 23****.*

Table 22. Raw data and calculated concentrations of colistin in samples. Sample replicate one was deemed irrelevant due to what appeared sample preparation error. Blanks were not injected into the system between sample replicates as they were assumed to increase in concentration, so the area for replicate 1 at 1h was disregarded due to carry-over.

Time (h)	Replicate #	Area	Average area	Standard deviation	RSD (%)	Concentration (µg/mL)
0	1	690931				
	2	3079387	3613802.3	3223477.0	89.20%	6.25
	3	7071089				
1	1	53063				
	2	8462	7083.0	1950.2	27.53%	0.96
	3	5704				
2	1	5005				
	2	1749	2851.0	1865.6	65.44%	0.95
	3	1799				
4	1	1174				
	2	1527	1240.0	260.4	21.00%	0.95
	3	1019				
6	1	1155				
	2	785	877.7	244.5	27.86%	0.95
	3	693				
9	1	615				
	2	580	551.3	81.9	14.85%	0.95
	3	459				

12	1	510				
	2	589	557.0	41.6	7.47%	0.95
	3	572				
18	1	572				
	2	422	469.7	88.7	18.88%	0.95
	3	415				
24	1	461				
	2	613	1222.0	1188.9	97.29%	0.95
	3	2592				
30	1	40467				
	2	8175	29199.3	18223.3	62.41%	0.95
	3	38956				
36	1	324547				
	2	5184	119339.3	178090.1	149.23%	0.91
	3	28287				
48	1	634897				
	2	254042	540034.0	252310.0	46.72%	2.48
	3	731163				
72	1	298806				
	2	737698	833022.3	587705.4	70.55%	3.36
	3	1462563				

Table 23 Raw data used to create the two calibration curves used in the second quantitative determination. Only calibration solutions with concentrations 1 through 10 were used for both days due to the inexplicably sudden signal loss below 1 µg/mL.

Day 1	Area	RT (min)	Concentration (µg/mL)
	374	1.1	0
	226	1.11	0.001
	355	1.12	0.0025
	345	1.12	0.005
	146	1.12	0.01
	124	1.1	0.025
	91.52	1.11	0.05
	92	1.1	0.1
	137	1.1	0.25
	73	1.11	0.5
	278864	1.09	1
	443563	1.11	2
	1443832	1.1	3
	3361685	1.11	6
	6237313	1.12	10
Day 2	**Area**	**RT (min)**	**Concentration (µg/mL)**
	0	0	0
	170	1.09	0.001

	37	1.1	0.0025
	82	1.09	0.005
	69	1.09	0.01
	59	1.1	0.025
	33	1.11	0.05
	57	1.1	0.1
	20	1.09	0.25
	30	1.11	0.5
	149531	1.11	1
	232526	1.09	2
	767747	1.09	3
	1671886	1.09	6
	3066446	1.11	10

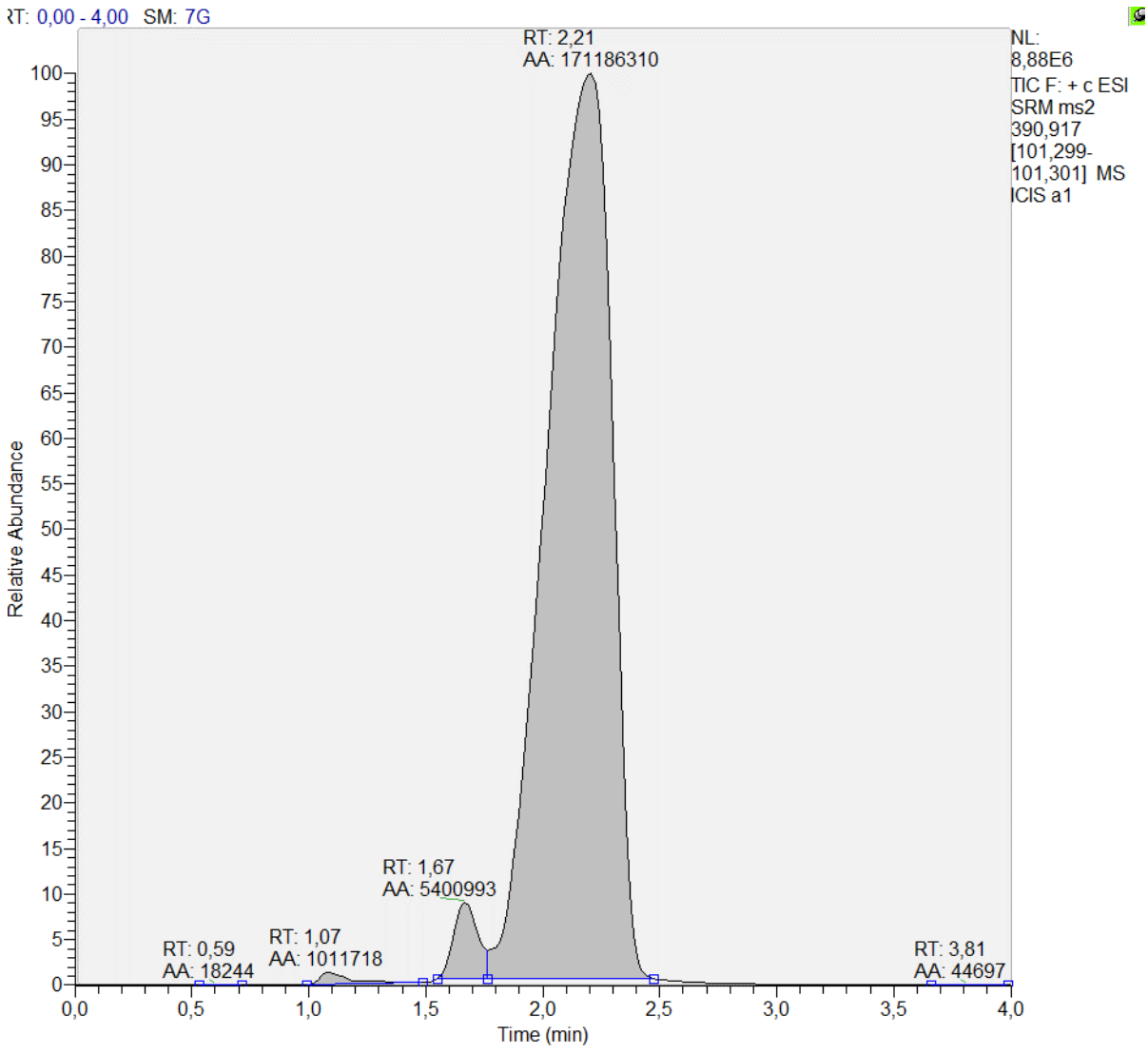

Figure 45 Representative single-channel MRM chromatogram for replicates of sample 1 (0h. With the slightly altered method used in this analysis (as described in section 5.2.2), colistin had a retention time of 1.1 minutes. The MRM transition illustrated is that of m/z 390.917→101.299. The massive area of the peak at 2.21 minutes (approximately 27

times that of the highest calibration solution at 10µg/mL) is believed to come from liposome-embedded colistin or some other contaminant.

9.8.3 H3 – Raw data from the first stability/adsorption test

Raw data obtained from the first stability study of colistin is summarized in **Table 24**, **Table 25**, **Table 26**, and **Table 27**.

Table 24. Raw data obtained from the first stability study of colistin. A single sequence contained a calibration set from each of the four groups (Control, Buffer, Ascorbic acid + buffer, and Polymyxin B1 + buffer, respectively). Each sequence took approximately four hours to complete. Sequence 0 is therefore t=0, 2 = 4h, 3=8h, 4=12h, 5=16h, 6=20h, 7=24h, and 8=28h. This table shows the raw data obtained from the control set.

Control (No changes)	**Calibration solution no.**	**1**	**2**	**3**	**4**	**5**	**6**
	Concentration (µg/mL)	10	6	3	2	1	0
Sequence 1	RT (min)	2.57	2.6	2.66	2.61	2.64	2.64
	Area	4835849	2649715	1124383	630981	180662	0
Sequence 2	RT (min)	2.49	2.44	2.49	2.58	2.6	2.64
	Area	9007205	5033857	2180363	1220964	382322	0
Sequence 3	RT (min)	2.27	2.35	2.37	2.37	2.48	2.48
	Area	8792196	4902823	2093739	1170512	359329	0
Sequence 4	RT (min)	2.45	2.49	2.57	2.62	2.64	2.64
	Area	8562942	4686043	2049120	1134074	357743	0
Sequence 5	RT (min)	2.41	2.44	2.52	2.58	2.64	2.64
	Area	4469901	2423698	1083954	595826	179021	0
Sequence 6	RT (min)	2.33	2.37	2.39	2.42	2.48	2.48
	Area	8546082	4760464	2029892	1093021	337678	0
Sequence 7	RT (min)	2.39	2.41	2.43	2.53	2.5	2.5
	Area	8434203	4622989	1991957	1084401	335837	0
Sequence 8	RT (min)	2.16	2.25	2.27	2.36	2.44	2.44
	Area	8370370	4641029	1982699	1073545	327891	0

Table 25. Raw data obtained from the first stability study of colistin. A single sequence contained a calibration set from each of the four groups (Control, Buffer, Ascorbic acid + buffer, and Polymyxin B1 + buffer, respectively). Each sequence took approximately four hours to complete. Sequence 0 is therefore t=0, 2 = 4h, 3=8h, 4=12h, 5=16h, 6=20h, 7=24h, and 8=28h. This table shows the raw data obtained from the buffer set.

Buffer (10mM ammonium formate, pH 4)	**Calibration solution no.**	**1**	**2**	**3**	**4**	**5**	**6**
	Concentration (µg/mL)	10	6	3	2	1	0
Sequence 1	RT (min)	2.43	2.52	2.58	2.64	2.64	2.87
	Area	6436233	3823306	1744829	1042252	206744	963
Sequence 2	RT (min)	2.4	2.41	2.46	2.53	2.6	2.78
	Area	11344830	6653989	3092614	1851397	803909	2570
Sequence 3	RT (min)	2.29	2.31	2.33	2.41	2.47	2.65
	Area	11125244	6495384	2984620	1810562	775332	4006

Sequence 4	RT (min)	2.37	2.41	2.44	2.5	2.54	2.73
	Area	11074893	6403033	2924964	1757318	762169	4038
Sequence 5	RT (min)	2.35	2.36	2.47	2.52	2.56	2.73
	Area	5812366	3334959	1534286	933007	394990	2754
Sequence 6	RT (min)	2.4	2.47	2.59	2.44	2.5	2.69
	Area	10939981	6383189	2904066	1757738	776123	7225
Sequence 7	RT (min)	2.39	2.41	2.44	2.53	2.56	2.66
	Area	10879652	6286093	2883950	1733637	761777	9180
Sequence 8	RT (min)	2.28	2.27	2.31	2.33	2.4	2.41
	Area	10924582	6269397	2917288	1741302	764174	12051

Table 26. Raw data obtained from the first stability study of colistin. A single sequence contained a calibration set from each of the four groups (Control, Buffer, Ascorbic acid + buffer, and Polymyxin B1 + buffer, respectively). Each sequence took approximately four hours to complete. Sequence 0 is therefore t=0, 2 = 4h, 3=8h, 4=12h, 5=16h, 6=20h, 7=24h, and 8=28h. This table shows the raw data obtained from the ascorbic acid + buffer set.

Ascorbic acid (20mM) + buffer	**Calibration solution no.**	**1**	**2**	**3**	**4**	**5**	**6**
	Concentration (µg/mL)	10	6	3	2	1	0
Sequence 1	RT (min)	2.37	2.44	2.48	2.5	2.57	2.79
	Area	5760847	3302486	1534913	937563	392283	462
Sequence 2	RT (min)	2.35	2.39	2.48	2.52	2.57	2.83
	Area	10371752	5959621	2786590	1702891	703984	1881
Sequence 3	RT (min)	2.33	2.39	2.41	2.41	2.45	2.66
	Area	10104234	5812782	2710263	1668221	673368	2019
Sequence 4	RT (min)	2.36	2.44	2.47	2.46	2.49	2.73
	Area	10036063	5702652	2680547	1648056	651752	2066
Sequence 5	RT (min)	2.18	2.23	2.24	2.31	2.41	2.72
	Area	5216034	3013371	1443593	880985	342181	1058
Sequence 6	RT (min)	2.45	2.47	2.54	2.56	2.64	2.8
	Area	9631840	5460417	2615044	1602400	641705	2129
Sequence 7	RT (min)	2.45	2.46	2.52	2.54	2.57	2.74
	Area	9410661	5352936	2579294	1563358	624700	2080
Sequence 8	RT (min)	2.36	2.39	2.4	2.43	2.47	2.65
	Area	9311382	5316180	2529261	1548709	608445	2128

Table 27. Raw data obtained from the first stability study of colistin. A single sequence contained a calibration set from each of the four groups (Control, Buffer, Ascorbic acid + buffer, and Polymyxin B1 + buffer, respectively). Each sequence took approximately four hours to complete. Sequence 0 is therefore t=0, 2 = 4h, 3=8h, 4=12h, 5=16h, 6=20h, 7=24h, and 8=28h. This table shows the raw data obtained from the polymyxin B1 + buffer set.

Polymyxin B1 (47.6 µg/mL) + buffer	**Calibration solution no.**	**1**	**2**	**3**	**4**	**5**	**6**
	Concentration (µg/mL)	10	6	3	2	1	0
Sequence 1	RT	2.54	2.58	2.61	2.61	2.87	2.73
	Area	5852592	3616745	1771442	1175693	588603	2921
Sequence 2	RT	2.33	2.41	2.41	2.53	2.52	2.66
	Area	10986395	6635896	3226780	2108887	1058849	5238
Sequence 3	RT (min)	2.58	2.64	2.64	2.62	2.64	2.73
	Area	10854492	6504494	3183844	2092344	1041590	7682

Sequence 4	RT (min)	2.57	2.61	2.61	2.66	2.69	2.7
	Area	10918565	6525758	3176666	2103974	1044859	28159
Sequence 5	RT (min)	2.4	2.52	2.48	2.48	2.53	2.53
	Area	5556655	3359354	1672491	1104726	554648	12723
Sequence 6	RT (min)	2.53	2.57	2.58	2.64	2.66	2.72
	Area	10705844	6327494	3155185	2076228	1024025	27214
Sequence 7	RT (min)	2.52	2.6	2.64	2.66	2.7	2.76
	Area	10623098	6600674	3101995	2059181	1009554	29029
Sequence 8	RT (min)	2.6	2.62	2.64	2.69	2.64	2.7
	Area	10475830	6462216	3062469	2023278	1005676	33528

9.8.4 H4 – Raw data from the second stability/adsorption test

Table 28. Raw data obtained from the second stability study of colistin. A single sequence contained a calibration set from each of the four groups (Control, Buffer, Ascorbic acid + buffer, and Polymyxin B1 + buffer, respectively). Each sequence took approximately four hours to complete. Sequence 0 is therefore t=0, 2 = 4h, 3=8h, 4=12h, 5=16h, 6=20h, 7=24h, and 8=28h. This table shows the raw data for all four groups.

Control (No changes)	**Calibration solution no.**	**1**	**2**	**3**	**4**	**5**	**6**
	Concentration (µg/mL)	10	6	3	2	1	0
Sequence 1	RT (min)	2.35	2.4	2.48	2.47	2.51	
	Area	4069008	2182896	921082	460497	136592	0
Sequence 2	RT (min)	2.32	2.4	2.28	2.39	2.39	
	Area	4119394	2270740	977973	513311	163145	0
Sequence 3	RT (min)	2.39	2.44	2.47	2.47	2.51	
	Area	4000247	2193893	949082	498269	158820	0
Sequence 4	RT (min)	2.33	2.4	2.45	2.51	2.48	
	Area	3953629	2194464	942067	494989	154101	0
Sequence 5	RT (min)	2.42	2.43	2.43	2.45	2.51	
	Area	3943193	2154471	935958	494046	138412	0
Sequence 6	RT (min)	2.39	2.48	2.44	2.48	2.51	
	Area	3928485	2153650	924531	481738	140617	0
Sequence 7	RT (min)	2.26	2.26	2.31	2.32	2.22	
	Area	3992284	2187684	950969	491833	140603	0
Sequence 8	RT (min)	2.4	2.39	2.51	2.52	2.56	
	Area	4014007	2221231	959580	493437	141442	0
Buffer (10mM ammonium formate, pH 4)	Calibration solution no.	1	2	3	4	5	6
	Concentration (µg/mL)	10	6	3	2	1	0
Sequence 1	RT (min)	2.36	2.41	2.45	2.51	2.39	2.51
	Area	5054357	2919142	1365815	823811	354855	6171
Sequence 2	RT (min)	2.35	2.35	2.4	2.39	2.41	2.57
	Area	4885696	2801549	1322424	803399	349302	5542
Sequence 3	RT (min)	2.37	2.37	2.44	2.44	2.47	2.6
	Area	4802885	2761152	1287594	788093	342083	6576
Sequence 4	RT (min)	2.16	2.16	2.28	2.23	2.31	2.45
	Area	4749751	2748614	1283222	772693	341624	7576

Sequence 5	RT (min)	2.43	2.48	2.55	2.52	2.57	2.65
	Area	4784668	2740593	1280180	769519	343810	7553
Sequence 6	RT (min)	2.39	2.44	2.42	2.49	2.55	2.66
	Area	4746191	2748507	1280781	778340	340669	8112
Sequence 7	RT (min)	2.24	2.3	2.39	2.41	2.3	2.47
	Area	4821582	2807381	1323804	787433	345089	9601
Sequence 8	RT (min)	2.35	2.36	2.38	2.45	2.45	2.48
	Area	4876690	2812096	1312507	786529	348062	9204
Ascorbic acid (20mM) + buffer	Calibration solution no.	1	2	3	4	5	6
	Concentration (µg/mL)	10	6	3	2	1	0
Sequence 1	RT (min)	2.4	2.49	2.44	2.45	2.49	
	Area	3994018	2308304	1129301	727181	280790	0
Sequence 2	RT (min)	2.45	2.48	2.53	2.53	2.52	
	Area	3781470	2187577	1076089	677206	264247	0
Sequence 3	RT (min)	2.43	2.45	2.48	2.48	2.48	
	Area	3743014	2126331	1052290	659878	257922	0
Sequence 4	RT (min)	2.24	2.4	2.32	2.39	2.41	
	Area	3680588	2109513	1041160	662455	257092	0
Sequence 5	RT (min)	2.34	2.4	2.4	2.47	2.49	
	Area	3632630	2087281	1018944	644201	252834	0
Sequence 6	RT (min)	2.43	2.48	2.49	2.52	2.57	
	Area	3639717	2069823	1021840	648731	252523	0
Sequence 7	RT (min)	2.37	2.43	2.39	2.45	2.47	
	Area	3647437	2101017	1028395	651999	253531	0
Sequence 8	RT (min)	2.36	2.4	2.44	2.45	2.49	
	Area	3629225	2078071	1016276	652415	246713	0
Polymyxin B1 (47.6 µg/mL) + buffer	Calibration solution no.	1	2	3	4	5	6
	Concentration (µg/mL)	10	6	3	2	1	0
Sequence 1	RT (min)	2.32	2.34	2.38	2.32	2.43	2.37
	Area	5224668	2965715	1433966	1054776	481468	15641
Sequence 2	RT (min)	2.42	2.51	2.55	2.61	2.61	2.67
	Area	4946161	2857008	1376123	994040	466962	17137
Sequence 3	RT (min)	2.49	2.53	2.58	2.53	2.55	2.66
	Area	4851158	2836264	1509579	981828	466916	17487
Sequence 4	RT (min)	2.36	2.4	2.4	2.47	2.45	2.48
	Area	4857492	2839924	1523166	947842	463298	18910
Sequence 5	RT (min)	2.48	2.45	2.48	2.48	2.49	2.59
	Area	4865525	2831318	1498428	938241	464586	19507
Sequence 6	RT (min)	2.34	2.4	2.51	2.48	2.49	2.55
	Area	4913009	2872689	1455747	939746	467372	21804
Sequence 7	RT (min)	2.49	2.57	2.57	2.59	2.64	2.61
	Area	4961291	2904722	1454358	942634	478645	27086
Sequence 8	RT (min)	2.47	2.56	2.53	2.6	2.57	2.61
	Area	4957761	2894877	1474177	933518	482484	25577

9.8.5 **H5 - Raw data from the third stability/adsorption test**

This appendix contains the raw data from the third stability/adsorption test described in section 5.3.1 (see **Table 29)**.

Table 29 Raw data obtained from the third stability/adsorption study of colistin. A single sequence was used to measure all samples. 'Sequence N' denotes the Nth time the calibration set was measured. These sets were measured ten times each.

Control (No changes)	#	1	2	3	4	5	6	7	8
	Concentration (µg/mL)	2	1	0.75	0.5	0.25	0.1	0.05	0
Sequence 1	RT (min)	2.52	2.59	2.56	2.65	2.73	2.91		
	Area	1397791	602699	413476	174590	47536	4442	0	0
	Time (h)	0	0	0	0	0	0	0	0
Sequence 2	RT (min)	2.47	2.47	2.48	2.51	2.53	2.91		
	Area	1368259	577482	392710	162944	42176	612	0	0
	Time (h)	4.5	4.5	4.5	4.5	4.5	4.5	4.5	4.5
Sequence 3	RT (min)	2.43	2.46	2.48	2.48	2.53			
	Area	1301795	551887	375695	152881	37230	0	0	0
	Time (h)	9	9	9	9	9	9	9	9
Sequence 4	RT (min)	2.42	2.41	2.43	2.45	2.52			
	Area	1265668	527666	357360	146202	35185	0	0	0
	Time (h)	13.5	13.5	13.5	13.5	13.5	13.5	13.5	13.5
Sequence 5	RT (min)	2.4	2.45	2.45	2.48	2.52			
	Area	1265598	532588	350257	142160	33685	0	0	0
	Time (h)	18	18	18	18	18	18	18	18
Sequence 6	RT (min)	2.4	2.44	2.44	2.48	2.52			
	Area	1250830	522619	352156	137796	32054	0	0	0
	Time (h)	22.5	22.5	22.5	22.5	22.5	22.5	22.5	22.5
Sequence 7	RT (min)	2.4	2.43	2.43	2.48	2.52			
	Area	1291645	535762	356757	143495	32501	0	0	0
	Time (h)	27	27	27	27	27	27	27	27
Sequence 8	RT (min)	2.4	2.45	2.47	2.45	2.49			
	Area	1290874	549206	360040	141957	31246	0	0	0
	Time (h)	31.5	31.5	31.5	31.5	31.5	31.5	31.5	31.5
Sequence 9	RT (min)	2.43	2.43	2.44	2.48	2.52			
	Area	1324473	550548	354923	142331	31316	0	0	0
	Time (h)	36	36	36	36	36	36	36	36
Sequence 10	RT (min)	2.38	2.45	2.43	2.47	2.51			
	Area	1340676	565333	371436	143607	29770	0	0	0
	Time (h)	40.5	40.5	40.5	40.5	40.5	40.5	40.5	40.5
Buffer (100mM ammonium formate, pH 4)	#	1	2	3	4	5	6	7	8
	Concentration (µg/mL)	2	1	0.75	0.5	0.25	0.1	0.05	0
Sequence 1	RT (min)	2.51	2.55	2.54	2.56	2.61	2.65	2.64	

	Area	2280305	1059253	735657	466283	197053	61026	20891	0
	Time (h)	0	0	0	0	0	0	0	0
Sequence 2	RT (min)	2.43	2.48	2.47	2.52	2.55	2.56	2.61	
	Area	2193856	1019279	705038	442831	188877	55649	16355	0
	Time (h)	4.5	4.5	4.5	4.5	4.5	4.5	4.5	4.5
Sequence 3	RT (min)	2.42	2.51	2.47	2.49	2.51	2.55	2.64	
	Area	2110540	972312	662235	419161	177758	53032	13556	0
	Time (h)	9	9	9	9	9	9	9	9
Sequence 4	RT (min)	2.43	2.47	2.45	2.47	2.49	2.55	2.58	2.69
	Area	2072029	946147	653243	409948	173340	50780	12824	2050
	Time (h)	13.5	13.5	13.5	13.5	13.5	13.5	13.5	13.5
Sequence 5	RT (min)	2.4	2.45	2.43	2.45	2.47	2.53	2.6	2.7
	Area	2065352	945393	657766	404528	172043	49423	11896	2586
	Time (h)	18	18	18	18	18	18	18	18
Sequence 6	RT (min)	2.41	2.43	2.44	2.45	2.47	2.45	2.57	2.65
	Area	2084859	966626	669571	408561	170787	49602	10403	3180
	Time (h)	22.5	22.5	22.5	22.5	22.5	22.5	22.5	22.5
Sequence 7	RT (min)	2.38	2.44	2.44	2.47	2.49	2.47	2.59	2.62
	Area	2148603	989527	675320	421051	170768	51746	11519	4841
	Time (h)	27	27	27	27	27	27	27	27
Sequence 8	RT (min)	2.41	2.44	2.45	2.45	2.51	2.53	2.59	2.68
	Area	2184320	1004803	691509	424540	178007	50440	11172	5306
	Time (h)	31.5	31.5	31.5	31.5	31.5	31.5	31.5	31.5
Sequence 9	RT (min)	2.44	2.43	2.43	2.51	2.51	2.51	2.59	2.65
	Area	2200686	1010443	693447	431478	175054	50443	10489	6716
	Time (h)	36	36	36	36	36	36	36	36
Sequence 10	RT (min)	2.45	2.44	2.43	2.45	2.43	2.49	2.57	2.6
	Area	2234023	1027105	705652	437359	179600	49967	9816	7591
	Time (h)	40.5	40.5	40.5	40.5	40.5	40.5	40.5	40.5
Buffer + 10% ACN	#	1	2	3	4	5	6	7	8
	Concentration (µg/mL)	2	1	0.75	0.5	0.25	0.1	0.05	0
Sequence 1	RT (min)	2.48	2.51	2.51	2.55	2.57	2.63	2.61	
	Area	2221192	1023860	744073	469558	214552	69633	30632	0
	Time (h)	0	0	0	0	0	0	0	0
Sequence 2	RT (min)	2.44	2.49	2.45	2.49	2.49	2.59	2.57	
	Area	2143657	988348	709452	450229	202009	65932	26463	0
	Time (h)	4.5	4.5	4.5	4.5	4.5	4.5	4.5	4.5
Sequence 3	RT (min)	2.4	2.41	2.44	2.45	2.46	2.55	2.55	
	Area	2066114	950917	694113	431243	193788	60747	25111	0
	Time (h)	9	9	9	9	9	9	9	9
Sequence 4	RT (min)	2.37	2.41	2.45	2.47	2.49	2.51	2.57	
	Area	2044809	940818	676519	421767	196305	59247	26393	0
	Time (h)	13.5	13.5	13.5	13.5	13.5	13.5	13.5	13.5
Sequence 5	RT (min)	2.4	2.46	2.41	2.43	2.43	2.49	2.57	

	Area	2038812	935687	678425	432941	187417	57551	23435	0
	Time (h)	18	18	18	18	18	18	18	18
Sequence 6	RT (min)	2.38	2.41	2.43	2.48	2.46	2.51	2.55	2.73
	Area	2108499	965023	693773	432946	198943	60476	23449	1401
	Time (h)	22.5	22.5	22.5	22.5	22.5	22.5	22.5	22.5
Sequence 7	RT (min)	2.41	2.43	2.44	2.45	2.47	2.48	2.56	2.77
	Area	2135810	981675	708067	443602	195659	59969	24540	1700
	Time (h)	27	27	27	27	27	27	27	27
Sequence 8	RT (min)	2.4	2.4	2.44	2.4	2.49	2.53	2.53	2.72
	Area	2175601	985309	710673	446562	200293	62472	24918	2559
	Time (h)	31.5	31.5	31.5	31.5	31.5	31.5	31.5	31.5
Sequence 9	RT (min)	2.41	2.43	2.45	2.48	2.49	2.49	2.53	2.69
	Area	2199796	1006812	733142	452212	197248	60842	24159	773
	Time (h)	36	36	36	36	36	36	36	36
Sequence 10	RT (min)	2.4	2.47	2.45	2.48	2.47	2.48	2.54	2.73
	Area	2230740	1010794	733287	463301	200082	61155	24442	2376
	Time (h)	40.5	40.5	40.5	40.5	40.5	40.5	40.5	40.5

9.8.6 H6 - Raw data from the fourth stability/adsorption test

The raw data produced from the fourth stability/adsorption test conducted on colistin can be seen in **Table 30**. This stability/adsorption study was conducted while maintaining autosampler temperature at 20 C.

Table 30 Raw data from the fourth stability/adsorption study of colistin, comparing the effects of buffered solutions at varying concentrations (1, 5, and 10 µg/mL) on the loss of signal due to adsorption and degradation.

		Buffer (100 mM ammonium formate, pH 4)			**Water**		
Time (h)	Concentration	1 µg/mL	5 µg/mL	10 µg/mL	1 µg/mL	5 µg/mL	10 µg/mL
0	Area	1184722	7074682	14877473	416106	4651719	9985029
	RT (min)	2.48	2.39	2.23	2.4	2.32	2.27
1	Area	1238634	7081881	15023609	397498	4629378	9915315
	RT (min)	2.37	2.34	2.24	2.45	2.35	2.28
2	Area	1248578	7145063	15019885	381725	4605616	10010830
	RT (min)	2.39	2.28	2.25	2.4	2.27	2.28
3	Area	1241790	7167935	15003360	375657	4578386	9949289
	RT (min)	2.39	2.3	2.26	2.43	2.34	2.24
4	Area	1249444	7096326	14881037	378916	4569062	9972055
	RT (min)	2.39	2.33	2.27	2.39	2.32	2.28
5	Area	1257644	7173779	14932995	364750	4558628	9929065
	RT (min)	2.39	2.28	2.33	2.39	2.27	2.22
6	Area	1268704	7153145	15068049	359745	4498793	9932474
	RT (min)	2.33	2.27	2.2	2.37	2.26	2.2
7	Area	1253004	7172597	14912141	352128	4461875	9954674
	RT (min)	2.36	2.28	2.19	2.33	2.27	2.22

8	Area	1250796	7131432	14948529	341612	4436196	9913904
	RT (min)	2.39	2.27	2.22	2.43	2.32	2.26
9	Area	1267668	7130468	14992093	346780	4437772	9804118
	RT (min)	2.35	2.28	2.24	2.41	2.28	2.23
10	Area	1269790	7176229	14867570	328278	4362981	9772809
	RT (min)	2.39	2.27	2.19	2.4	2.3	2.23
11	Area	1252857	7079013	14946833	322758	4416126	9748835
	RT (min)	2.41	2.36	2.29	2.45	2.35	2.27
12	Area	1264047	7065789	14784444	321128	4391440	9709237
	RT (min)	2.43	2.35	2.27	2.45	2.35	2.26
13	Area	1260045	7109007	14702139	308330	4343622	9710752
	RT (min)	2.41	2.3	2.24	2.44	2.39	2.31
14	Area	1261899	7115029	14772453	308028	4362427	9685287
	RT (min)	2.47	2.34	2.27	2.48	2.37	2.32
15	Area	1253709	7061853	14678751	302500	4315408	9679267
	RT (min)	2.49	2.38	2.31	2.51	2.37	2.31

9.8.7 H7 – Initial assessment of the limit of quantification

Table 31. Area of colistin peak for a long calibration curve. Solutions were measured twice, in increasing concentrations, with three blank injections between the highest calibration solution of the first sequence and the lowest calibration solution of the second.

Calibration solution concentration (µg/mL)	Area 1	Area 2
0	860	677
0.001	920	2098
0.0025	630	1228
0.005	1275	1455
0.01	721	845
0.025	1839	1972
0.05	516	611
0.1	2821	2968
0.25	21177	13676
0.5	71659	43536
1	198366	147285
2	1337016	1312756
3	2507433	2405734
6	6409674	6027178
10	10626729	9918286

9.9 APPENDIX I - RAW DATA FROM THE METHOD B EVALUATION

9.9.1 I1 – LOQ

The LOQ was established by measuring increasingly concentrated colistin standards, measuring the signal-to-noise ratio, and the area. With the LOD defined as a peak with a signal-to-noise ratio of three, and the LLOQ defined as three times the LOQ, a signal-to-noise ratio of nine would give the LLOQ. It was observed that 0.025 µg/mL gave a signal-to-noise ratio of 12, which was considered sufficiently close to 9 to qualify as the LLOQ.

*Table 32 Area of various colistin concentrations in buffered solutions (100mM ammonium formate, pH 4). The cLOQ was established at 0.025 µg/mL. As the LOD is defined as when the signal-to-noise ratio is equal to 3, and the LOQ is equal to 3 times the LOD, a signal-to-noise ratio of 12 (observed) is sufficiently close to the theoretical value (9) of the LOQ for this work. This data is graphically illustrated in **Figure 36**.*

Concentration (µg/mL)	Area	Signal-to-noise ratio
0.01	0	N/A
0.025	*9557*	*12*
0.1	58674	57
0.25	218361	313
0.5	477858	766
1	1053153	647
5	6580564	1264
10	13904555	1550

9.9.2 I2 – Carry-over

Carry-over was determined by injecting solutions at the ULOQ, followed by blanks with an identical matrix. Carry-over was measured as the percentage ratio of colistin in blanks to colistin at the ULOQ (see **Table 33**).

Table 33 Areas of 10 µg/mL solutions of colistin and subsequent blanks were used to assess the system carry-over, which overall remained low (< 0.1 %).

Concentration (µg/mL)	Area	Carry-over (%)	Mean carry-over	ST.DEV	RSD (%)
10	13904555				
0	9340	0.0672 %	0.0646 %	0.0087 %	13.42%
10	13817046				
0	9237	0.0669 %			
10	13920034				
0	7251	0.0521 %			
10	13941135				
0	10058	0.0721 %			

9.9.3 I3 – Intra-day precision

Intra-day precision was determined by producing six replicates for a total of four concentrations: LLOQ: 0.025 µg/mL, 1.2ULOQ: 0.030µg/mL, 0.5ULOQ:5µg/mL, ULOQ: 10µg/mL. The areas measured for these six replicates and the calibration solutions measured can be seen in **Table 34** and **Table 35**, respectively. For this determination, a non-weighted log-log calibration curve was used. For a non-weighted example, see section 9.12.1.

Table 34 Areas for the solutions used to assess the intra-day precision. Six replicates were prepared and measured in random order. Calibration solutions were measured both before and after the sequence run, and both measurements were used to prepare the calibration curve. (LLOQ: 0.025 µg/mL, 1.2ULOQ: 0.030µg/mL, 0.5ULOQ:5µg/mL, ULOQ: 10µg/mL).

	Replicate 1	Replicate 2	Replicate 3	Replicate 4	Replicate 5	Replicate 6
LLOQ	10068	7290	6305	6733	8374	12151
1.2LLOQ	14987	11016	12097	10899	14855	11082
0.5ULOQ	6625137	6497824	6521428	6519572	6501058	6558190
ULOQ	13569955	13372884	13568982	13708768	13283266	13234593

*Table 35 Areas for the calibration solutions measured during the assessment of the intra-day precision. All solutions were measured twice, used to determine the concentrations of the solutions measured in **Table 34**.*

Name	Concentration (µg/mL)	Area (day 1)
LLOQ	0.025	**10068**
1.2LLOQ	0.03	**14987**
Cal4	0.05	**23001**
Cal5	0.1	**84936**
Cal6	0.5	**491276**
Cal7	1	**1120323**
Cal8	3	**3860697**
Cal9	5	**6965895**
Cal10	10	**14606763**
LLOQ	0.025	**10068**
1.2LLOQ	0.03	**14987**
Cal4	0.05	**22113**
Cal5	0.1	**81902**
Cal6	0.5	**487812**
Cal7	1	**1108011**
Cal8	3	**3795900**
Cal9	5	**6863267**
Cal10	10	**14323371**

Table 36 back-calculated concentrations from the intra-day precision experiment. R [n] stands for replicate n. Data are presented.

Concentration (µg/mL)

	R 1	R 2	R 3	R 4	R 5	R 6	Mean	ST.DEV	RSD (%)
LLOQ	0.0244	0.0188	0.0167	0.0176	0.0210	0.0284	0.0211	0.0041	19.38%
1.2LLOQ	0.0336	0.0262	0.0283	0.0260	0.0334	0.0263	0.0290	0.0033	11.36%
0.5ULOQ	4.6343	4.5622	4.5756	4.5745	4.5640	4.5964	4.5845	0.0249	0.54%
ULOQ	8.2757	8.1783	8.2752	8.3441	8.1340	8.1099	8.2195	0.0845	1.03%

9.9.4 I4 – inter-day precision

Inter-day precision was assessed by measuring four control solutions (same as for intra-day precision). All solutions were made from scratch using a new standard every day. Raw areas can be seen in **Table 37** and **Table 38**.

Table 37 Areas measured for calibration solutions on separate days (dates shown).

Date	**4/21/2021**	**4/22/2021**	**4/23/2021**	**4/28/2021**	**4/29/2021**	**4/30/2021**
Concentration (µg/mL)	Area day 1	Area day 2	Area day 3	Area day 4	Area day 5	Area day 6
0	0	0	0	0	0	0
0.025	10068	10191	10866	10614	8893	9473
0.03	14987	12566	12637	14637	9066	12616
0.05	23001	24042	25428	23931	22174	15946
0.1	84936	68618	84820	67588	52704	60744
0.5	491276	[6]	477310	460939	370970	439463
1	1120323	1035231	1108105	921126	834808	948363
3	3860697	3736009	3655828	3523809	2912224	3450584
5	6965895	6628029	6653574	6134938	5188016	6049565
10	14606763	14237997	13900482	13058636	11184306	12708898
0	0	0	0	0	0	0
0.025	10068	10191	10866	10614	8893	9473
0.03	14987	12566	12637	14637	9066	12616
0.05	22113	23764	28154	24545	21430	13571
0.1	81902	67867	82858	69203	53849	57626
0.5	487812	[7]	492910	474908	392289	429873
1	1108011	1014104	1134600	949918	871785	927866
3	3795900	3665659	3733676	3527968	2947730	3384448
5	6863267	6522534	6688858	6078639	5236604	5864846
10	14323371	14070329	14060151	12981154	11115277	12588488

Table 38 Raw areas measured for control solutions on separate days used to assess the inter-day precision.

Day 1	LLOQ	10068

[6] Not measured due to sample contamination that was only observed post-measurements.
[7] Not measured due to sample contamination that was only observed post-measurements.

	1.2LLOQ	14987
	0.5ULOQ	6625137
	ULOQ	13569955
Day 2	LLOQ	10191
	1.2LLOQ	12566
	0.5ULOQ	6646557
	ULOQ	14619729
Day 3	LLOQ	10866
	1.2LLOQ	12637
	0.5ULOQ	6834735
	ULOQ	14220921
Day 4	LLOQ	10614
	1.2LLOQ	14637
	0.5ULOQ	5716943
	ULOQ	13183090
Day 5	LLOQ	8893
	1.2LLOQ	9066
	0.5ULOQ	5339687
	ULOQ	11211754
Day 6	LLOQ	9473
	1.2LLOQ	12616
	0.5ULOQ	6027766
	ULOQ	12456012

9.9.5 I5 – Reinjection reproducibility

By injecting the same sample of colistin 20 times directly after one another, the reinjection reproducibility from the instrument itself was assessed. This is expressed as the RSD (%) and was equal to 0.50 % for the qualifier transition and 0.42 % for the quantifier transition. This was done without the use of a calibration curve and rather the peak area itself. This also showed a constant relationship between the quantifier and qualifier transition ratios, with the qualifier transition having a 30 % intensity of the quantifier transition.

Table 39 Areas of a 10 µg/mL solution of colistin, injected 20 times in sequence. The areas for the quantifier and qualifier transition peaks were measured and compared.

Injection #	Quantifier Area	Qualifier Area	Relative ratio (Qualifier/Quantifier) (%)
1	8458905	2478704	29.30%
2	8480795	2494781	29.42%
3	8474736	2479134	29.25%
4	8481676	2495276	29.42%
5	8486468	2477895	29.20%
6	8529856	2507813	29.40%
7	8534480	2509388	29.40%

8	8512277	2506857	29.45%
9	8580042	2516565	29.33%
10	8534179	2510327	29.41%
11	8489450	2505009	29.51%
12	8589237	2507198	29.19%
13	8545944	2507472	29.34%
14	8560614	2494888	29.14%
15	8505718	2499636	29.39%
16	8563172	2507745	29.29%
17	8508805	2514850	29.56%
18	8519557	2504626	29.40%
19	8518575	2502352	29.38%
20	8550553	2527555	29.56%

9.9.6 I6 – Matrix effects

Matrix effects were addressed by comparing areas of equal concentrations of colistin in various buffers. The raw data can be seen in **Table 40**. Furthermore, confirmation that in-solutions salts did not co-elute with colistin E1 can be seen as the white band of ion suppression present in **Figure 46**.

*Table 40 Areas of colistin in varying concentrations in various buffers. '0' means no peak was observed. X means the solution was mishandled during sample preparation. This table is an excerpt from **Table 41**, **Table 42**, **Table 43,** and **Table 44.***

Matrix (Buffer)	**Tris**	**Ammonium formate**	**PBS**	**Citric acid**
Concentration (µg/mL)	Area	Area	Area	Area
0	0	0	0	0
0.025	0	X	0	4186
0.05	0	13571	0	7629
0.1	11860	57626	0	19269
0.25	59026	X	0	77715
0.5	161549	429873	39397	204399
1	445896	927866	326239	1153513
5	3294264	5864846	3312011	7239821
10	7244480	12588488	7665390	15433526

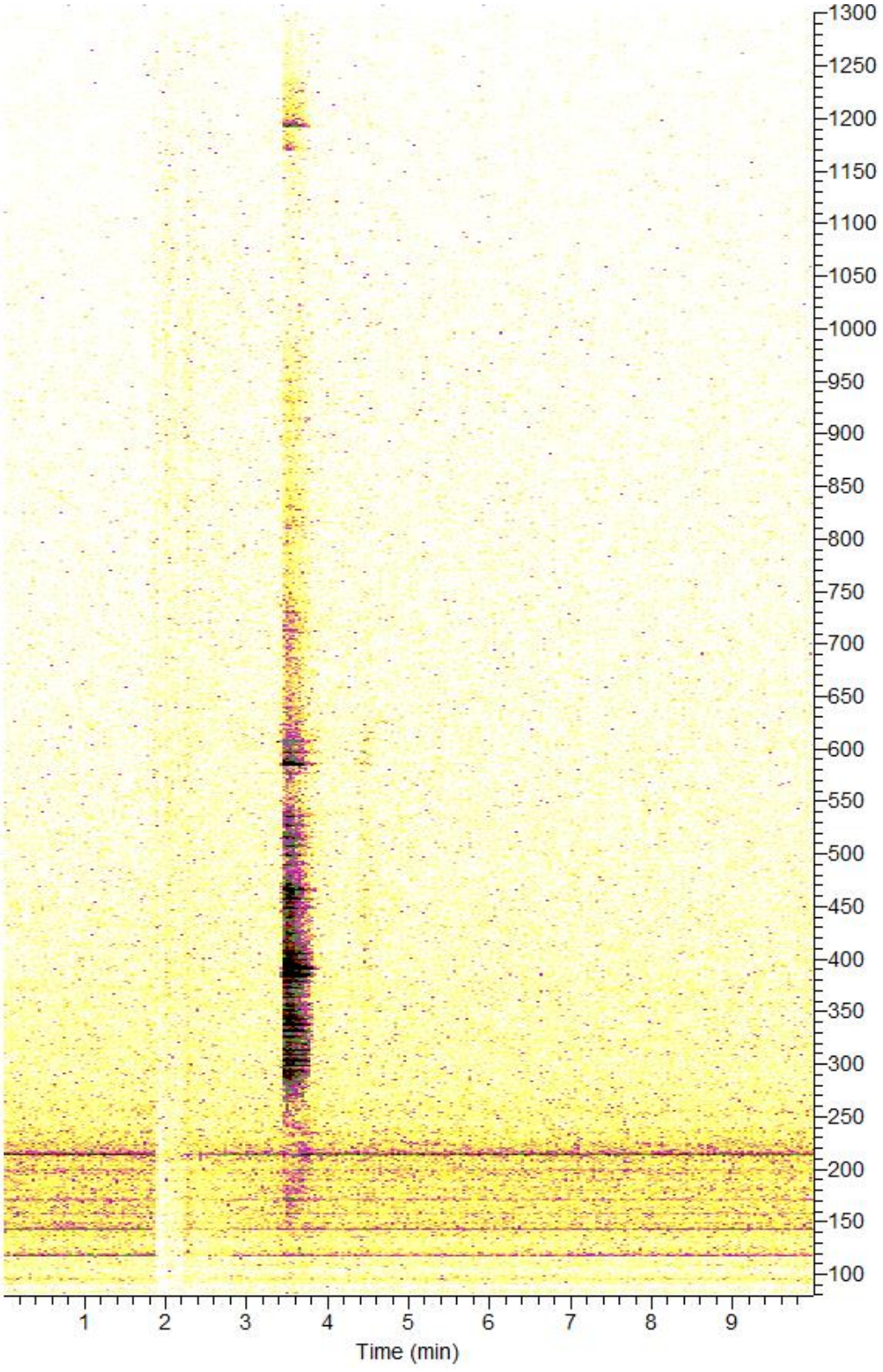

Figure 46 Full scan ion map chromatogram of a 10 µg/mL solution of polymyxin E1, with time in minutes on the x-axis and m/z value on the y-axis. Intensity is displayed via. a color scheme (white->yellow->purple->black). This injection required manual control of both MS and LC instruments, and the retention time is significantly longer than in automated injections. However, elution of ammonium formate can be seen clearly as ion suppression around the two-minute mark, with polymyxin E1 eluting around one and a half minutes later.

Table 41 Raw areas over time for colistin solutions in 50 mM ammonium formate buffer (pH apx. 3.5). $t1, t2$ and t_3 are measurements done 6.5, 13, and 19.5 hours after $t0$, respectively. A dash means the solution was mishandled during sample preparation.

#	Conc. [µg/mL]	t0	t1	t2	t3
1	0	0	0	0	0
2	0,025	-	-	-	-
3	0,05	13571	14017	12609	12321
4	0,1	57626	56620	55623	51572
5	0,25	-	-	-	-
6	0,5	429873	441030	433570	427438
7	1	927866	958199	963229	954025
8	5	5864846	6258327	6257790	6321956
9	10	12588488	13211319	13287325	13337467

Table 42 Raw areas over time for colistin solutions in 50 mM PBS buffer (pH apx. 7.4). $t1, t2$ and t_3 are measurements done 6.5, 13, and 19.5 hours after $t0$, respectively.

#	Conc. [µg/mL]	t0	t1	t2	t3
1	0	0	0	0	0
2	0,025	0	0	0	0
3	0,05	0	0	0	0
4	0,1	11860	8819	3055	0
5	0,25	59026	47843	33868	31375
6	0,5	161549	141543	130910	128479
7	1	445896	398619	398202	400051
8	5	3294264	3105339	3189072	3176213
9	10	7244480	6849310	7013086	7009567

Table 43 Raw areas over time for colistin solutions in 50 mM tris buffer (pH apx. 7.2). $t1, t2$ and t_3 are measurements done 6.5, 13, and 19.5 hours after $t0$, respectively.

#	Conc. [µg/mL]	t0	t1	t2	t3
1	0	0	0	0	0
2	0,025	0	0	0	0
3	0,05	0	0	0	0
4	0,1	0	0	0	0
5	0,25	0	0	0	0
6	0,5	39397	33876	30952	28532
7	1	326239	302272	290847	277784
8	5	3312011	3279995	3217869	3167535
9	10	7665390	7555421	7481446	7418054

Table 44 Raw areas over time for colistin solutions in 50 mM citric acid buffer (pH apx. 5.5). $t1, t2$ and t_3 are measurements done 6.5, 13, and 19.5 hours after $t0$, respectively.

#	Conc. [µg/mL]	t0	t1	t2	t3
1	0	0	0	0	7392
2	0,025	4186	3848	3538	4468
3	0,05	7629	5973	6346	5101
4	0,1	19269	18129	20758	17218
5	0,25	77715	75735	68202	72643
6	0,5	204399	202522	202591	198391
7	1	1153513	1205047	1227821	1208498
8	5	7239821	7501436	7565606	7427915
9	10	15433526	15974557	16155581	15802455

9.9.7 I7 – Effect of different ammonium formate concentrations

The effect of the ammonium formate concentrations on solutions of colistin ranging from 0.025 to 1 µg/mL was examined by creating calibration solutions in ammonium formate buffers at pH 3, but concentrations of 100, 150, and 200 mM ammonium formate. The data obtained showed no significant difference in response (areas), and it was concluded that a higher concentration than 100mM yielded no significant improvement in signal nor reduction of adsorption (see **Figure 47**).

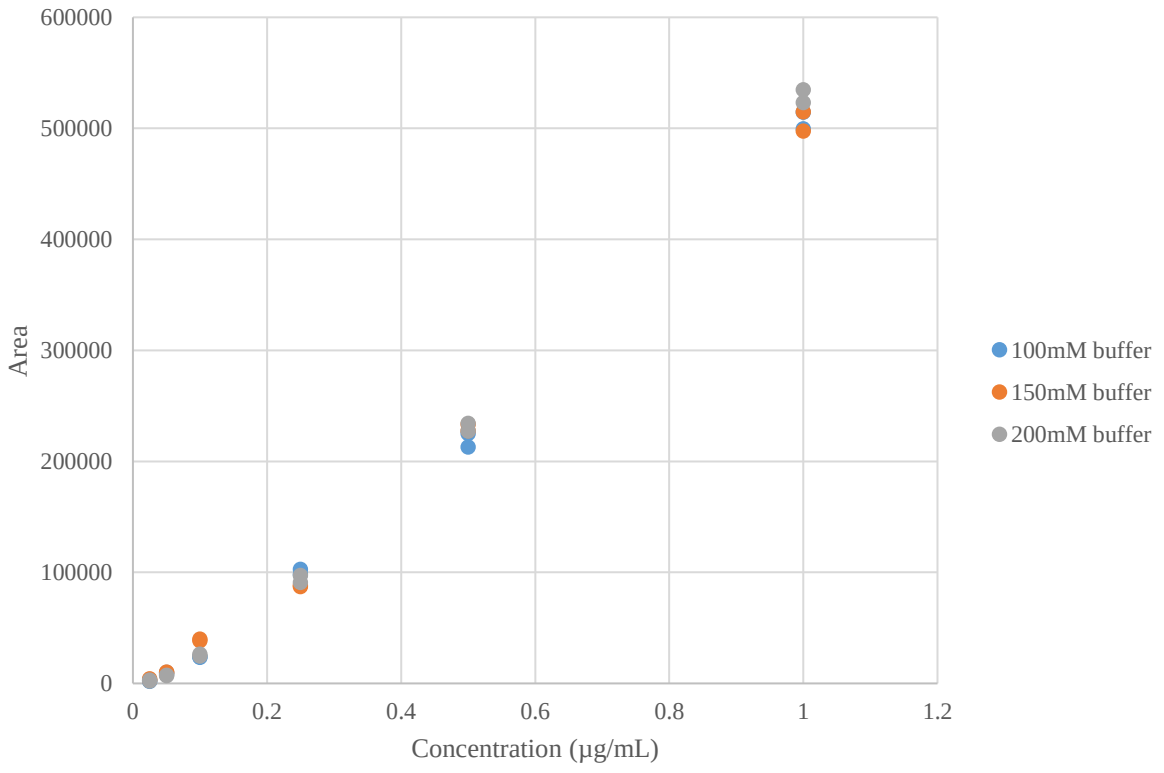

*Figure 47 Area versus concentration of colistin solutions ranging from 0.025 to 1 µg/mL, solutions at pH 3, and ammonium formate concentrations of 100, 150, and 200 mM. The graph was produced using the data from **Table 45**.*

Table 45 Areas for calibration solutions of colistin in buffered solutions of ammonium formate, with ammonium formate concentrations of 100, 150, and 200 mM. Solutions were measured twice, with the lower set being the latter measurement.

	Area		
Colistin concentration (µg/mL)	100mM buffer	150mM buffer	200mM buffer
1	499603	497413	523224
0.5	212923	227481	227280
0.25	98216	87110	91046
0.1	23468	38386	24634
0.05	9787	9568	7273
0.025	2447	4099	2008
1	514487	514781	534705
0.5	224898	233363	234114
0.25	102692	88253	97326
0.1	23895	39885	26281
0.05	8513	10240	6855
0.025	1737	3096	2888

9.9.8 I8 – Effect of pH

The effect of the pH on colistin loss (adsorption/degradation) was assessed using a 100mM ammonium formate buffer, modified using ammonia and formic acid to achieve pH 3, 6, and 9. These buffers were then used as diluents to prepare working solutions and calibration solutions, showing a clear trend clarifying that a low pH was necessary to reduce colistin loss. Each calibration solution was measured a total of three times (see **Figure 48**). This means that strict control of pH is required to reduce colistin loss to adsorptive effects and degradation. This is made clear in **Figure 49**, showing a distinctly decreasing trend in signal over time for colistin solutions at pH 9 versus pH 3. The same trend was observed for pH 6 but not equally visible at first glance, and an illustration was therefore omitted.

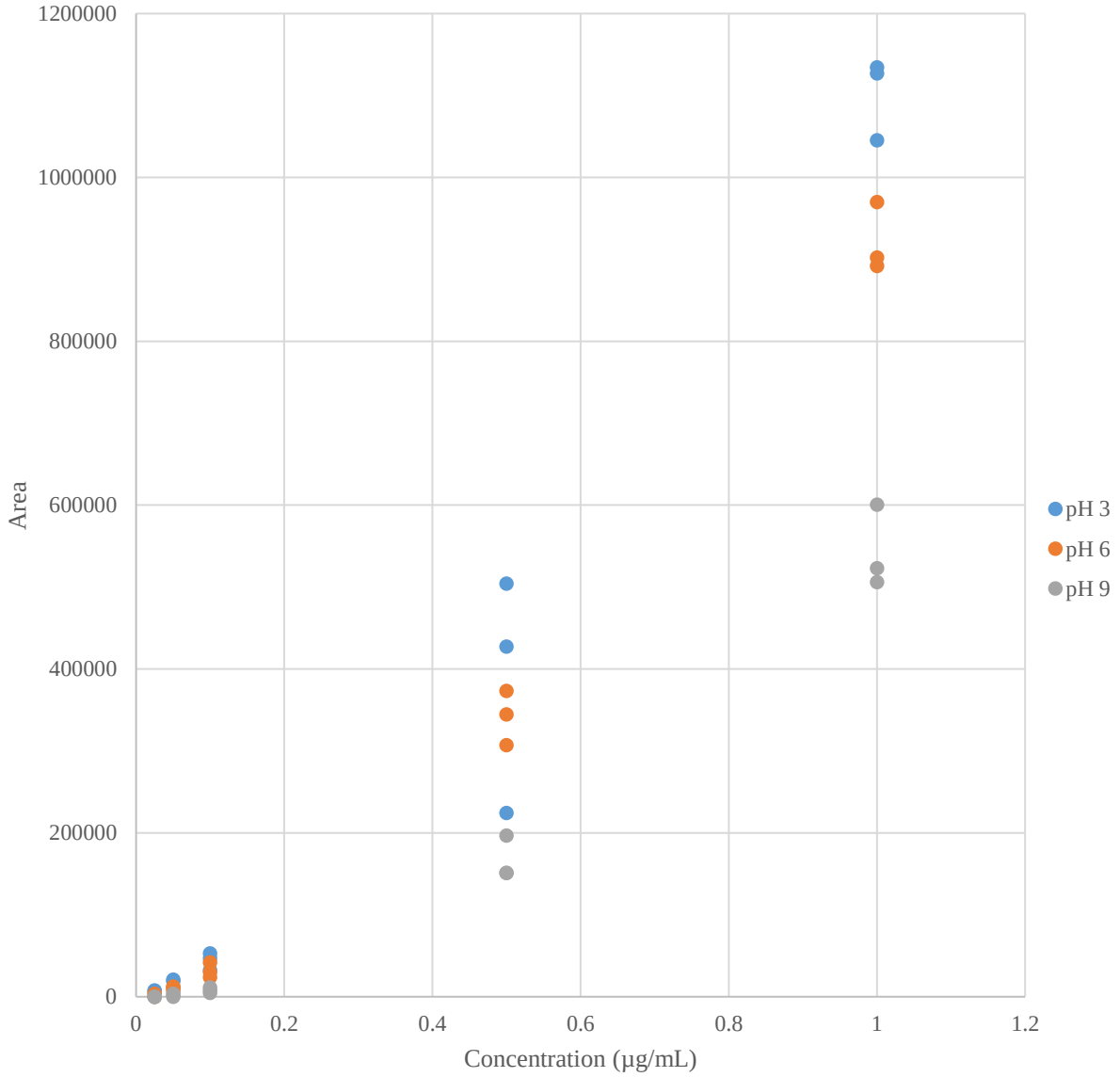

Figure 48 Area versus concentration for calibration curves with 100mM ammonium formate solutions, pH-adjusted to pH 3, 6, and 9. The data shows an apparent decrease in signal as the pH increases. The graph was produced using data from ***Table 46****.*

Table 46 Areas for solutions of colistin at varying concentrations at various pH points, showing a clear trend where signal strength decreases as the pH increases.

	Area		
Concentration (µg/mL)	pH 3	pH 6	pH 9
0.025	7359	3618	0
0.05	20694	12500	3455
0.1	52979	41629	11351
0.5	504230	373070	196684
1	1134188	969911	600690
0.025	7506	2369	0
0.05	19010	9814	2225
0.1	46884	30055	7466

0.5	224183	344394	150866
1	1126815	902063	523024
0.025	4980	0	0
0.05	11456	7121	0
0.1	32287	23733	4485
0.5	427456	307136	150895
1	1045295	891949	506160

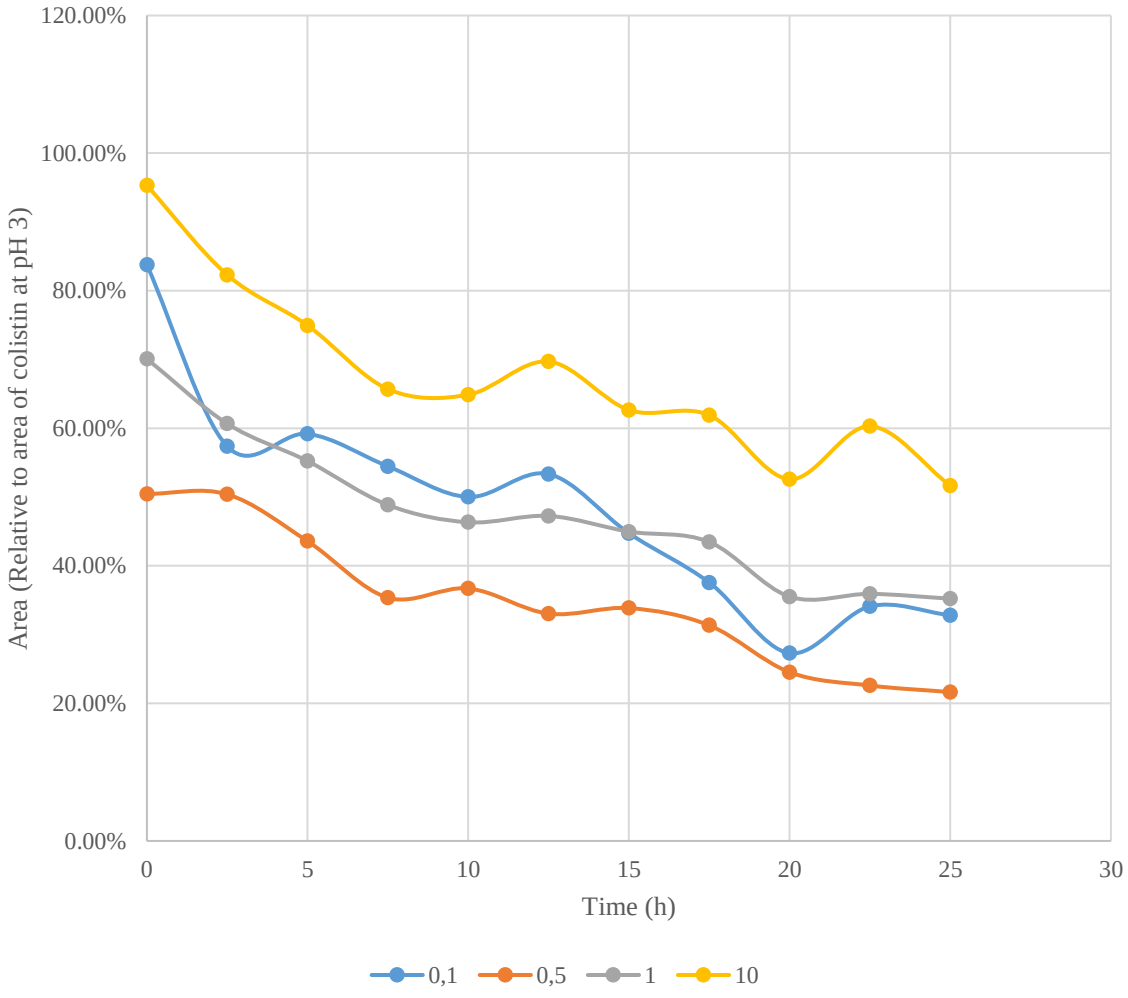

*Figure 49 Area of solutions of colistin at 0.1, 0.5, 1, and 10 µg/mL at pH 9, relative to solutions of equal colistin concentrations at pH 3, showing a distinctly decreasing trend in signal over time. The graph was produced using data from **Table 47**.*

Table 47 Areas over time for solutions at pH 3, 6, and 9 for colistin solutions of concentrations of 0.1, 0.5, 1, and 10 µg/mL, used to assess the effect of pH on stability of buffered solutions. MS ion source contamination is thought to be responsible for the significant spread of the signals for the same solutions, and assessment was performed using relative signals.

	(pH 3)			
Concentration (µg/ml)	0.1	0.5	1	10

	0	15104	126461	314036	4345421
	2.5	25419	153325	397670	5787990
	5	27634	174195	460290	6724893
	7.5	29172	189666	490559	7079721
	10	28192	179491	470348	6538359
Time (h)	12.5	26872	181187	447823	6348923
	15	32392	172909	451343	6383119
	17.5	34152	175520	450339	6254966
	20	33535	161692	399779	5517131
	22.5	27171	138070	335164	4743312
	25	27676	141711	358202	4989588
		(pH 6)			
	Concentration (µg/ml)	0.1	0.5	1	10
	0	15064	113285	318827	4890429
	2.5	16568	135510	399731	6230816
	5	18096	147426	422114	6900220
	7.5	18320	153785	421797	6872503
	10	18265	145061	396362	6396491
Time (h)	12.5	17997	143484	396221	6497737
	15	18317	142101	392508	6123775
	17.5	17319	138941	406248	6288344
	20	14309	114238	310357	4885694
	22.5	14696	119283	314014	4808834
	25	13982	113022	320828	5008872
		(pH 9)			
	Concentration (µg/ml)	0.1	0.5	1	10
	0	12649	63802	220091	4140648
	2.5	14582	77259	241218	4762943
	5	16354	75909	254203	5039760
	7.5	15886	67066	239594	4650033
	10	14096	65889	217888	4241108
Time (h)	12.5	14333	59862	211582	4424587
	15	14489	58531	202960	3998809
	17.5	12829	55011	195714	3871528
	20	9153	39664	141993	2901064
	22.5	9265	31196	120388	2859526
	25	9079	30668	126170	2576850

9.9.9 I9 - Retention times

The retention time for colistin was determined using data from **Appendix H3** – Raw data from the first stability/adsorption test and **H4** – Raw data from the second stability/adsorption test. The retention time for polymyxin B1, less examined in this work, was determined by 60

injections of a mixture of polymyxin E1 and polymyxin B1, both with a concentration of 10 µg/mL in a 100 mM solution of ammonium formate at pH 3. The recorded retention times for polymyxin E1 and B1 are listed in **Table 48**. With 60 data points, this gave average retention times of 2,35 ± 0,03 and 3,40 ± 0,05 minutes for polymyxin E1 and polymyxin B1, respectively.

Table 48 Retention times for a mixture of polymyxin E1 and B1, with a 10 µg/mL concentration for both analytes.

	RT (minutes)	
Injection #	Polymyxin E1	Polymyxin B1
1	2,38	3,46
2	2,38	3,44
3	2,38	3,45
4	2,36	3,45
5	2,38	3,43
6	2,36	3,44
7	2,37	3,4
8	2,33	3,38
9	2,35	3,39
10	2,33	3,37
11	2,37	3,4
12	2,34	3,39
13	2,34	3,37
14	2,31	3,35
15	2,31	3,37
16	2,33	3,37
17	2,3	3,35
18	2,34	3,42
19	2,34	3,39
20	2,35	3,39
21	2,35	3,4
22	2,34	3,38
23	2,31	3,35
24	2,34	3,39
25	2,36	3,4
26	2,37	3,43
27	2,38	3,43
28	2,38	3,43
29	2,36	3,43
30	2,38	3,43
31	2,39	3,45
32	2,36	3,45
33	2,37	3,44
34	2,36	3,43

35	2,38	3,47
36	2,39	3,47
37	2,38	3,45
38	2,39	3,45
39	2,39	3,44
40	2,37	3,45
41	2,34	3,44
42	2,39	3,44
43	2,38	3,44
44	2,38	3,44
45	2,35	3,41
46	2,39	3,45
47	2,31	3,35
48	2,34	3,37
49	2,33	3,36
50	2,34	3,35
51	2,31	3,39
52	2,3	3,36
53	2,35	3,36
54	2,31	3,32
55	2,28	3,31
56	2,25	3,28
57	2,29	3,32
58	2,3	3,32
59	2,27	3,28
60	2,28	3,27

9.10 APPENDIX J – ATTEMPTED LIQUID CHROMATOGRAPHY WITH ULTRAVIOLET AND REFRACTIVE INDEX DETECTION

Attempts were made at measuring colistin using an LC-UV-RI system. This system is described in detail in the next section.

9.10.1 J1 - Experimental

All components of the LC-UV-RI system came from Shimadzu. It consisted of a SIL10ADvp autosampler, two LC10ADvp pumps, a DGU14A degasser, a CTO10Avp column oven, a SCL10Avp system controller, an SPD-M10Avp diode array detector (DAD), and a RID10a refractive index detector. Shimadzu LCsolution software was used in this setup.

The column temperature was set to 40ºC. The flow rate was set to 1.0 mL per minute. An xBridge C18 column (4.6mm x 50mm) was used for testing the suitability of UV-RI detection. Mobile phase A consisted of neat type 1 water. Mobile phase B consisted of LC-grade ACN.

For each, a flow rate of 1.2 and 0.5 mL/min were used. The runtime for all flow programs was 16 minutes (where the last 5 minutes were used to re-equilibrate the column). The system was then auto-purged (5 mL/min) for five minutes. The attempted flow programs can be seen in **Table 49**.

Table 49. Various attempted flow programs were used in the attempted UV detection of polymyxin B1 and E1. Mobile phase B was ACN + 0.1% formic acid. Mobile phase A was H_2O with 0.1% formic acid.

Flow program	%B at the start	% B at the end	Run time (min)
Isocratic	10		16
Isocratic	50		16
Isocratic	80		16
Gradient	10	80	16
Gradient	10	90	16
Gradient	90	10	16
Gradient	80	10	16

Absorption spectra for the two analytes were measured using a NanoDrop 2000 with a 1 mm light path from ThermoFisher.

9.10.1.1 Size exclusion chromatography with ultraviolet and refractive index detection

For the SEC-UV-RI method development, the LC-UV-RI system described in the former section was used. Mobile phase A consisted of neat type 1 water, and mobile phase B consisted of 50/50 type 1 water/methanol (v/v). Mobile phase A was the only one used, while mobile phase B was used for flushing the system before instrument shutdown to prevent bacterial growth when the instrument stood idle. Mobile phase A was replaced daily for this exact reason.

9.10.2 J2 - Liquid chromatography with ultraviolet and refractive index detection for the measurement of colistin

Despite reports that the significant constituents of polymyxin E1 possess a low UV absorbance [117-120], the LC-UV-RI system was used to detect both polymyxin E1 and the IS (polymyxin B1) used. Injections of 10 µg/mL solutions of polymyxin B1 and E1, respectively, were injected

into the system with increasing volumes, ranging from 10 to 100 µL. No signals outside the solvent front were observed in any chromatograms, and various flow programs were attempted (see **Table 49**, section 9.10.1).

As no signals were observed even when injecting 1 mg/mL solutions, absorption spectra for both polymyxins were analyzed by the NanoDrop described in section 9.10.1. These revealed low UV absorbance above 200 nm. As a result of the insufficient sensitivity, UV and RI-based detection were discarded as a viable option. For more details, see **Appendix J** – Attempted liquid chromatography with ultraviolet and refractive index detection

Thus, following several attempts and a low UV absorbance (see **Figure 51** in **Appendix J** – Attempted liquid chromatography with ultraviolet and refractive index detection), UV detection was deemed impossible without derivatization. Derivatization was not considered a viable option, as the original aim of the thesis was to observe the interactions and kinetics between polymyxin E1 and liposomes. RI-based detection has an inherently lower sensitivity than UV [121] and provided a similar lack of chromatographic peaks, and was also deemed unfit for the analysis of aqueous solutions of polymyxins in free solution with concentrations $\leq$ 0.1 mg/mL.

9.10.3 J3 - Method development for the determination of free and encapsulated polymyxin E1 using size exclusion chromatography

To measure the released amount of polymyxin E1 and the encapsulated polymyxin E1 without having to dialyze the samples of loaded liposomes, separation of free and encapsulated colistin was required, using the SEC column described in section 4.2. These liposomes could be perturbed later, so the polymyxin E1 content within could be measured.

As described in section 2.4.2, the SEC column should be pre-saturated with perturbed liposomes, pseudo-free phospholipids, to ensure reproducibility. Therefore, an HPSEC method would involve regular re-injections of sonicated liposomes to maintain intra-day and intra-run phospholipid saturation on the SEC particles to maintain repeatability.

9.10.3.1 J3.1 - Column saturation and fractionation development

Phospholipids are known to cause contamination in ESI-MS systems [122]. For this reason, it was preferable to use the LC-UV-RI system for the development of a fractionation method and to test the SEC column described in section 4.2 with solutions of both perturbed (sonicated) and intact liposomes. Using pure or buffered water and no organic mobile phase components for the elution of liposomes in SEC columns has been done numerous times [123-127] and was

thought to help maintain the structural stability of the liposomes. While there exists some literature using low amounts (< 10%) of organic solvents [128], pure water was chosen for the sake of simplicity.

While RI-based detection is a viable option for measuring liposomes and less sensitive to liposome morphology than some other detectors [129], it was desirable to utilize UV detection as this remains overall more sensitive and has a more extended linear range [121]. This detector was also part of the instrumentation present. To find a useful wavelength, UV absorption spectra were measured using the Nanodrop described in section 9.10.1. The UV absorption spectra are shown in the next section.

The spectra show an evident absorption around apx. 190 nm for DMPC-PEG liposomes. This wavelength remains a viable option if a mobile phase without organic modifiers or constituents is used, as these typically have UV absorption near the low end of the UV range [130]. Therefore, if these must be used, a higher wavelength must also be used so that the analyte signal does not become lower than the higher background signal from the mobile phase. However, due to time constraints, the SEC-UV-RI system was not used further, but as described in section 6, it retains significant potential worthy of further investigation.

9.10.3.2 J3.2 – Absorbance spectra

Figure 50 and **Figure 51** show UV absorption spectra for liposomes and polymyxins, respectively.

(A)

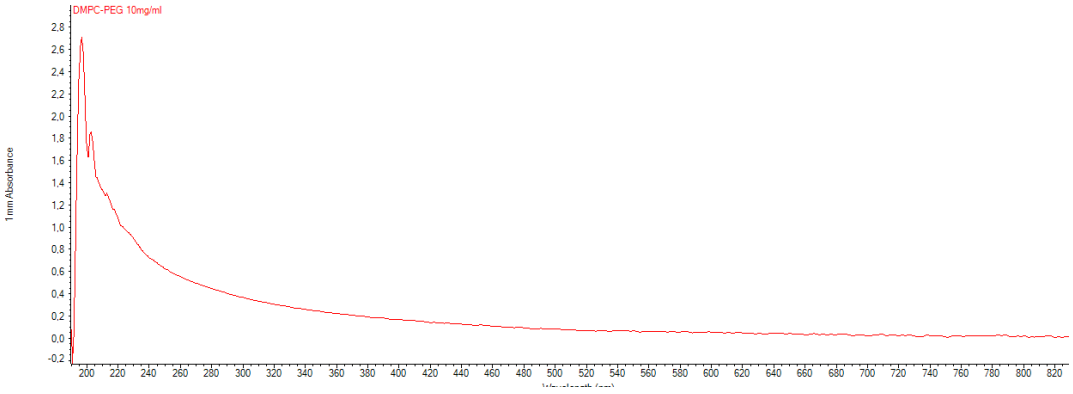

(B)

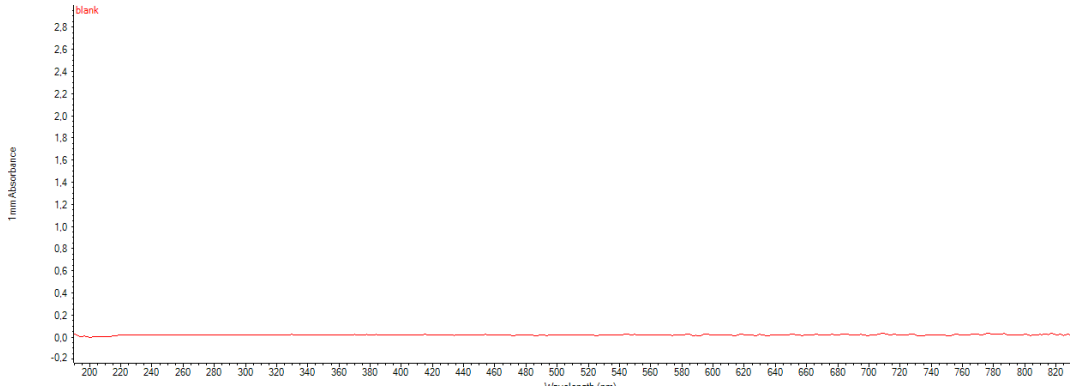

Figure 50 UV-VIS absorption spectra of (A) solution of 10 mg/mL DMPC-PEG liposomes and (B) blank, type 1 water.

(1)

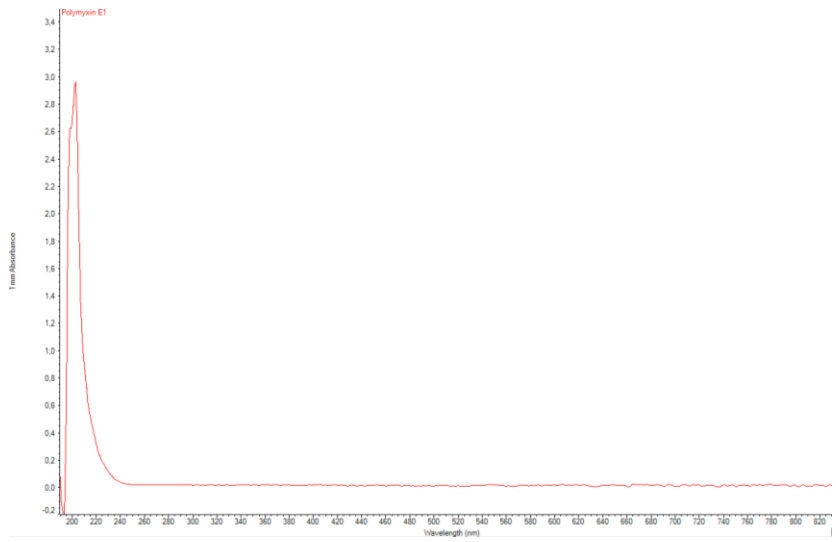

(2)

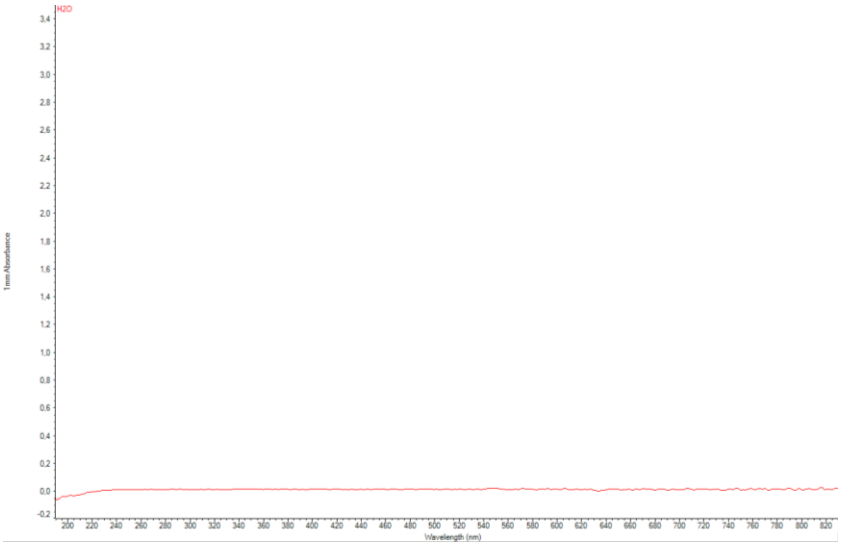

(3)

Figure 51. UV absorption spectra measured on a Nanodrop 2000 in UV-VIS mode. (1) UV-VIS spectrum for polymyxin B1. (2) UV-VIS spectrum for polymyxin E1. (3) UV-VIS spectrum of blank (Type 1 H_2O). All samples were referenced against a blank (Type 1 H_2O).

9.11 Appendix K – Colistin pH estimation

In the following calculation, the pH of a 10 µg/mL solution of colistin is estimated to be around 10. In this calculation, pH effects from carbonate and other effects are ignored. The calculation, however, is based on the following assumptions:

- Carbonate from the atmosphere does not interact with colistin
- Colistin is only protonated once (and not up to five times)
- The most basic state of colistin (pKa of 10.2) is assumed to be the fully unprotonated state of colistin.

The predicted value for pK_b is calculated.

$$pK_a = 10.2 => pK_b = 14 - 10.2 \quad (1)$$

$$pK_b = 3.8 \quad (2)$$

The equilibrium equation for a generic, single-protonated base is

$$K_b = \frac{[OH^-][HA^+]}{[A]} \quad (3)$$

Insertion of (2) into (3) gives (4)

$$10^{-3.8} = \frac{[OH^-][HA^+]}{[A]} \quad (4)$$

Which can be written as

$$10^{-3.8} = \frac{x^2}{a - x} \quad (5)$$

Where a is the starting concentration of colistin. To calculate the molarity of 10 µg/mL colistin, the molar mass of polymyxin E1 is used

$$M_{polymyxin\ E1} = 1168.8 g/mol \quad (6)$$

Calculating a in a 10 µg/mL solution gives

$$n_{10\ \mu g/mL} = \frac{0{,}01\ g\ /\ L}{1168.8\ g\ /mol} \quad (7)$$

$$n_{10\ \mu g/mL} = 0{,}00000856\ M \quad (8)$$

Inserting a = (8) into (5), the following expression is obtained

$$10^{-3.8} = \frac{x^2}{0.0085mM - x} \quad (9)$$

$$(0.0085 * 10^{-3} M * 10^{-3.8}) - 10^{-3.8} x - x^2 = 0$$

Which yields

$$x_1 = 1.66 * 10^{-4}\ M \quad (10)$$

$$x_2 = -8.09 * 10^{-6}\ M$$

Calculating pOH using x_1 from (10) gives

$$pOH = -\log_{10}(1.66 * 10^{-4}) \quad (11)$$

$$pOH = 3.78$$

Calculating pH from pOH

$$pH = 14 - pOH \quad (12)$$

Insertion of (11) into (12) gives the theoretical pH.

$$pH = 14 - 3.78 \quad (13)$$

$$pH = 10{,}22$$

9.12 APPENDIX L - STATISTICS

9.12.1 L1 - Calibration curve fittings

When the range on the x-axis is extensive (more than one order of magnitude), the assumption of homoscedasticity made in the standard linear regression often causes errors in the lower end of the calibration solution. With a more considerable variance at higher concentrations, these

influence (weight) the calibration curve equation more strongly than those at lower concentrations, often causing lower accuracy at lower concentrations [131-133].

However, the easiest way to negate this effect is to use a weighted least-squares linear regression. Data points are 'weighted' based on the dependent (area) or independent (concentration) variables. This can be justified with the extensive range on the x-axis and an F-test or a visual plot of the residuals of the calibration curve. If this shows heteroscedasticity, a weighted calibration curve may be justifiably used, given that it provides more accurate concentrations when back-calculating the concentrations of the calibration solutions. In this work, only linear, non-weighted curve fittings were implemented before the method validation (Section 5.3). Following this section, a quadratic, unweighted fitting of log-log transformed data curve was used to create the calibration curve, the choice of which is justified and explained in this section.

To exemplify, the data from the intra-day precision (see section 9.9.3) is used in this section. When using a non-weighted calibration curve, all data points are assumed to have equal variance (homoscedastic) across the calibration range. The non-weighted calibration curve prepared for this can be seen in **Figure 52**.

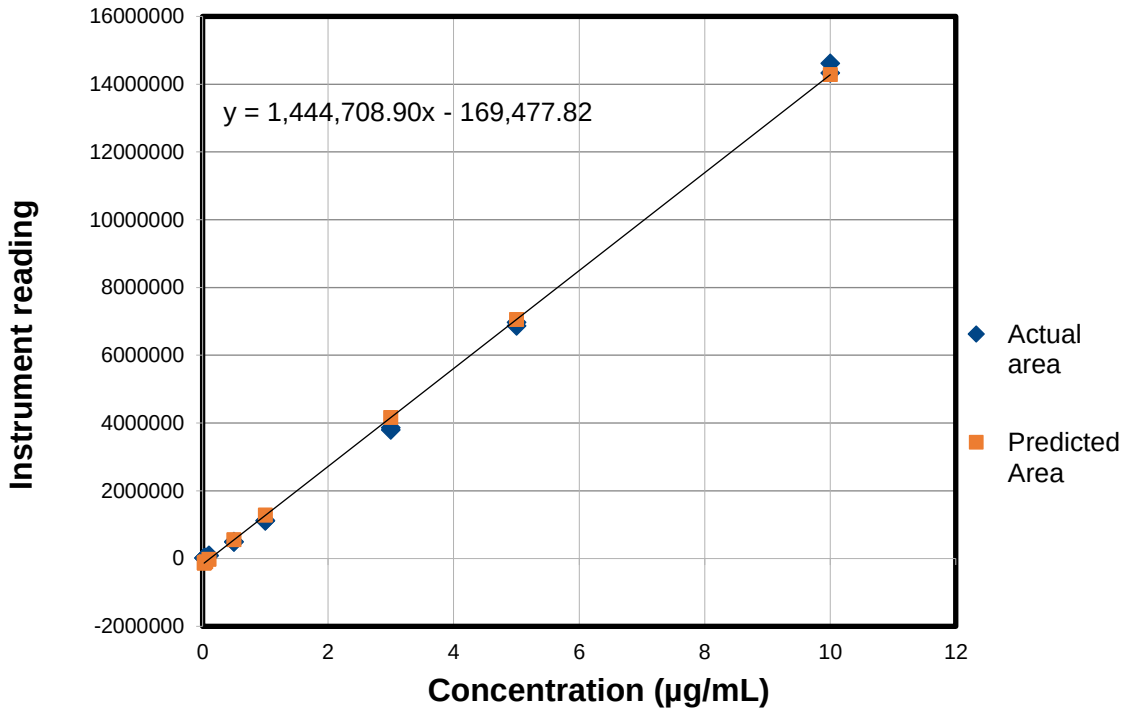

*Figure 52 Non-weighted calibration curve for the calibration solutions prepared to assess the intra-day precision; see **Table 35**. This gives an R^2 of 0.9985.*

Note the significantly low intersect on the y-axis. If a weighted calibration curve is used (with a weighting of $1/x$) is used, we get **Figure 53**. Note the difference in the intersect, which becomes reduced by more than an order of magnitude.

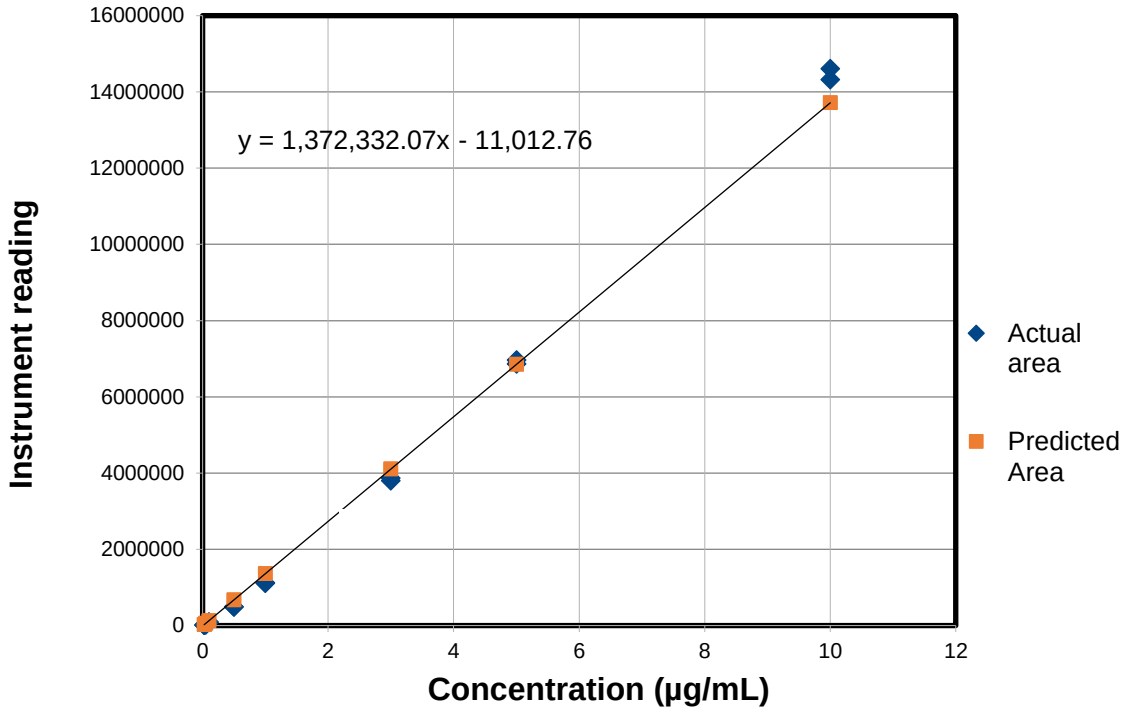

*Figure 53 Weighted calibration curve for the calibration solutions prepared to assess the intra-day precision; see **Table 35**. Weighted using a $1/x$ relationship. This gives an R^2 of 0,9926.*

It is worth noting that a linear calibration curve with more substantial weighting (such as $1/x^2$) should not be used, as this gives a poor fit for higher calibration points without a significant improvement in back-calculated accuracy (see **Figure 54**).

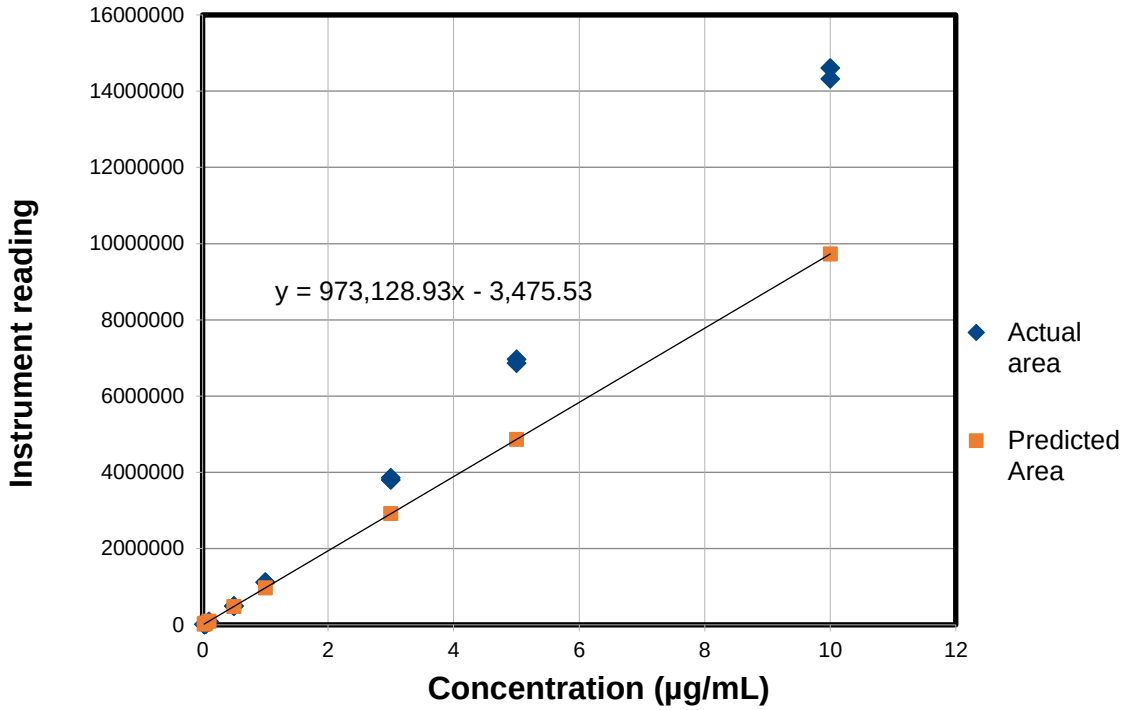

Figure 54 Weighted calibration curve for the calibration solutions prepared to assess the intra-day precision; see ***Table 35****. Weighted using a* $1/x^2$ *relationship. This gives an* R^2 *of 0,8820.*

Back-calculating the concentrations using the three methods presented in **Figure 52**, **Figure 53**, and **Figure 54**, we get a clear improvement when using a weighted $(1/x)$ calibration curve, as shown readily in **Table 50.**

Table 50 Back-calculated concentrations using different means of weighing (and not weighing) the calibration curve. The deviation held by the back-calculated concentration from the nominal concentration is expressed as the relative error percentage. Errors above 20% are highlighted with bold text. All concentrations are in µg/mL.

Nominal concentration (µg/mL)	**No weighing**		**$1/X$**		**$1/X^2$**	
	Concentration (µg/mL)	*Error*	Concentration (µg/mL)	*Error*	Concentration (µg/mL)	*Error*
0.025	0.124	***397%***	0.015	***-39%***	0.014	***-44%***
0.03	0.128	***326%***	0.019	***-37%***	0.019	***-37%***
0.05	0.133	***166%***	0.025	***-50%***	0.027	***-46%***
0.1	0.176	***76%***	0.070	***-30%***	0.091	*-9%*
0.5	0.457	*-9%*	0.366	***-27%***	0.508	*2%*
1	0.893	*-11%*	0.824	*-18%*	1.155	*15%*
3	2.790	*-7%*	2.821	*-6%*	3.971	***32%***
5	4.939	*-1%*	5.084	*2%*	7.162	***43%***
10	10.228	*2%*	10.652	*7%*	15.014	***50%***

However, other methods for back-calculating concentrations from calibration solutions also exist, such as the log-log transformation approach. The calibration curve is produced by using

the logarithm of the concentration and area. This up-scales lower concentrations and down-scales larger concentrations operate similarly to the weighted calibration curves exemplified in **Figure 53** and **Figure 54**. To see a log-log calibration curve fitting, see **Figure 55**.

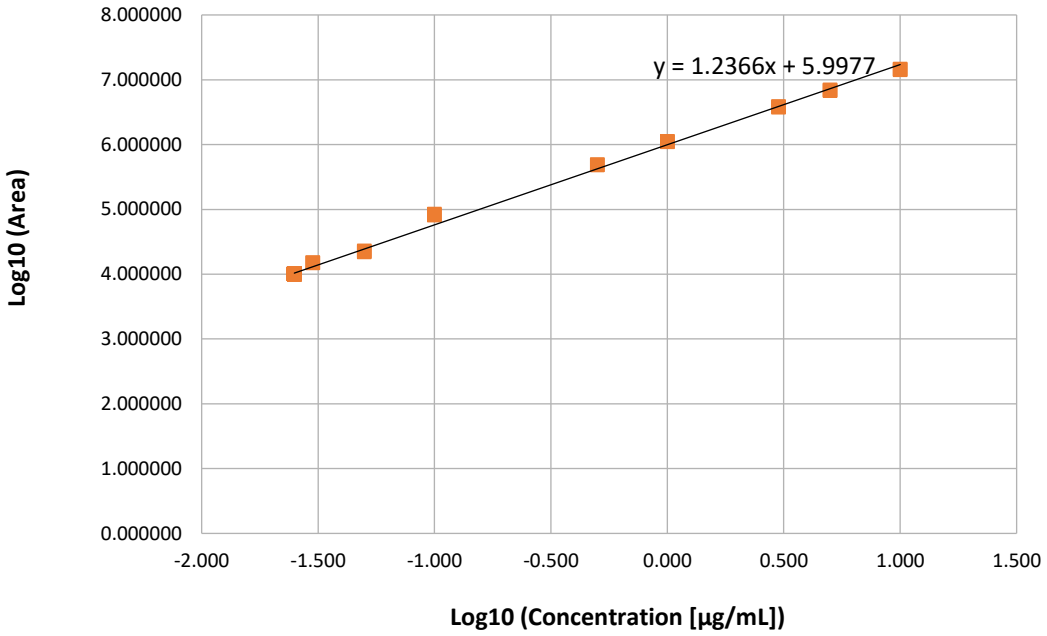

*Figure 55 Log-log calibration curve for the calibration solutions prepared to assess the intra-day precision; see **Table 35**. This gives an R^2 of 0,9981.*

This approach yielded the most accurate compared to the other fitting approaches described and compared in **Table 50**, as shown in **Table 51**, and warranted further investigation. While other methods such as the linear interpolation approach (commonly also called the bracket method) also exist, this remains tedious as many calibration points have to be produced and given an even spacing to ensure the interpolation does not become excessively faulty. This approach assumes complete linearity between calibration points and does not cope well with random errors in measurements. Finally, quadratic and cubic calibration curves also exist, but attempts to fit the calibration points to a quadratic or cubic curve yielded increasingly significant errors closer to the bottom of the calibration curve (173% relative error at the LLOQ for a quadratic fit, 69% error for a cubic fit) and were therefore not considered suitable for this work. Log-log transformations appeared to be most suitable based on the back-calculated accuracy, but this approach requires proper justification.

As described earlier in this section, heteroscedasticity may be observed quite directly by plotting the relative residuals against concentration. With the linearly fitted, unweighted data

obtained from the intra-day precision study, heteroscedasticity may still be observed in **Figure 56**. This means the weighting does not entirely negate the heteroscedasticity of the data.

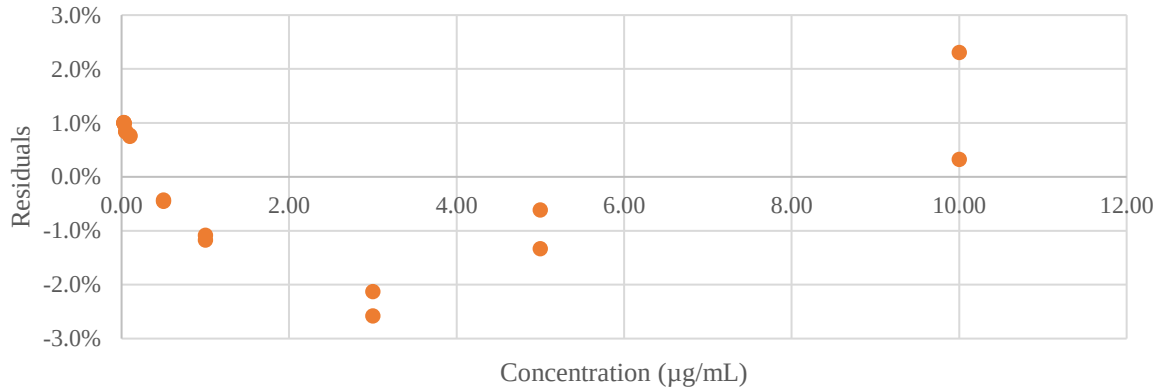

*Figure 56 Residuals versus concentrations for the calibration curve produced by a linear, non-weighted fit of data. The linear fit is illustrated in **Figure 52**. Data used to produce this can be found in **Table 35**. The trend shows a distinctly heteroscedastic set of data.*

For this reason, a weighted or log-log curve fitting is both justified and highly suitable. However, as shown, log-log transformations of data yield higher back-calculated accuracy and remain preferable. Logarithmic transformations of data narrow the numerical range of the calibration curve (making it easier to assess visually), turns heteroscedastic data homoscedastic, and gives a more uniform weighing, as described (downscaling of high values, upscaling of low values), and remains more suitable for large ranges in calibration curves [134-138]. Using this method, all calibration solutions except one (0.10 µg/mL) met the 15% criteria presented by the ICH of the EMA [139].

When dealing with transformed data, one must be wary of putting too much meaning into the slope and R^2. The value of the calibration fit does not *directly* describe the relationship of signal versus concentration but rather that of the transformed data. Back-calculating concentrations from various fitting methods were therefore considered the ideal way to evaluate calibration curve fittings. In **Table 51**, the relative error of the back-calculated concentrations compared to the nominal concentrations can be seen for log-log transformed data subjected to linear and quadratic unweighted fittings, as well as weighted fittings of quadratic curves. A weighted (factor: X) quadratic fit of log-log transformed data should be used to achieve maximum accuracy. However, this remains impractical and overly complex, and a simple quadratic fit is used instead in this work.

Table 51 Comparison of quadratic and linearly fitted calibration curves of log-log transformed data on the calibration points, with and without weighting. The relative error of back-calculated concentrations is used to assess the goodness of the calibration curve fitting.

	Relative error (%)			
Nominal concentration (µg/mL)	Linear	Quadratic	Quadratic (Weighted, X)	Quadratic (Weighted, 1/X)
0.025	-2.5%	-3.6%	-8.8%	-2.4%
0.03	12.1%	7.3%	2.8%	7.9%
0.05	-4.9%	-11.7%	-14.4%	-11.8%
0.1	36.7%	18.9%	19.2%	17.1%
0.5	13.1%	-2.6%	0.0%	-4.9%
1	10.1%	-2.1%	0.7%	-4.2%
3	-0.2%	-2.2%	-0.7%	-2.7%
5	-3.5%	1.5%	1.6%	2.4%
10	-12.2%	3.5%	0.8%	7.0%

9.13 APPENDIX M – SOURCES FROM APPENDICES

Sources referenced in appendices can be found in this section.

1. Preuss, H.G., *Basics of Renal Anatomy and Physiology.* Clinics in Laboratory Medicine, 13 (**1993**) 1-11.
2. *BioRender*. (**2020**); Available from: https://biorender.com/.
3. Jafari, F. and S. Elyasi, *Prevention of colistin induced nephrotoxicity: a review of preclinical and clinical data.* Expert Review of Clinical Pharmacology, (**2021**)
4. Li, J., R.W. Milne, R.L. Nation, J.D. Turnidge, T.C. Smeaton, and K. Coulthard, *Use of High-Performance Liquid Chromatography To Study the Pharmacokinetics of Colistin Sulfate in Rats following Intravenous Administration.* Antimicrobial Agents and Chemotherapy, 47 (**2003**) 1766-1770.
5. Gai, Z., S.L. Samodelov, G.A. Kullak-Ublick, and M. Visentin, *Molecular Mechanisms of Colistin-Induced Nephrotoxicity.* Molecules, 24 (**2019**).
6. Strimbu, K. and J.A. Tavel, *What are biomarkers?* Current opinion in HIV and AIDS, 5 (**2010**) 463-466.
7. Ptolemy, A.S. and N. Rifai, *What is a biomarker? Research investments and lack of clinical integration necessitate a review of biomarker terminology and validation schema.* Scandinavian Journal of Clinical and Laboratory Investigation, 70 (**2010**) 6-14.
8. Keirstead, N.D., M.P. Wagoner, P. Bentley, M. Blais, C. Brown, L. Cheatham, P. Ciaccio, Y. Dragan, D. Ferguson, J. Fikes, M. Galvin, A. Gupta, M. Hale, N. Johnson, W. Luo, F. McGrath, M. Pietras, S. Price, A.G. Sathe, J.C. Sasaki, D. Snow, R.L. Walsky, and G. Kern, *Early Prediction of Polymyxin-Induced Nephrotoxicity With Next-Generation Urinary Kidney Injury Biomarkers.* Toxicological Sciences, 137 (**2013**) 278-291.
9. Ghlissi, Z., A. Hakim, H. Mnif, F.M. Ayadi, K. Zeghal, T. Rebai, and Z. Sahnoun, *Evaluation of colistin nephrotoxicity administered at different doses in the rat model.* Renal Failure, 35 (**2013**) 1130-1135.
10. Ordooei Javan, A., S. Shokouhi, and Z. Sahraei, *A review on colistin nephrotoxicity.* European Journal of Clinical Pharmacology, 71 (**2015**) 801-810.
11. Soni, S.S., C. Ronco, N. Katz, and D.N. Cruz, *Early Diagnosis of Acute Kidney Injury: The Promise of Novel Biomarkers.* Blood Purification, 28 (**2009**) 165-174.
12. Ajiboye, T.O., *Colistin sulphate induced neurotoxicity: Studies on cholinergic, monoaminergic, purinergic and oxidative stress biomarkers.* Biomedicine & Pharmacotherapy, 103 (**2018**) 1701-1707.
13. Spapen, H., R. Jacobs, V. Van Gorp, J. Troubleyn, and P.M. Honoré, *Renal and neurological side effects of colistin in critically ill patients.* Annals of intensive care, 1 (**2011**) 14-14.
14. Jin, L., J. Li, R.L. Nation, and J.A. Nicolazzo, *Brain Penetration of Colistin in Mice Assessed by a Novel High-Performance Liquid Chromatographic Technique.* Antimicrobial Agents and Chemotherapy, 53 (**2009**) 4247-4251.
15. Wang, J., M. Yi, X. Chen, I. Muhammad, F. Liu, R. Li, J. Li, and J. Li, *Effects of colistin on amino acid neurotransmitters and blood-brain barrier in the mouse brain.* Neurotoxicology and Teratology, 55 (**2016**) 32-37.
16. Tamai, I., H. Yabuuchi, J.-i. Nezu, Y. Sai, A. Oku, M. Shimane, and A. Tsuji, *Cloning and characterization of a novel human pH-dependent organic cation transporter, OCTN1.* FEBS Letters, 419 (**1997**) 107-111.
17. Adibi, S.A., *The oligopeptide transporter (Pept-1) in human intestine: Biology and function.* Gastroenterology, 113 (**1997**) 332-340.

18. Dai, C., J. Li, S. Tang, J. Li, and X. Xiao, *Colistin-Induced Nephrotoxicity in Mice Involves the Mitochondrial, Death Receptor, and Endoplasmic Reticulum Pathways.* Antimicrobial Agents and Chemotherapy, 58 (**2014**) 4075-4085.
19. Dai, C., J. Li, and J. Li, *New insight in colistin induced neurotoxicity with the mitochondrial dysfunction in mice central nervous tissues.* Experimental and Toxicologic Pathology, 65 (**2013**) 941-948.
20. Cai, Y., W. Lee, and A.L. Kwa, *Polymyxin B versus colistin: an update.* Expert Review of Anti-infective Therapy, 13 (**2015**) 1481-1497.
21. Sweet, D.H. and J.B. Pritchard, *The molecular biology of renal organic anion and organic cation transporters.* Cell Biochemistry and Biophysics, 31 (**1999**) 89-118.
22. Lim, L.M., N. Ly, D. Anderson, J.C. Yang, L. Macander, A. Jarkowski III, A. Forrest, J.B. Bulitta, and B.T. Tsuji, *Resurgence of Colistin: A Review of Resistance, Toxicity, Pharmacodynamics, and Dosing.* Pharmacotherapy: The Journal of Human Pharmacology and Drug Therapy, 30 (**2010**) 1279-1291.
23. Sarkar, S., E.R.H. DeSantis, and J. Kuper, *Resurgence of colistin use.* American Journal of Health-System Pharmacy, 64 (**2007**) 2462-2466.
24. Yousef, J.M., G. Chen, P.A. Hill, R.L. Nation, and J. Li, *Melatonin Attenuates Colistin-Induced Nephrotoxicity in Rats.* Antimicrobial Agents and Chemotherapy, 55 (**2011**) 4044-4049.
25. Sirijatuphat, R., S. Limmahakhun, V. Sirivatanauksorn, R.L. Nation, J. Li, and V. Thamlikitkul, *Effect of ascorbic acid on colistin-associated nephrotoxicity: A preliminary clinical study.* Antimicrobial Agents and Chemotherapy, (**2015**) AAC.00280-15.
26. Aslan, T., E.M. Guler, A. Cakir, T. Dundar, A.S. Gulgec, O. Huseyinbas, M. Celikten, G. Coban, I.N. Hakyemez, A. Kocyigit, and B. Durdu, *Dexpanthenol and ascorbic acid ameliorate colistin-induced nephrotoxicity in rats.* European Review for Medical and Pharmacological Science, 25 (**2021**) 1016-1023.
27. Eljaaly, K., M.R. Bidell, R.G. Gandhi, S. Alshehri, M.A. Enani, A. Al-Jedai, and T.C. Lee, *Colistin Nephrotoxicity: Meta-Analysis of Randomized Controlled Trials.* Open Forum Infectious Diseases, 8 (**2021**) 1-6.
28. Naeini, M.B., V. Bianconi, M. Pirro, and A. Sahebkar, *The role of phosphatidylserine recognition receptors in multiple biological functions.* Cellular & Molecular Biology Letters, 25 (**2020**) 23-23.
29. Ichimura, T., J.V. Bonventre, V. Bailly, H. Wei, C.A. Hession, R.L. Cate, and M. Sanicola, *Kidney injury molecule-1 (KIM-1), a putative epithelial cell adhesion molecule containing a novel immunoglobulin domain, is up-regulated in renal cells after injury.* Journal of Biological Chemistry, 273 (**1998**) 4135-42.
30. Ichimura, T., C.C. Hung, S.A. Yang, J.L. Stevens, and J.V. Bonventre, *Kidney injury molecule-1: a tissue and urinary biomarker for nephrotoxicant-induced renal injury.* American Journal of Physiology-Renal Physiology, 286 (**2004**) F552-F563.
31. Ichimura, T., C.R. Brooks, and J.V. Bonventre, *Kim-1/Tim-1 and immune cells: shifting sands.* Kidney International, 81 (**2012**) 809-811.
32. Song, J., J. Yu, G.W. Prayogo, W. Cao, Y. Wu, Z. Jia, and A. Zhang, *Understanding kidney injury molecule 1: a novel immune factor in kidney pathophysiology.* American journal of translational research, 11 (**2019**) 1219-1229.
33. Bailly, V., Z. Zhang, W. Meier, R. Cate, M. Sanicola, and J.V. Bonventre, *Shedding of Kidney Injury Molecule-1, a Putative Adhesion Protein Involved in Renal Regeneration*.* Journal of Biological Chemistry, 277 (**2002**) 39739-39748.
34. Rees, A.J. and R. Kain, *Kim-1/Tim-1: from biomarker to therapeutic target?* Nephrol Dial Transplant, 23 (**2008**) 3394-6.

35. Lim, A.I., S.C.W. Tang, K.N. Lai, and J.C.K. Leung, *Kidney injury molecule-1: More than just an injury marker of tubular epithelial cells?* Journal of Cellular Physiology, 228 (**2013**) 917-924.
36. Vaidya, V.S., V. Ramirez, T. Ichimura, N.A. Bobadilla, and J.V. Bonventre, *Urinary kidney injury molecule-1: a sensitive quantitative biomarker for early detection of kidney tubular injury.* American Journal of Physiology-Renal Physiology, 290 (**2006**) F517-F529.
37. Huo, W., K. Zhang, Z. Nie, Q. Li, and F. Jin, *Kidney injury molecule-1 (KIM-1): a novel kidney-specific injury molecule playing potential double-edged functions in kidney injury.* Transplantation Reviews, 24 (**2010**) 143-146.
38. Chiusolo, A., R. Defazio, E. Zanetti, M. Mongillo, N. Mori, P. Cristofori, and A. Trevisan, *Kidney Injury Molecule-1 Expression in Rat Proximal Tubule after Treatment with Segment-Specific Nephrotoxicants:A Tool for Early Screening of Potential Kidney Toxicity.* Toxicologic Pathology, 38 (**2010**) 338-345.
39. Bonventre, J.V., *Kidney injury molecule-1 (KIM-1): a urinary biomarker and much more.* Nephrology Dialysis Transplantation, 24 (**2009**) 3265-3268.
40. Bonventre, J.V., *Kidney Injury Molecule-1 (KIM-1): A specific and sensitive biomarker of kidney injury.* Scandinavian Journal of Clinical and Laboratory Investigation, 68 (**2008**) 78-83.
41. Monney, L., C.A. Sabatos, J.L. Gaglia, A. Ryu, H. Waldner, T. Chernova, S. Manning, E.A. Greenfield, A.J. Coyle, R.A. Sobel, G.J. Freeman, and V.K. Kuchroo, *Th1-specific cell surface protein Tim-3 regulates macrophage activation and severity of an autoimmune disease.* Nature, 415 (**2002**) 536-541.
42. Kaplan, G., A. Totsuka, P. Thompson, T. Akatsuka, Y. Moritsugu, and S.M. Feinstone, *Identification of a surface glycoprotein on African green monkey kidney cells as a receptor for hepatitis A virus.* The EMBO journal, 15 (**1996**) 4282-4296.
43. Bonventre, J.V., *Dedifferentiation and Proliferation of Surviving Epithelial Cells in Acute Renal Failure.* Journal of the American Society of Nephrology, 14 (**2003**) S55-S61.
44. Thadhani, R., M. Pascual, and J.V. Bonventre, *Acute Renal Failure.* New England Journal of Medicine, 334 (**1996**) 1448-1460.
45. Wallin, A., G. Zhang, T.W. Jones, S. Jaken, and J.L. Stevens, *Mechanism of the nephrogenic repair response. Studies on proliferation and vimentin expression after 35S-1,2-dichlorovinyl-L-cysteine nephrotoxicity in vivo and in cultured proximal tubule epithelial cells.* Laboratory investigation; a Journal of Technical Methods and Pathology, 66 (**1992**) 474-484.
46. Nony, P.A. and R.G. Schnellmann, *Mechanisms of Renal Cell Repair and Regeneration after Acute Renal Failure.* Journal of Pharmacology and Experimental Therapeutics, 304 (**2003**) 905-912.
47. Witzgall, R., D. Brown, C. Schwarz, and J.V. Bonventre, *Localization of proliferating cell nuclear antigen, vimentin, c-Fos, and clusterin in the postischemic kidney. Evidence for a heterogenous genetic response among nephron segments, and a large pool of mitotically active and dedifferentiated cells.* The Journal of Clinical Investigation, 93 (**1994**) 2175-2188.
48. Kobayashi, N., P. Karisola, V. Peña-Cruz, D.M. Dorfman, M. Jinushi, S.E. Umetsu, M.J. Butte, H. Nagumo, I. Chernova, B. Zhu, A.H. Sharpe, S. Ito, G. Dranoff, G.G. Kaplan, J.M. Casasnovas, D.T. Umetsu, R.H. Dekruyff, and G.J. Freeman, *TIM-1 and TIM-4 glycoproteins bind phosphatidylserine and mediate uptake of apoptotic cells.* Immunity, 27 (**2007**) 927-940.

49. Ichimura, T., E.J.P.v. Asseldonk, B.D. Humphreys, L. Gunaratnam, J.S. Duffield, and J.V. Bonventre, *Kidney injury molecule–1 is a phosphatidylserine receptor that confers a phagocytic phenotype on epithelial cells.* The Journal of Clinical Investigation, 118 (**2008**) 1657-1668.
50. Humphreys, B.D., S. Czerniak, D.P. DiRocco, W. Hasnain, R. Cheema, and J.V. Bonventre, *Repair of injured proximal tubule does not involve specialized progenitors.* Proceedings of the National Academy of Sciences, 108 (**2011**) 9226-9231.
51. Daniel C. Harris, C.A.L., *Quantitative Chemical Analysis*. 9 ed. (**2016**): W.H. Freeman and Company.
52. Snyder, L.R., J.J. Kirkland, and J.W. Dolan, *Introduction to Modern Liquid Chromatography*. (**2011**): Wiley.
53. Desmet, G. and K. Broeckhoven, *Extra-column band broadening effects in contemporary liquid chromatography: Causes and solutions.* TrAC Trends in Analytical Chemistry, 119 (**2019**) 115619.
54. Farkas, T. and G. Guiochon, *Contribution of the Radial Distribution of the Flow Velocity to Band Broadening in HPLC Columns.* Analytical Chemistry, 69 (**1997**) 4592-4600.
55. Astashkina, A.I., B.K. Mann, G.D. Prestwich, and D.W. Grainger, *Comparing predictive drug nephrotoxicity biomarkers in kidney 3-D primary organoid culture and immortalized cell lines.* Biomaterials, 33 (**2012**) 4712-4721.
56. Ranga, A., N. Gjorevski, and M.P. Lutolf, *Drug discovery through stem cell-based organoid models.* Advanced Drug Delivery Reviews, 69-70 (**2014**) 19-28.
57. Lin, A., F. Sved Skottvoll, S. Rayner, S. Pedersen-Bjergaard, G. Sullivan, S. Krauss, S. Ray Wilson, and S. Harrison, *3D cell culture models and organ-on-a-chip: Meet separation science and mass spectrometry.* Electrophoresis, 41 (**2020**) 56-64.
58. Zhang, M., C. Xu, L. Jiang, and J. Qin, *A 3D human lung-on-a-chip model for nanotoxicity testing.* Toxicology Research, 7 (**2018**) 1048-1060.
59. Danoy, M., M.L. Bernier, K. Kimura, S. Poulain, S. Kato, D. Mori, T. Kido, C. Plessy, H. Kusuhara, A. Miyajima, Y. Sakai, and E. Leclerc, *Optimized protocol for the hepatic differentiation of induced pluripotent stem cells in a fluidic microenvironment.* Biotechnology and Bioengineering, 116 (**2019**) 1762-1776.
60. Hao, W., G. Chenlei, G. Ying, W. Xinwei, Z. Kai, H. Ning, and W. Ping, *Sensor-free and Sensor-based Heart-on-a-chip Platform: A Review of Design and Applications.* Current Pharmaceutical Design, 24 (**2018**) 5375-5385.
61. Haring, A.P., H. Sontheimer, and B.N. Johnson, *Microphysiological Human Brain and Neural Systems-on-a-Chip: Potential Alternatives to Small Animal Models and Emerging Platforms for Drug Discovery and Personalized Medicine.* Stem Cell Reviews and Reports, 13 (**2017**) 381-406.
62. Takasato, M., P.X. Er, H.S. Chiu, and M.H. Little, *Generation of kidney organoids from human pluripotent stem cells.* Nature Protocols, 11 (**2016**) 1681-1692.
63. Skardal, A., T. Shupe, and A. Atala, *Organoid-on-a-chip and body-on-a-chip systems for drug screening and disease modeling.* Drug Discovery Today, 21 (**2016**) 1399-1411.
64. Cláudia C. Miranda, T.G.F.M.M.D.J.M.S.C., *Towards Multi-Organoid Systems for Drug Screening Applications.* Bioengineering, 5 (**2018**).
65. Catherman, A.D., O.S. Skinner, and N.L. Kelleher, *Top Down proteomics: Facts and perspectives.* Biochemical and Biophysical Research Communications, 445 (**2014**) 683-693.
66. Gregorich, Z.R., Y.-H. Chang, and Y. Ge, *Proteomics in heart failure: top-down or bottom-up?* Pflugers Archiv : European journal of physiology, 466 (**2014**) 1199-1209.

67. Kelleher, N.L., *Top-down proteomics.* Anal Chem, 76 (**2004**) 197a-203a.
68. El-Aneed, A., A. Cohen, and J. Banoub, *Mass Spectrometry, Review of the Basics: Electrospray, MALDI, and Commonly Used Mass Analyzers.* Applied Spectroscopy Reviews, 44 (**2009**) 210-230.
69. Zhang, Y., B.R. Fonslow, B. Shan, M.-C. Baek, and J.R. Yates, *Protein Analysis by Shotgun/Bottom-up Proteomics.* Chemical Reviews, 113 (**2013**) 2343-2394.
70. Yates III, J.R., *Mass spectrometry and the age of the proteome.* Journal of Mass Spectrometry, 33 (**1998**) 1-19.
71. Fournier, M.L., J.M. Gilmore, S.A. Martin-Brown, and M.P. Washburn, *Multidimensional Separations-Based Shotgun Proteomics.* Chemical Reviews, 107 (**2007**) 3654-3686.
72. Swaney, D.L., C.D. Wenger, and J.J. Coon, *Value of Using Multiple Proteases for Large-Scale Mass Spectrometry-Based Proteomics.* Journal of Proteome Research, 9 (**2010**) 1323-1329.
73. Tsiatsiani, L. and A.J.R. Heck, *Proteomics beyond trypsin.* The FEBS Journal, 282 (**2015**) 2612-2626.
74. Giansanti, P., L. Tsiatsiani, T.Y. Low, and A.J.R. Heck, *Six alternative proteases for mass spectrometry–based proteomics beyond trypsin.* Nature Protocols, 11 (**2016**) 993-1006.
75. Burkhart, J.M., C. Schumbrutzki, S. Wortelkamp, A. Sickmann, and R.P. Zahedi, *Systematic and quantitative comparison of digest efficiency and specificity reveals the impact of trypsin quality on MS-based proteomics.* Journal of Proteomics, 75 (**2012**) 1454-1462.
76. Olsen, J.V., S.-E. Ong, and M. Mann, *Trypsin Cleaves Exclusively C-terminal to Arginine and Lysine Residues*.* Molecular & Cellular Proteomics, 3 (**2004**) 608-614.
77. Rodriguez, J., N. Gupta, R.D. Smith, and P.A. Pevzner, *Does Trypsin Cut Before Proline?* Journal of Proteome Research, 7 (**2008**) 300-305.
78. Loziuk, P.L., J. Wang, Q. Li, R.R. Sederoff, V.L. Chiang, and D.C. Muddiman, *Understanding the role of proteolytic digestion on discovery and targeted proteomic measurements using liquid chromatography tandem mass spectrometry and design of experiments.* Journal of Proteome Research, 12 (**2013**) 5820-9.
79. Cristobal, A., F. Marino, H. Post, H.W.P. van den Toorn, S. Mohammed, and A.J.R. Heck, *Toward an Optimized Workflow for Middle-Down Proteomics.* Analytical Chemistry, 89 (**2017**) 3318-3325.
80. Olaitan, A.O., S. Chabou, L. Okdah, S. Morand, and J.-M. Rolain, *Dissemination of the mcr-1 colistin resistance gene.* The Lancet Infectious Diseases, 16 (**2016**) 147.
81. Liakopoulos, A., D.J. Mevius, B. Olsen, and J. Bonnedahl, *The colistin resistance mcr-1 gene is going wild.* Journal of Antimicrobial Chemotherapy, 71 (**2016**) 2335-2336.
82. Nang, S.C., J. Li, and T. Velkov, *The rise and spread of mcr plasmid-mediated polymyxin resistance.* Critical Reviews in Microbiology, 45 (**2019**) 131-161.
83. Hartl, R., H. Kerschner, S. Lepuschitz, W. Ruppitsch, F. Allerberger, and P. Apfalter, *Detection of the mcr-1 Gene in a Multidrug-Resistant Escherichia coli Isolate from an Austrian Patient.* Antimicrobial Agents and Chemotherapy, 61 (**2017**) e02623-16.
84. Sonnevend, Á., A. Ghazawi, M. Alqahtani, A. Shibl, W. Jamal, R. Hashmey, and T. Pal, *Plasmid-mediated colistin resistance in Escherichia coli from the Arabian Peninsula.* International Journal of Infectious Diseases, 50 (**2016**) 85-90.
85. Malhotra-Kumar, S., B.B. Xavier, A.J. Das, C. Lammens, P. Butaye, and H. Goossens, *Colistin resistance gene mcr-1 harboured on a multidrug resistant plasmid.* The Lancet Infectious Diseases, 16 (**2016**) 283-284.

86. Fernandes, M.R., Q. Moura, L. Sartori, K.C. Silva, M.P. Cunha, F. Esposito, R. Lopes, L.K. Otutumi, D.D. Gonçalves, M. Dropa, M.H. Matté, D.F. Monte, M. Landgraf, G.R. Francisco, M.F. Bueno, D. de Oliveira Garcia, T. Knöbl, A.M. Moreno, and N. Lincopan, *Silent dissemination of colistin-resistant Escherichia coli in South America could contribute to the global spread of the mcr-1 gene.* Eurosurveillance, 21 (**2016**) 30214.
87. Stoesser, N., A.J. Mathers, C.E. Moore, N.P.J. Day, and D.W. Crook, *Colistin resistance gene mcr-1 and pHNSHP45 plasmid in human isolates of Escherichia coli and Klebsiella pneumoniae.* The Lancet Infectious Diseases, 16 (**2016**) 285-286.
88. Zhang, R., L. Liu, H. Zhou, E.W. Chan, J. Li, Y. Fang, Y. Li, K. Liao, and S. Chen, *Nationwide Surveillance of Clinical Carbapenem-resistant Enterobacteriaceae (CRE) Strains in China.* EBioMedicine, 19 (**2017**) 98-106.
89. Saavedra, S.Y., L. Diaz, M. Wiesner, A. Correa, S.A. Arévalo, J. Reyes, A.M. Hidalgo, E. de la Cadena, M. Perenguez, L.A. Montaño, J. Ardila, R. Ríos, M.V. Ovalle, P. Díaz, P. Porras, M.V. Villegas, C.A. Arias, M. Beltrán, and C. Duarte, *Genomic and Molecular Characterization of Clinical Isolates of Enterobacteriaceae Harboring mcr-1 in Colombia, 2002 to 2016.* Antimicrobial Agents and Chemotherapy, 61 (**2017**) e00841-17.
90. Hasman, H., A.M. Hammerum, F. Hansen, R.S. Hendriksen, B. Olesen, Y. Agersø, E. Zankari, P. Leekitcharoenphon, M. Stegger, R.S. Kaas, L.M. Cavaco, D.S. Hansen, F.M. Aarestrup, and R.L. Skov, *Detection of mcr-1 encoding plasmid-mediated colistin-resistant Escherichia coli isolates from human bloodstream infection and imported chicken meat, Denmark 2015.* Eurosurveillance, 20 (**2015**) 30085.
91. Ortega-Paredes, D., P. Barba, and J. Zurita, *Colistin-resistant Escherichia coli clinical isolate harbouring the mcr-1 gene in Ecuador.* Epidemiology and Infection, 144 (**2016**) 2967-2970.
92. Lima Barbieri, N., D.W. Nielsen, Y. Wannemuehler, T. Cavender, A. Hussein, S.-g. Yan, L.K. Nolan, and C.M. Logue, *mcr-1 identified in Avian Pathogenic Escherichia coli (APEC).* PLOS ONE, 12 (**2017**) e0172997.
93. Brauer, A., K. Telling, M. Laht, P. Kalmus, I. Lutsar, M. Remm, V. Kisand, and T. Tenson, *Plasmid with Colistin Resistance Gene mcr-1 in Extended-Spectrum-β-Lactamase-Producing Escherichia coli Strains Isolated from Pig Slurry in Estonia.* Antimicrobial Agents and Chemotherapy, 60 (**2016**) 6933-6936.
94. Falgenhauer, L., S.-E. Waezsada, Y. Yao, C. Imirzalioglu, A. Käsbohrer, U. Roesler, G.B. Michael, S. Schwarz, G. Werner, L. Kreienbrock, and T. Chakraborty, *Colistin resistance gene mcr-1 in extended-spectrum β-lactamase-producing and carbapenemase-producing Gram-negative bacteria in Germany.* The Lancet Infectious Diseases, 16 (**2016**) 282-283.
95. Juhász, E., M. Iván, E. Pintér, J. Pongrácz, and K. Kristóf, *Colistin resistance among blood culture isolates at a tertiary care centre in Hungary.* Journal of Global Antimicrobial Resistance, 11 (**2017**) 167-170.
96. Cannatelli, A., T. Giani, A. Antonelli, L. Principe, F. Luzzaro, and G.M. Rossolini, *First Detection of the mcr-1 Colistin Resistance Gene in Escherichia coli in Italy.* Antimicrobial Agents and Chemotherapy, 60 (**2016**) 3257-3258.
97. Ohsaki, Y., W. Hayashi, S. Saito, S. Osaka, Y. Taniguchi, S. Koide, K. Kawamura, Y. Nagano, Y. Arakawa, and N. Nagano, *First detection of Escherichia coli harboring mcr-1 gene from retail domestic chicken meat in Japan.* Japanese Journal of Infectious Diseases, advpub (**2017**).

98. Ruzauskas, M. and L. Vaskeviciute, *Detection of the mcr-1 gene in Escherichia coli prevalent in the migratory bird species Larus argentatus.* Journal of Antimicrobial Chemotherapy, 71 (**2016**) 2333-2334.
99. Yu, C.Y., G.Y. Ang, P.S. Chin, Y.F. Ngeow, W.-F. Yin, and K.-G. Chan, *Emergence of mcr-1-mediated colistin resistance in Escherichia coli in Malaysia.* International Journal of Antimicrobial Agents, 47 (**2016**) 504-505.
100. Leangapichart, T., P. Gautret, P. Brouqui, Z. Mimish, D. Raoult, and J.-M. Rolain, *Acquisition of mcr-1 Plasmid-Mediated Colistin Resistance in Escherichia coli and Klebsiella pneumoniae during Hajj 2013 and 2014.* Antimicrobial Agents and Chemotherapy, 60 (**2016**) 6998-6999.
101. Kluytmans–van den Bergh, M.F., P. Huizinga, M.J. Bonten, M. Bos, K. De Bruyne, A.W. Friedrich, J.W. Rossen, P.H. Savelkoul, and J.A. Kluytmans, *Presence of mcr-1-positive Enterobacteriaceae in retail chicken meat but not in humans in the Netherlands since 2009.* Eurosurveillance, 21 (**2016**) 30149.
102. Robin, F., R. Beyrouthy, J. Colot, P. Saint-Sardos, A. Berger-Carbonne, G. Dalmasso, J. Delmas, and R. Bonnet, *MCR-1 in ESBL-producing Escherichia coli responsible for human infections in New Caledonia.* Journal of Antimicrobial Agents and Chemotherapy, 72 (**2017**) 946-947.
103. Jørgensen, S.B., A. Søraas, L.S. Arnesen, T. Leegaard, A. Sundsfjord, and P.A. Jenum, *First environmental sample containing plasmid-mediated colistin-resistant ESBL-producing Escherichia coli detected in Norway.* APMIS, 125 (**2017**) 822-825.
104. Castanheira, M., M.A. Griffin, L.M. Deshpande, R.E. Mendes, R.N. Jones, and R.K. Flamm, *Detection of mcr-1 among Escherichia coli Clinical Isolates Collected Worldwide as Part of the SENTRY Antimicrobial Surveillance Program in 2014 and 2015.* Antimicrobial Agents and Chemotherapy, 60 (**2016**) 5623-5624.
105. Campos, J., L. Cristino, L. Peixe, and P. Antunes, *MCR-1 in multidrug-resistant and copper-tolerant clinically relevant Salmonella 1,4,[5],12:i:- and S. Rissen clones in Portugal, 2011 to 2015.* Eurosurveillance, 21 (**2016**) 30270.
106. Perreten, V., C. Strauss, A. Collaud, and D. Gerber, *Colistin resistance gene mcr-1 in avian pathogenic Escherichia coli in South Africa.* Antimicrobial Agents and Chemotherapy, (**2016**).
107. Lim, S.-K., H.Y. Kang, K. Lee, D.-C. Moon, H.-S. Lee, and S.-C. Jung, *First detection of the mcr-1 gene in Escherichia coli isolated from livestock between 2013 and 2015 in South Korea.* Antimicrobial Agents and Chemotherapy, (**2016**) AAC.01472-16.
108. Hernández, M., M.R. Iglesias, D. Rodríguez-Lázaro, A. Gallardo, N. Quijada, P. Miguela-Villoldo, M.J. Campos, S. Píriz, G. López-Orozco, C. de Frutos, J.L. Sáez, M. Ugarte-Ruiz, L. Domínguez, and A. Quesada, *Co-occurrence of colistin-resistance genes mcr-1 and mcr-3 among multidrug-resistant Escherichia coli isolated from cattle, Spain, September 2015.* Eurosurveillance, 22 (**2017**) 30586.
109. Vading, M., M.H. Kabir, M. Kalin, A. Iversen, S. Wiklund, P. Nauclér, and C.G. Giske, *Frequent acquisition of low-virulence strains of ESBL-producing Escherichia coli in travellers.* Journal of Antimicrobial Chemotherapy, 71 (**2016**) 3548-3555.
110. Donà, V., O.J. Bernasconi, J. Pires, A. Collaud, G. Overesch, A. Ramette, V. Perreten, and A. Endimiani, *Heterogeneous Genetic Location of mcr-1 in Colistin-Resistant Escherichia coli Isolates from Humans and Retail Chicken Meat in Switzerland: Emergence of mcr-1-Carrying IncK2 Plasmids.* Antimicrobial Agents and Chemotherapy, 61 (**2017**) e01245-17.
111. Kuo, S.-C., W.-C. Huang, H.-Y. Wang, Y.-R. Shiau, M.-F. Cheng, and T.-L. Lauderdale, *Colistin resistance gene mcr-1 in Escherichia coli isolates from humans*

and retail meats, Taiwan. Journal of Antimicrobial Chemotherapy, 71 (**2016**) 2327-2329.
112. Runcharoen, C., K.E. Raven, S. Reuter, T. Kallonen, S. Paksanont, J. Thammachote, S. Anun, B. Blane, J. Parkhill, and S.J. Peacock, *Whole genome sequencing of ESBL-producing Escherichia coli isolated from patients, farm waste and canals in Thailand.* Genome medicine, 9 (**2017**) 1-11.
113. Grami, R., W. Mansour, W. Mehri, O. Bouallègue, N. Boujaâfar, J.-Y. Madec, and M. Haenni, *Impact of food animal trade on the spread of mcr-1-mediated colistin resistance, Tunisia, July 2015.* Eurosurveillance, 21 (**2016**) 30144.
114. Doumith, M., G. Godbole, P. Ashton, L. Larkin, T. Dallman, M. Day, M. Day, B. Muller-Pebody, M.J. Ellington, E. de Pinna, A.P. Johnson, K.L. Hopkins, and N. Woodford, *Detection of the plasmid-mediated mcr-1 gene conferring colistin resistance in human and food isolates of Salmonella enterica and Escherichia coli in England and Wales.* Journal of Antimicrobial Chemotherapy, 71 (**2016**) 2300-2305.
115. Meinersmann, R.J., S.R. Ladely, J.R. Plumblee, K.L. Cook, and E. Thacker, *Prevalence of mcr-1 in the Cecal Contents of Food Animals in the United States.* Antimicrobial Agents and Chemotherapy, 61 (**2017**) e02244-16.
116. Malhotra-Kumar, S., B.B. Xavier, A.J. Das, C. Lammens, H.T.T. Hoang, N.T. Pham, and H. Goossens, *Colistin-resistant Escherichia coli harbouring mcr-1 isolated from food animals in Hanoi, Vietnam.* The Lancet Infectious Diseases, 16 (**2016**) 286-287.
117. Decolin, D., P. Leroy, A. Nicolas, and P. Archimbault, *Hyphenated Liquid Chromatographic Method for the Determination of Colistin Residues in Bovine Tissues.* Journal of Chromatographic Science, 35 (**1997**) 557-564.
118. Li, J., R.W. Milne, R.L. Nation, J.D. Turnidge, K. Coulthard, and D.W. Johnson, *A simple method for the assay of colistin in human plasma, using pre-column derivatization with 9-fluorenylmethyl chloroformate in solid-phase extraction cartridges and reversed-phase high-performance liquid chromatography.* Journal of Chromatography B: Biomedical Sciences and Applications, 761 (**2001**) 167-175.
119. Ma, Z., J. Wang, J.P. Gerber, and R.W. Milne, *Determination of colistin in human plasma, urine and other biological samples using LC–MS/MS.* Journal of Chromatography B, 862 (**2008**) 205-212.
120. Jansson, B., M. Karvanen, O. Cars, D. Plachouras, and L.E. Friberg, *Quantitative analysis of colistin A and colistin B in plasma and culture medium using a simple precipitation step followed by LC/MS/MS.* Journal of Pharmaceutical and Biomedical Analysis, 49 (**2009**) 760-767.
121. Swartz, M., *HPLC DETECTORS: A BRIEF REVIEW.* Journal of Liquid Chromatography & Related Technologies, 33 (**2010**) 1130-1150.
122. Wojnicz, A., C. Belmonte, D. Koller, A. Ruiz-Nuño, M. Román, D. Ochoa, and F. Abad-Santos, *Effective phospholipids removing microelution-solid phase extraction LC-MS/MS method for simultaneous plasma quantification of aripiprazole and dehydro-aripiprazole: Application to human pharmacokinetic studies.* Journal of Pharmaceutical and Biomedical Analysis, 151 (**2018**) 116-125.
123. Andrieux, K., S. Lesieur, M. Ollivon, and C. Grabielle-Madelmont, *Methodology for vesicle permeability study by high-performance gel exclusion chromatography.* J Chromatogr B Biomed Sci Appl, 706 (**1998**) 141-7.
124. Holzer, M., S. Barnert, J. Momm, and R. Schubert, *Preparative size exclusion chromatography combined with detergent removal as a versatile tool to prepare unilamellar and spherical liposomes of highly uniform size distribution.* Journal of Chromatography A, 1216 (**2009**) 5838-5848.

125. Xu, R., A. Fitts, X. Li, J. Fernandes, R. Pochampally, J. Mao, and Y.-M. Liu, *Quantification of Small Extracellular Vesicles by Size Exclusion Chromatography with Fluorescence Detection.* Analytical Chemistry, 88 (**2016**) 10390-10394.
126. Dos Santos, N., C. Allen, A.-M. Doppen, M. Anantha, K.A.K. Cox, R.C. Gallagher, G. Karlsson, K. Edwards, G. Kenner, L. Samuels, M.S. Webb, and M.B. Bally, *Influence of poly(ethylene glycol) grafting density and polymer length on liposomes: Relating plasma circulation lifetimes to protein binding.* Biochimica et Biophysica Acta (BBA) - Biomembranes, 1768 (**2007**) 1367-1377.
127. Hwang, S.Y., H.K. Kim, J. Choo, G.H. Seong, T.B.D. Hien, and E.K. Lee, *Effects of operating parameters on the efficiency of liposomal encapsulation of enzymes.* Colloids and Surfaces B: Biointerfaces, 94 (**2012**) 296-303.
128. Nguyen, T.T.T.N., S. Stürup, J. Østergaard, U. Franzen, and B. Gammelgaard, *Simultaneous measurement of phosphorus and platinum by Size Exclusion Chromatography coupled to Inductively Coupled Plasma Mass Spectrometry (SEC-ICPMS) using xenon as reactive collision gas for characterization of platinum drug liposomes.* Journal of Analytical Atomic Spectrometry, 26 (**2011**) 1466-1473.
129. Lesieur, S., C. Grabielle-Madelmont, M. Paternostre, and M. Ollivon, *Study of size distribution and stability of liposomes by high performance gel exclusion chromatography.* Chemistry and Physics of Lipids, 64 (**1993**) 57-82.
130. Bidlingmeyer, B., *Liquid Chromatography Problem Solving and Troubleshooting.* Journal of Chromatographic Science, 39 (**2001**) 537-537.
131. Almeida, A.M., M.M. Castel-Branco, and A.C. Falcão, *Linear regression for calibration lines revisited: weighting schemes for bioanalytical methods.* Journal of Chromatography B, 774 (**2002**) 215-222.
132. Szabo, G.K., H.K. Browne, A. Ajami, and E.G. Josephs, *Alternatives to Least Squares Linear Regression Analysis for Computation of Standard Curves for Quantitation by High Performance Liquid Chromatography: Applications to Clinical Pharmacology.* The Journal of Clinical Pharmacology, 34 (**1994**) 242-249.
133. Mulholland, M. and D.B. Hibbert, *Linearity and the limitations of least squares calibration.* Journal of Chromatography A, 762 (**1997**) 73-82.
134. Miller-Ihli, N.J., T.C. O'Haver, and J.M. Harnly, *Calibration and curve fitting for extended range AAS.* Spectrochimica Acta Part B: Atomic Spectroscopy, 39 (**1984**) 1603-1614.
135. Mani, D.R., S.E. Abbatiello, and S.A. Carr, *Statistical characterization of multiple-reaction monitoring mass spectrometry (MRM-MS) assays for quantitative proteomics.* BMC Bioinformatics, 13 (**2012**) S9.
136. Aouri, M., A. Calmy, B. Hirschel, A. Telenti, T. Buclin, M. Cavassini, A. Rauch, and L.A. Decosterd, *A validated assay by liquid chromatography–tandem mass spectrometry for the simultaneous quantification of elvitegravir and rilpivirine in HIV positive patients.* Journal of Mass Spectrometry, 48 (**2013**) 616-625.
137. van Liempd, S., D. Cabrera, J.M. Mato, and J.M. Falcon-Perez, *A fast method for the quantitation of key metabolites of the methionine pathway in liver tissue by high-resolution mass spectrometry and hydrophilic interaction ultra-performance liquid chromatography.* Analytical and Bioanalytical Chemistry, 405 (**2013**) 5301-5310.
138. Singtoroj, T., J. Tarning, A. Annerberg, M. Ashton, Y. Bergqvist, N.J. White, N. Lindegardh, and N.P.J. Day, *A new approach to evaluate regression models during validation of bioanalytical assays.* Journal of Pharmaceutical and Biomedical Analysis, 41 (**2006**) 219-227.
139. Agency, E.M., *Guideline on bioanalytical method validation.* European Medicines Agency, (**2011**).